1-1-1977

The effect of shear on polymer crystallization kinetics.

Charles Herbert Sherwood
University of Massachusetts Amherst

THE EFFECT OF SHEAR ON POLYMER CRYSTALLIZATION KINETICS

A Dissertation Presented

By

Charles H. Sherwood

Submitted to the Graduate School of the
University of Massachusetts in partial fulfillment
of the requirements for the degree of

DOCTOR OF PHILOSOPHY

February 1977

Polymer Science and Engineering

THE EFFECT OF SHEAR ON POLYMER

CRYSTALLIZATION KINETICS

A Dissertation Presented

by

Charles H. Sherwood

Approved as to style and content by:

Chairman of Committee

Head of Department

Member

Member

Member

February 1977

In Memory of

Professor Fraser P. Price

ACKNOWLEDGEMENTS

This research project was conceived and directed by Dr. F. P. Price up until the time of his death. I am extremely indebted to him in ways too numerous to mention. I hope that this dissertation serves as an adequate representation of his ideas and the kind of work he would have produced.

I wish to thank Dr. R. S. Stein for his advice and interest during the course of these studies and for his invaluable contribution as director in the final stages of this research. I also wish to thank Dr. R. L. Laurence for his suggestions, criticisms and friendship which contributed to my personal as well as technical development. Thanks must also go to the other members of my committee, Dr. S. Middleman and Dr. F. E. Karasz for their suggestions and constructive criticisms.

Credit must also be given to Michael D. Wolkowicz for his assistance with certain experiments undertaken during this research and for his valuable input during frequent discussions of this work.

ABSTRACT

THE EFFECT OF SHEAR ON POLYMER
CRYSTALLIZATION KINETICS

February 1977

Charles H. Sherwood, B.S., Cornell University
M.S., University of Massachusetts
Ph.D., University of Massachusetts

Directed by: Professor Richard S. Stein

The effect of shear on polymer crystallization kinetics has been studied for three materials at several shear rates and degrees of supercooling. Two polyethylene oxide samples with molecular weights of 75,000 and 12,000 and a poly-ε-caprolactone material with a molecular weight of 9,400 were investigated. The apparatus used was a concentric cylinder viscometer which also functions as a dilatometer capable of detecting very small volume changes on crystallization. The shear rate range of the experiments was 0 sec^{-1} to 60 sec^{-1}. Avrami kinetics were used to describe the transformation process and the exponent was found to increase from the quiescent value of 3 to a value greater than 5 with increasing shear rate for all materials studied. The acceleration in the transformation process was associated with a reduction in induction time. The value of induction time at high shear rates did not significantly decrease with increasing shear rate indicating a saturation effect with shear. This was most pronounced in the low

molecular weight samples. The value of induction time for the high molecular weight polyethylene oxide sample under identical experimental conditions was substantially less than that of the low molecular weight material in all cases.

Shear stress and nuclei formation measurements were made for the crystallizing melt in separate experimental instruments. Shear stress was found to increase rapidly with small amounts of crystallinity. Nuclei formation under shear was very different from quiescent behavior and increased substantially with increasing shear rate. These experimental observations lead to the conclusion that accelerated crystallization is due to increased molecular chain extension and orientation under shear. This orientation greatly enhances the nucleation process which is thought to be the rate controlling step in the crystalline transformation. This enhancement results in shorter induction times and more rapid crystallization.

TABLE OF CONTENTS

TABLE OF CONTENTS (cont.)

LIST OF TABLES

LIST OF FIGURES

LIST OF FIGURES (cont.)

LIST OF FIGURES (cont.)

C H A P T E R I

INTRODUCTION

It is well known that the morphology of a polymeric material can greatly influence its mechanical properties and dictate its usefulness in certain applications. Extensive research over the past twenty years has shown that the processing conditions to which a polymer is subjected have a controlling effect on the resulting morphology. It was the purpose of this study to examine the effect of molecular weight, shear and undercooling on the kinetics of the crystallization process under well defined conditions in an attempt to elucidate the fundamental mechanism of crystallization under shear.

In order to form a cohesive picture of crystallization under shear, it is necessary to incorporate the results of this study with those reported by other researchers. This chapter divides the pertinent literature into three categories. The first section contains theories of the nucleation process and expressions describing the kinetics of the crystalline transformation. Several theoretical treatments of crystallization under stress are outlined in the second section. The last section contains a review of the numerous experimental observations obtained with shear crystallized systems.

Nucleation

The birth of a new phase in a mother phase begins with the formation of a thermodynamically stable nucleus. Nuclei formation under quiescent conditions can occur by one of two processes, heterogeneous or homogeneous nucleation. Homogeneous nucleation takes place in the pure supercooled melt and results from random fluctuations of molecular order. Heterogeneous nucleation is initiated on foreign particles or surfaces and occurs at lower degrees of undercooling than homogeneous nucleation. An expression for the rate of formation of nuclei has been formulated by Fisher and Turnbull[1] and is given below. Here I_o is

$$\dot{I} = I_o \exp(-\Delta F^*/kT) \exp(-\Delta G^*/kT) \qquad (1)$$

essentially independent of temperature, depends on molecular parameters and in the case of nucleation controlled growth, is a function of crystal geometry. The quantity ΔF^* is the energy required to transport material across the liquid-crystal interface. The quantity ΔG^* is the work required to build a nucleus of critical size. This term depends on surface energy contributions and the bulk free energy of fusion. At temperatures near the melting point, the contribution of ΔG^* is controlling and the temperature coefficient of the nucleation rate is negative. At temperatures near the glass transition temperature, the transport term,

ΔF^*, is dominant and the process has a positive temperature coefficient. In most shear crystallization studies it is assumed that the major barrier to crystallization lies in the work required to build a critical nucleus, ΔG^*.

Transformation Kinetics

The overall description of the transformation kinetics of polymer crystallization must contain the combined effects of the nucleation and growth processes. An initial treatment of this type was reported by Von Goler and Sachs[2]. Their theory, which is termed the free growth approximation, disregards the effect of impinging growth moieties and is therefore only applicable for the initial stages of the transformation. Avrami[3,4,5], in a theory originally formulated for metals, and others[6,7] have reported a more exact description of crystalline transformation kinetics.

The Avrami treatment is based on several assumptions which must be scrutinized when it is used to describe polymeric systems. The first of these assumptions is that the density of the transformed phase is constant. This is not true for polymers. The second assumption is that the rate of growth along a given growth axis does not vary with time. This is generally observed except when growing particles are near impingement[8]. It is also assumed that nuclei formation is random throughout the melt. This is acceptable providing nucleation does not take place on the surface of the

crystallization vessel[8]. This assumption must also be re-examined if shear is found to produce highly localized concentrations of nuclei. The final assumption requires either a zeroth or first order time dependence of nucleation. It has been observed experimentally that nucleation can be described by a combination of both rate equations[9].

In a treatment analagous to that of Avrami, Mandelkern[10] has developed an equation for polymer crystallization taking into account the fact that polymers do not achieve complete transformation. The expression is given below

$$X_{cr} = X_{\infty}(1 - \exp(-k/X_{\infty}(t)^{n})) \tag{2}$$

where X_{∞} is the weight fraction of polymer that is crystalline at the termination of the transformation, n and k are the Avrami exponent and rate constant respectively, and X_{cr} is the measured degree of crystallinity.

The rate constant, k, for a growing sphere is given by

$$k = \frac{\pi}{3} \frac{\rho_c}{\rho_L} \dot{I} \, G^3 \tag{3}$$

where G is the radial growth rate of the crystal, ρ_c and ρ_L are the densities of the crystalline and melt phase respectively, and $\dot{I}$ is the nucleation rate. For growth in systems where diffusion of the crystallizing chains to the interface is not controlling, the Avrami theory predicts integer values

of the exponent which reflect the time dependence of nucleation (zeroth or first order) and the dimensionality of the growing crystal. Hence, for a growing sphere (dimensionality of three) with heterogeneous nucleation (zeroth growth) the value of the exponent would be three. Non integer values of n are frequently observed[11], and this can be explained in part by the inaccurate description of the nucleation process discussed previously. Although in many cases the value of n has been found to correspond well with the observed crystalline morphology[12], it is not good practice to attempt to describe the nucleation and growth processes by these values alone.

Several authors have recognized the limitations of the Avrami equation and have attempted to include modifications to provide better agreement with experimental data[13,14]. These modifications are in the form of adjustable parameters and do not appear to provide significant improvement during the initial stages of the transformation. In general, the Avrami analysis does not always provide an accurate mechanistic description of the crystalline transformation process for polymeric materials. However, the author feels it still has value as a mathematical description of the kinetics and as a basis for comparison of experimental data.

Stress Crystallization Theory

Theoretical interpretations of the molecular mechanisms occurring during the crystallization process are rare indeed. The uncertainty concerning the configuration of chains and complexity of interactions between molecules have discouraged attempts to describe flow induced crystallization in the melt. Several theories have been formulated to explain crystallization in uniaxially extended cross linked systems and in dilute solutions subjected to transverse and elongational velocity gradients. It is instructive to examine these theories because with the appropriate sophistications they can serve as a basis for the molecular interpretation of melt crystallization in flowing systems.

Flory[15] has proposed a theory which describes the crystalline transformation in a stressed network of cross-linked polymer chains. The theory is based on a thermodynamic analysis of the fusion process which assumes equilibrium conditions, namely the crystallization process occurs after the sample deformation is complete. Changes in entropy associated with nuclei formation are considered insignificant. Gaussian statistics are used to describe chain configurations and as a consequence, the theory is not applicable at very high elongation ratios[16].

The retractive force after crystallization per unit of original cross-sectional area is given by

$$f_c = \sigma RT(\alpha - \frac{1}{\alpha^2} - (\frac{6n}{\pi})^{1/2} X_c)/(1-X_c) \quad (4)$$

where α is the ratio of stretched to unstretched length, n is the number of statistical segments per chain, σ is the number of chains per unit volume, and X_c is the equilibrium degree of crystallinity. This stress can be related to the stress in the sample prior to crystallization using

$$f_o = \sigma RT\ (\alpha - \frac{1}{\alpha^2}) \quad (5)$$

which is the reduced form of equation 4 for X_c equal to zero. The theory also predicts the incipient crystallization temperature, T_m.

$$\frac{1}{T_m} = \frac{1}{T_m^o} - \frac{R}{h_f}\ ((\frac{6}{n\pi})^{1/2}\alpha - \frac{\alpha^2}{2n} + \frac{1}{\alpha n}) \quad (6)$$

Here T_m^o is the incipient crystallization temperature at rest and h_f is the heat of fusion per statistical segment.

The predicted retractive force and incipient crystallization temperature are qualitatively in good agreement with experimental data except at low and very high elongations. The error at low elongations is due in part to an assumption which dictates the orientation of a crystallizing segment with respect to the end to end chain vector. Smith[17] relaxed this assumption and obtained expressions similar to those already given and in good agreement with experimental data for values of α in the range of 3 to 10. Gaylord has extended the theory to include morphologies

different than the extended chain configuration assumed by Flory[18] and has also employed a non-Gaussian distribution function to describe chain configuration[19]. For moderate elongation ratios, the results obtained with these modifications are similar to those of Flory and Smith.

Krigbaum and Roe[20] have derived an expression using free energy considerations to predict the incipient crystallization temperature as a function of extension ratio. This expression is

$$\frac{1}{T_m} = \frac{1}{T_m^o} - \frac{R}{2\Delta H_f' n}\left(\alpha^2 - \frac{2}{\alpha} - 3\right) \qquad (7)$$

where $\Delta H_f'$ is the heat of fusion per mole of statistical segments. Unlike the Flory treatment, this theory neglects the free energy change associated with the orientation of crystallites formed in the stretched network. The temperatures calculated from equation 7 fit their data on chloroprene rubber well at low elongations but are consistently too low for medium and high values of α.

McHugh[21] has derived a theory of molecular extension and crystal nucleation in dilute solution following a method employed by Peterlin[22]. The elastic dumbell model used considers the total hydrodynamic resistance of a molecule to be concentrated at its ends which are separated by an elastic force. The results for the extension ratio, α, in simple shear and extensional flow are

$$\alpha_{SH} = \left[\frac{3E^2 - 2\theta G^2}{3E^3} \right]^{1/2} \tag{8}$$

$$\alpha_{EX} = \left[\frac{E - \theta G}{(E-2\theta G)(E+\theta G)} \right]^{1/2} \tag{9}$$

where G is the deformation rate, θ is the relaxation time and E is a factor involving the inverse Langevin function introduced to account for non linear chain extension effects. The relaxation time can be employed to include molecular weight as a parameter in equations 8 and 9 through the use of equation 10 where η_o is the solvent

$$[\eta]_o = \frac{RT\theta}{\eta_o M_w} \tag{10}$$

viscosity and $[\eta]_o$ is the intrinsic viscosity of the polymer solution at zero shear.

The equation for the rate of formation of bundle-like nuclei from solution is given by[23]

$$\dot{I}_b = k_b\left(\frac{kT}{h}\right) n_o \exp\left(\frac{-\Delta F^*}{kT}\right) \exp\left(\frac{-32\sigma_s^2\sigma'_{end}}{kT(\Delta f^1)^2}\right) \exp\left(\frac{16\sigma_s^2 \ln v_2}{a(\Delta f^1)^2}\right) \tag{11}$$

where σ_s and σ_{end} are the surface energies of the side and ends of the nuclei respectively, v_2 is the volume fraction of polymer, Δf^1 is the free energy difference between a chain in an infinite fiber crystal and in an extended conformation in solution, h is Planck's constant, n_o is the number of molecules per unit volume, and k_b is a term that

depends on σ_{end}' and Δf^1. The free energy Δf^1 is evaluated using

$$\Delta f^1 = \Delta f + \Delta f_1 \tag{12}$$

where Δf is the free energy change associated with crystallization from a random coil to an infinite fiber and can be readily calculated. The term Δf_1 represents the free energy associated with the transition from a random coil to a partially extended conformation in solution. The equation for Δf_1 includes the first normal stress difference, the elongation ratio and other parameters. If it is assumed that Δf is the same for both the random coil to infinite fiber crystallization and the random coil to folded chain crystallization, then the ratio of the nucleation rates for these transformations is given by equation 13.

$$\frac{\dot{I}_{ex}}{\dot{I}_{f.c.}} = \exp \frac{32\sigma_s\sigma_e}{kT} \left(\frac{1}{\Delta_f^2} - \frac{1}{(\Delta f^1)^2}\right) \exp\left(\frac{16\sigma_s^2 \ln v_2}{a\ (\Delta f^1)^2}\right) \tag{13}$$

Substitution of the calculated Δf^1 values for simple shear and elongational flow into equation 13 indicates that the latter is orders of magnitude more effective in generating the extended chain morphology.

Crosslinked Systems

One of the initial investigations of crystallization under stress was conducted by Treloar[24] on uniaxially stretched samples of natural rubber. Birefringence and density measurements were employed to follow orientation and crystallite formation at several elongations and temperatures. It was found that the crystallization rate and the maximum degree of crystallinity increased with increasing extension ratio. Near perfect orientation of crystallite axes in the stretch direction was detected even at low elongations.

Gent[25] also investigated stressed natural rubber systems. Volume changes were measured and a kinetic treatment of the transformation process was formulated. The Avrami exponent[3] was found to decrease continuously from a value of 3 for the unstretched state to 1 at high extensions. It was noted that deviations from the theoretical crystallization curve occurred at advanced stages of the transformation. Stress relaxation as a function of crystallinity was monitored and values for the degree of crystallinity at zero stress were in good agreement with those predicted by Flory[15] for moderate elongations. At low extensions, lack of agreement was attributed to incomplete orientation leading to non aciform growth.

Andrews[26] used electron microscopy to examine the morphology, nucleation, and growth of crystals formed in uniaxially stretched natural rubber. Crystal structure in the unstrained state was found to be spherulitic. As the extension ratio was increased, alignment of needle-like structures, termed α filaments, perpendicular to the stretch direction predominated. At strains greater than 300 percent, γ filaments, which were parallel to the stretch direction, were formed. It was suggested that small amounts of γ filament structures are formed at moderate degrees of stretch which then serve as nuclei for the formation of α filaments.

Nucleation was measured versus time and was found to increase with increasing strain and decreasing temperature. Nucleation density at the end of the transformation process was a function of strain only, greater strain producing more nuclei. The growth rate of the crystal filaments was found to be essentially independent of strain up to measured elongations of 200 percent, but was markedly increased by decreasing crystallization temperatures.

Kim and Mandelkern[27] analyzed the kinetics of strained natural rubber crystallization using the Avrami equation. Degrees of crystallinity were calculated using Flory's theory relating X_{cr} to stress in the sample and extension ratio. Values of the exponent n decreased with stretch ratio to a limiting value of 1 at an elongation of 600 percent. The crystallinity versus time curves were superposable,

with appropriate shifts in the time axis, for a given degree of stretch at different temperatures. It was concluded from this that major nucleation and growth processes are independent of temperature at a given elongation ratio. Estimates of incipient crystallization temperatures were made as a function of elongation ratio and were found to agree well with theoretical values[15] at moderate and high elongations.

The orientation of crystallites in stress crystallized polychloroprene rubber was investigated by Krigbaum and Roe using X-ray diffraction[20]. An orientation distribution function for the stretched amorphous network chains was developed and compared to the measured orientation function for the crystalline chains. It was concluded that orientation in the melt was much less than found in the crystals. Assuming a rate expression for nucleation based on the amorphous chain orientation function, the dimensions of a critical size nucleus were calculated.

Judge and Stein[28] and Kawai, Iquchi and Tonami[29] crystallized elongated radiation crosslinked polyethylene melts and examined crystallite orientation with X-ray diffraction and electron microscopy. The crystals exhibited a axis orientation at low elongations and c axis orientation at higher elongations. Judge and Stein attributed this behavior to a transition from lamellar to bundled fibril crystal structure whereas Kawai et al. reported the presence of stacked lamellae structures throughout with the

chain axes in the lamellae undergoing rotation toward the stretch direction as elongation increased. The existence of extended chain crystals, oriented in the stretch direction, as a precursor to lamellae structure was considered plausible but could not be substantiated by experimental data. Kawai et al. concluded that the factor governing crystallization was not macroscopic deformation but the degree of molecular orientation prior to crystallization.

Hashiyama[83] examined the crystallization under stress of cis-1,4-polyisoprene using X-ray diffraction, birefringence, and light scattering measurements. Examination of the V_v light scattering pattern indicated that crystal nuclei are formed with some preferential order in the stretching direction. X-ray diffraction measurements showed a large degree of chain axis orientation close to the stretching direction. H_v light scattering patterns led to the conclusion that crystalline scattering entities are aligned at a slight angle to the stretching direction at higher elongations. A possible explanation of this tilting was derived from the analagous behavior observed in single crystals where tilting relieves the crowding due to chain folds.

Keller and Machin [36,51] examined crystallization of crosslinked and uncrosslinked films of polyethylene in the stretched state. Electron microscopy, X-ray diffraction and thermal analysis were used to measure orientation and

to investigate the mechanism of crystal nucleation. Observations from X-ray diffraction experiments were similar to those reported previously, but the "row structure" model proposed to explain them is somewhat different. Keller states that nucleation occurs along rows parallel to the stress direction in the deformed melt. These nuclei, which are composed of very high melting polymer crystallites not heterogeneities[51], form the site for accelerated growth of folded chain crystals. The orientation of the chain axes in the stacked lamellae change with increasing stress. At low stress values, the lamellae appear as twisted ribbons perpendicular to the stress direction (b axis growth) but with randomly oriented a and c axes. At high stress values, the lamellae resemble flat plates with near perfect c axis orientation in the stress direction. The morphology of the nuclei could not be determined but the high melting point indicates a possible combination of extended and folded chain crystals.

Yeh and coworkers[80-82] have interpreted the morphology of stress crystallized materials in terms of two processes, strain induced crystallization (SIC) and thermally induced crystallization (TIC). It was concluded that any strain above a critical value is sufficient to generate a fibrillar morphology in the SIC process. These fibrils have diameters of approximately 150 Å, exhibit a high degree of c axis orientation, have highly elevated melting points, and contain

crystallites with limiting crystal dimensions. The crystallites are thought to consist of nodules, each composed of several chain folds, rather than extended chain material.

Actual crystallization under stress in most experiments is a combination of SIC and TIC in which nodules are able to realign and reduce their fold period. Aligned nodules, and connective chains (chain segments attached at one or both ends to nodules) then crystallize in lamellae oriented perpendicular to the stress direction. The formation of lamellae is governed by temperature (no lamellae formation can ocurr above T_m^o) and imposed stress or strain only influences the rate and ease of formation.

Solution Crystallization

Considerable interest in the field of flow induced crystallization was generated by the experiments of Pennings and Kiel[30] in which fibrous crystals were produced during shearing of dilute (one to five percent) solutions of polyehtylene in xylene. Electron micrographs, birefringence and melting point measurements indicated that the backbone of these fibers was composed of extended chain crystals. At lower concentrations and different shearing conditions, an overgrowth of ribbon type crystals, composed of folded chains, became more prominent.

Other researchers have found similar structures formed in shear crystallized solutions of polyvinyl

alcohol[31,32], isotactic polystyrene[33] and polyethylene oxide[34]. This fiber-ribbon overgrowth composite was termed the shish kebab morphology[35]. Further research in this area can be divided into two categories. The first category deals with the morphological investigations of the shish kebab structure while the second is concerned with the hydrodynamic conditions necessary to produce this morphology.

Morphology. Keller and Machin[36] examined electron micrographs of the shish kebab morphology and determined that the central thread, composed of extended chains, appeared ribbon-like with dimensions of 30 Å thick and 70 Å wide. Regularly spaced overgrowths of folded chain lamellar platelets extending from this core had length dimensions of 300 Å to 1000 Å. As the temperature of crystallization was lowered, the size and complexity of this structure increased.

Wikjord and St. John Manley[37] investigated the morphology of stirrer crystallized polyethylene after chemical modification. Nitric acid etching was used to attack tie molecules, amorphous segments and chain folds. The remaining material was then dissolved by repeated exposure to hot solvent vapors. The dissolution of the lamellar overgrowths left only the central core for examination. Crystal dimensions were similar to those observed by Keller and Machin. An interesting observation was that periodicity of

structures along the fiber axis was comparable to the calculated length of an extended chain molecule.

Krueger and Yeh[39] reported that drawing of solution crystallized shish kebabs produced a continuous fibrous structure. The conclusion reached from these results was that the platelets are not overgrowths but part of the core material. A clarification must be made at this point to distinguish between the platelets of Krueger and Yeh and those discussed by other researchers. It has been reported that platelets of large dimensions (1000 Å) have formed around the central core. It appears that this material is an overgrowth and is not associated with the same crystallization process producing the central filament.

Additional insight into this matter was provided by Mackley[38] who rotated fine wire gauze in a solution of polyethylene under laminar flow conditions. The resulting morphology was the typical shish kebab structure with a central thread (d = 160 Å) and regularly spaced lamellar platelets (d = 250 Å). Additional chain folded overgrowths and fiber aggregation were noted and attributed to the crystallization processes occurring in simple shear flow. The central thread and platelet formation was attributed to longitudinal velocity gradients produced by flow through the wire mesh.

Hydrodynamics. Pennings et al.[40] examined the formation of fibrous crystals in a concentric cylinder apparatus

with inner and outer cylinder rotation. It was postulated that the high rotational speeds necessary to create fibrous crystals produced an elongational flow region due to the formation of Taylor vortices[41,42]. Further research[43] measured crystallization rate as a function of molecular weight and rotational speed. For low molecular weight polyethylene (M_w = 9200) fibrous crystals were not formed at any rotational speed. A transition from lamellar to fibrous crystals was noted at a critical speed for high molecular weight polyethylene (M_w = 720,000). Above this critical value, the crystallization rate was found to increase with increased rotational speed. Although elongational flow was deemed necessary for fibrous crystal formation, Pennings et al.[44] examined the effect of simple shear flow on the acceleration of the crystal growth rate in solution. A seed crystal was steadily withdrawn from a sheared solution at a speed equal to its longitudinal growth rate. The growth of the material formed in this manner was 16 times faster than that measured in quiescent spherulitic growth systems at the same temperature.

Mackley[45], with a theoretical treatment describing conditions similar to those in Pennings' experiments, calculated the flow field around an ellipsoid simulating a growing fibrous crystal. The viscosity of the flowing solution was assumed to be 1 poise producing a Reynolds number, based on the length of the long axis of the ellipse, of 20. The

longitudinal and transverse velocity gradients in the region near the ellipse were large and theoretically calculated to be sufficient to elongate molecules of moderate length. A mechanism of growth was hypothesized in which molecules extended by the longitudinal gradient at the tip of the fiber will attach and grow, increasing the fiber length. Molecules attaching at the side of the fiber will not be completely reeled in due to the rapidly decreasing velocity gradient moving out from the fiber. The dangling chain end will attempt to adopt a random coil conformation and subsequently crystallizes in a folded chain morphology explaining why platelets appear to be attached to the central core.

Seyer and Hlavacek[46,47] present a theoretical analysis of the extension of a polymer molecule in shear and elongational flow which differs in origin from those previously discussed[21,22]. Their conclusion that elongational flow is necessary to produce extended chain shish-kebab structures is similar to those reached by previous researchers.

Torza[48] built a modified four roller apparatus from an original design by Taylor[41]. Extensional velocity gradients are developed along a streamline in the central region of the apparatus and preliminary experiments with polyethylene solutions produced the typical fibrous structures. McHugh and Schultz[49] designed their own apparatus to produce elongation flow. It consisted of an egg shaped bob which oscillated vertically in the sample chamber. Their results (DSC

and electron microscopy) indicated fibrous structures were produced and the rate of crystallization was found to increase with increasing plunging rate.

Mackley and Keller[50] extensively examined crystallization from solution in an impinging jet apparatus. The flow field was analyzed using a dispersion of drops for cases of blowing, sucking and different vertical and horizontal jet separations. Theoretical strain rates were calculated from models of the velocity profiles which best fit the experimental data. The maximum temperature at which crystallization would proceed was measured as a function of strain rate and molecular weight. As expected, increases in either molecular weight or strain rate raised the maximum crystallization temperature. Birefringence was found to increase and level off as a function of increasing strain rate. Estimates of orientation in suck jet flow were made by comparing birefringence values extrapolated to 100 percent polymer with those calculated for fully extended chains. This method led to the conclusion that chains were fully aligned by the flow. It was also noted from electron micrographs that once a crystal was nucleated (which depended on the imposed velocity gradient) lateral growth of the backbone was limited and did not depend on the imposed velocity gradient. This is good experimental justification for the theory of growth hypothesized by Mackley[45].

Melt Crystallization

Polymers are predominantly processed in the melt state and it is during these operations that orientation and initial stages of crystallization may occur. Solution crystallization experiments provide a useful approximation in which hydrodynamic interactions are minimized and morphological investigation is less complex. However, to adequately assess behavior in the melt, better simulation of actual processing conditions must be attempted.

Parallel Plate System. Haas and Maxwell[52] studied polyethylene and polybutene-1 melts crystallized in a parallel plate shearing device composed of two glass slides mounted on a microscope stage. A characteristic time associated with a certain degree of crystal formation was used as a measure of the kinetics of the process. It was found that low molecular weight samples of polyethylene crystallized more rapidly at high shear stress than the high molecular weight materials. This was attributed to increased molecular mobility of the shorter chains and lack of viscous heating effects. Polybutene-1, at low shear stresses, crystallized into resolvable spherulites which could be followed with time lapse photography. At high shear stress values, profuse nucleation resulted in a structure composed of row nuclei with lamellae growing perpendicular to the stress direction. Werata and Gogos[53] also conducted

experiments with polybutene-1 in a similar apparatus. X-ray diffraction studies showed that shear produced two distinct crystal forms (I and II) directly from the strained melt. Quiescent experiments resulted in the formation of form II only.

The experiments of Lagasse and Maxwell[54] were also done in a glass parallel plate apparatus. The time scale of the crystallization process was characterized by an induction time defined as the time from the start of the shearing to the rise in melt viscosity. The lowest molecular weight polyethylene studied (M_w = 189,000) showed a critical value of shear rate below which the induction time was constant. Higher molecular weight samples showed decreasing induction times with increasing shear rate and decreasing temperature over the entire shear rate range studied.

Two other experiments were conducted to investigate the nucleation process. Pure polypropylene and samples containing dispersed carbon black were crystallized quiescently and under stress. Inclusion of the carbon black was found to have no effect on the kinetics of crystallization. In a similar experiment, nucleating agents were dispersed in ethylene-propylene rubber samples. Induction times for the material containing the nucleating agents were relatively constant and lower with increasing shear rate than those for the pure polymer up to a certain value of shear rate. Above this critical value, the induction times for

nucleating agent material decreased and were equal to those for the pure polymer. The authors concluded that enhanced crystallization under shear cannot be attributed to effects caused by heterogeneities, but must be due to molecular extension arising from chain entanglements.

Williamson and Busse[55] have formulated a theory to explain enhanced nucleation and molecular extension. It is based on the experimental observation of Keith et al.[56] that intercrystalline links exist between lamellae in sheared samples, their density being inversely proportional to the distance between the lamellae. According to the theory, these links are formed when two entangled chains are reeled into different lamellae. The force exerted on the entangled ends produces crystallization in an extended configuration. It is postulated that an analagous process occurs in the supercooled melt between dangling ends in clusters rotating and translating in "elastic turbulent flow". The extended chain segments serve as nuclei for fiber formation which includes the crystalization of clusters to form a continuous filament.

Extrusion and Molding. Orientation during capillary and channel flow has been examined by many authors due to its industrial significance. Van der Vegt and Smit[57] extended a wide variety of polymers near their melting points in a capillary rheometer. It was found that at a critical shear rate, which increased with extrusion

temperature, solidification occurred. The conclusion that crystallization was due to orientation during flow was confirmed by X-ray diffraction. Sieglaff and O'Leary[58] noted similar behavior and found that orientation was greater at lower processing temperatures. Folt[59] discovered that increased L/D capillary ratio, increased molecular weight and lower temperature all caused more rapid crystallization.

Southern and Porter[60] and Griswold and Cucolo[61] produced transparent crystalline strands of polyethylene and polyethylene terephthalate respectively, using a combination of critical pressure and shear rate. These crystals contained highly oriented chains which were thought to form in elongational flow gradients at the capillary entrance. Collier et al.[62] were able to continuously produce transparent filaments of polyethylene and polypropylene during extrusion without significant pressure by imposing an axial temperature gradient in the die. Orientation produced in this manner was very high throughout the fiber.

Clark[63] analyzed the morphology of polyoxymethylene produced during injection molding. Crystal structure was dependent on distance from the channel wall. The region closest to the wall was characterized by lamellae oriented perpendicular to the direction of flow and the surface. The middle region contained lamellae perpendicular to the surface with no preferred orientation in the flow direction. The core material was composed of spherulites. Increasing

pressure drop or radial temperature gradient increased the thickness of the oriented layer.

Melt Spinning. Crystallization in the melt spinning process occurs with molecular orientation and usually under non-isothermal conditions. Mathematical description of the process is very complex and contains many approximations[64,65]. Discussion will consequently be limited to qualitative observations which may prove useful in the interpretation of the results of the present study.

Ziabicki and Kedzierska[66] examined the melt spinning process of polycapronamide using X-ray diffraction and birefringence. It was concluded that the measured orientation was a function of elongational velocity gradient, spinline tension, and the relaxation processes of the polymer chains. An apparatus which continuously measured small and wide angle X-ray diffraction, fiber diameter and temperature, and take up tension was used by Katayama et al.[68] to study crystallization during the melt spinning of polyethylene. Wide angle diffraction patterns showed a decrease in c axis orientation with distance from the die. This was attributed to a tilting of the c axis within the lamellae. Similar experiments by Dees and Spruiell[67] interpreted these results to indicate a row nucleation mechanism where the outer skin material forms stacked lamellae with perfect c axis orientation. As the skin crystallizes, it bears more of the stress leaving the interior of the fiber,

subjected to reduced stress, to crystallize in twisted ribbons. The transition from spherulitic (as seen in gravitationally spun fibers) to twisted ribbon morphology was postulated to occur at very low levels of spinline stress. Other authors studying different polymers[69,70] have reached conclusions similar to those of Dees and Spruiell.

Melt Extensional Flow. The impinging jet apparatus was used by Mackley and Keller[71] to study polyethylene melts as well as dilute solutions. It was found in the suck jet mode that crystals produced at the outer end of the jet consisted of two different morphologies. The first was composed of extended chains elongated by the longitudinal velocity gradient. The other fraction was mainly folded chain material which was thought to be dragged along by the fiber lubricating the flow process and eventually crystallizing under a low stress condition. In a second experiment, fine wire gauze was placed in the reservoir away from the entrance to the jet. The fibers at the jet outlet were found to contain a higher extended chain content caused by elongational flow regions created around the wire gauze.

Manley et al.[72] used a modified jet apparatus, which consisted of a single jet attached to a rheometer barrell, to study crystal growth in a flow field. It was found that stable growing fibers protruded from the jet into the reservoir at a certain temperature and mean velocity into the jet.

Changing the flow rate or temperature destroyed the dynamic equilibrium and resulted in either blockage or lack of crystallization. Morphological examination of these crystals indicated that they were continuously produced in the orifice region. The velocity profiles near the orifice were analyzed and a critical local strain rate necessary for nucleation and continuous growth was calculated.

Simple Shear Flow. In much of the previous discussion it has been implied that longitudinal velocity gradients are necessary to produce significant orientation and alter crystalline morphology and transformation kinetics. This may be true for solutions but several experiments conducted with melts in laminar shear flows indicate that this is not the case.

Tan and Gogos[73] produced transparent polyethylene films in a biconical rheometer at shear rates below 10 sec^{-1}. These films exhibited two melting peaks when analyzed using DSC. The high melting temperature was similar to those reported by Southern and Porter[60] for ultra oriented crystals. Kawai and coworkers[74] observed accelerated crystallization for polyethylene samples in a cone and plate rheometer at shear rates in the range of 0.5 sec^{-1} to 2.5 sec^{-1}. Electron micrographs of this material indicated regions of stacked lamellae growing perpendicular to the shear direction. X-ray diffraction patterns showed substantial c axis orientation which increased with shear rate.

Kobayashi and Nagasawa[75] crystallized high (M_w = 50,000) and low (M_w = 2,700) molecular weight linear polyethylene in a concentric cylinder viscometer over a wide range of shear rates (2.7 sec^{-1} to 5500 sec^{-1}). Quantitative kinetic interpretations were impossible due to non isothermal conditions but an important qualitative result of this work was that crystallization was accelerated under shear even for the low molecular weight material which was substantially below the critical entanglement value.

Manrique and Porter[76] and Krueger and Yeh[77] sheared linear polyethylene in concentric cylinders under isothermal conditions. Manrique found the crystalline material to exhibit some orientation, but at a level below that of the transparent morphologies produced in extrusion. In contrast, Krueger and Yeh were able to produce transparent material. The different results may be attributed to the lower crystallization temperature and shear rates used by Krueger and Yeh. In their experiments it was found that there existed a unique induction strain, defined as the product of shear rate and induction time, for the initiation of crystallization. This strain was dependent on temperature but independent of the imposed shear rate. The authors concluded from this that shear rates approaching 0 sec^{-1} were capable of producing oriented crystalline morphologies.

In kinetic experiments similar to those conducted in this study, Fritzsche et al.[78,79] found that shear

drastically reduced induction times and accelerated the transformation process. Over the shear rate range studied (30 sec^{-1} to 150 sec^{-1}) little difference was noted between induction times at different shear rates for the same crystallization temperature. Avrami kinetics were used to analyze the data and the exponent was found to have values as high as 9. No general trend was noted, but the largest exponent values appeared to occur at the highest crystallization temperatures. Addition of a small amount of high molecular weight material (five percent) greatly reduced the induction time, but the observed Avrami exponent value for the mixture was smaller. This indicated that nucleation occurred more rapidly but the overall transformation was slower.

CHAPTER II

INSTRUMENTATION

The initial problem encountered in this research was to construct an apparatus capable of measuring small volume changes during crystallization under well defined temperature and shear rate conditions. Previous research by Fritzsche[84] produced the basic instrument which was modified for use in these experiments. Figure 1 is a photograph of the modified shearing dilatometer.

The instrument is a concentric cylinder viscometer which also functions as a dilatometer. A schematic drawing of the concentric cylinder section of the apparatus is shown in Figure 2. The inner cylinder has a radius of 1.187 inches (3.016 cm) and is 6.625 inches (16.83 cm) long. The gap between the two cylinders is .047 inches (.119 cm). The resulting annular volume is 2.362 in^3 (38.70 cm^3) which corresponds to approximately 40 grams of molten polymer in a typical charge.

The region below the annulus is filled with mercury. This mercury is connected via a sidearm to a glass capillary tube with a constant diameter of 5 mm. The height of the mercury in the sight tube is measured using a cathetometer. The height difference observed for 10% crystallinity is between 3 and 4 cm.

FIGURE 1 Photograph of Shearing Dilatometer including instrument panel, main bath and shearing assembly.

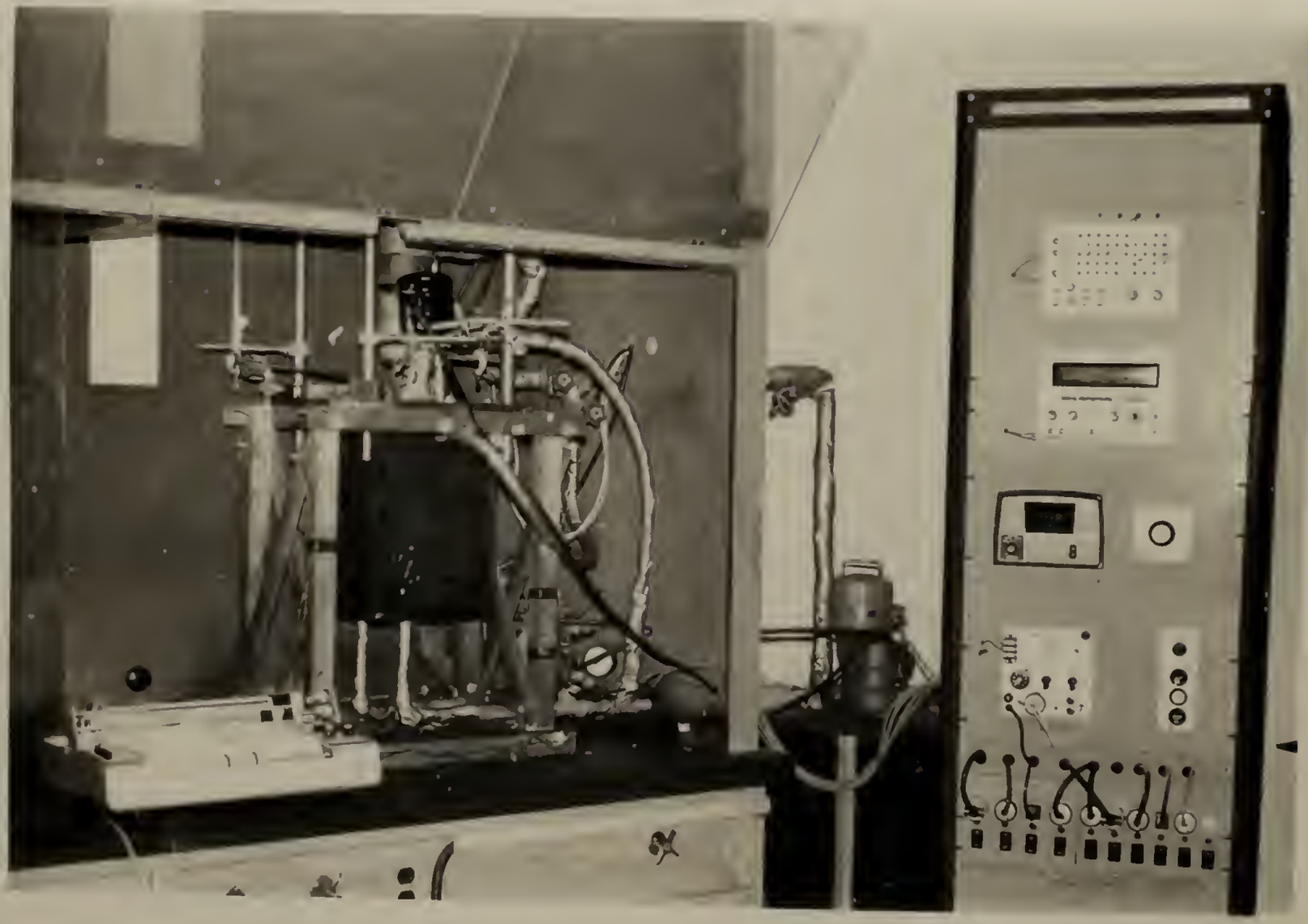

FIGURE 2 Schematic diagram of concentric cylinders.

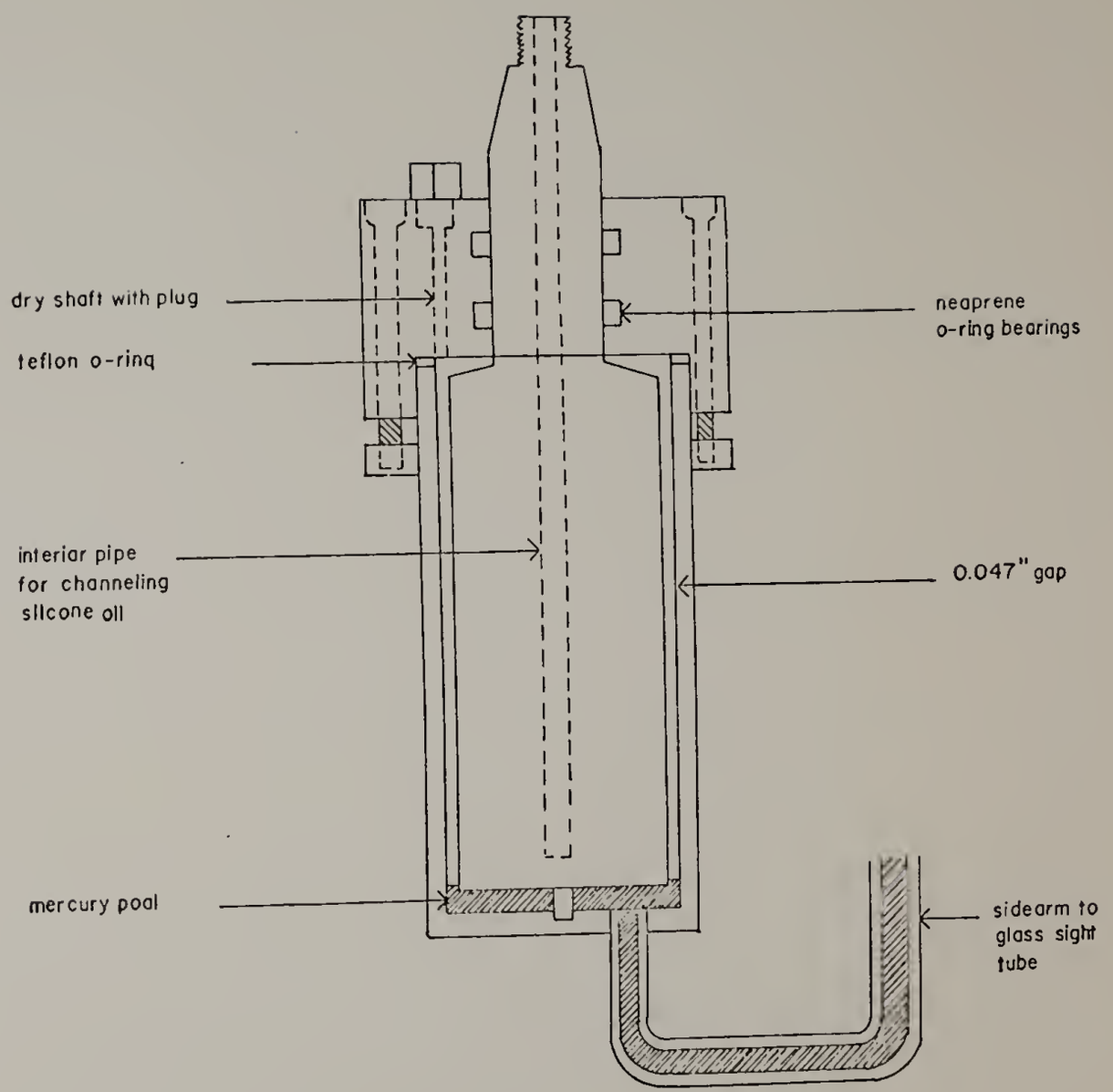
dry shaft with plug
teflon o-ring
interior pipe
for channeling
silicone oil
mercury pool
neaprene
o-ring bearings
0.047" gap
sidearm to
glass sight
tube

The driveshaft and cylinders are constructed of type 304 stainless steel. This material was chosen despite the fact that it has a low thermal conductivity compared to copper or carbon steel because it is relatively inert to solvents and moisture. The head, which supports the outer cylinder as shown in Figure 3, is constructed of brass. A soft material was chosen for this part to minimize the possibility of binding of rotating parts in close proximity.

The system is sealed by two sets of gaskets. A teflon O-ring provides the seal between the outer cylinder and the brass head. Two neoprene rubber gaskets are used to seal the area between the rotating inner shaft and the brass head.

Drive Train

As crystallization proceeds, a large increase in the viscosity of the sample can be observed. It was therefore necessary to select a motor which could maintain a constant speed with different torque outputs. The unit selected was a Boston Gear model V9500 3/4 horsepower D.C. shunt motor with Boston Ratiotrol E75 variable speed selection control. The maximum speed of the motor is 1750 rpm. Two reductors, Boston Gear models F315D and F324D, were employed separately and in series to reduce the speed of the drive shaft. Model F315D reduces the speed by a factor of 10 whereas Model F324D produces a reduction of

FIGURE 3 Schematic diagram of head and drive shaft section showing internal heating system.

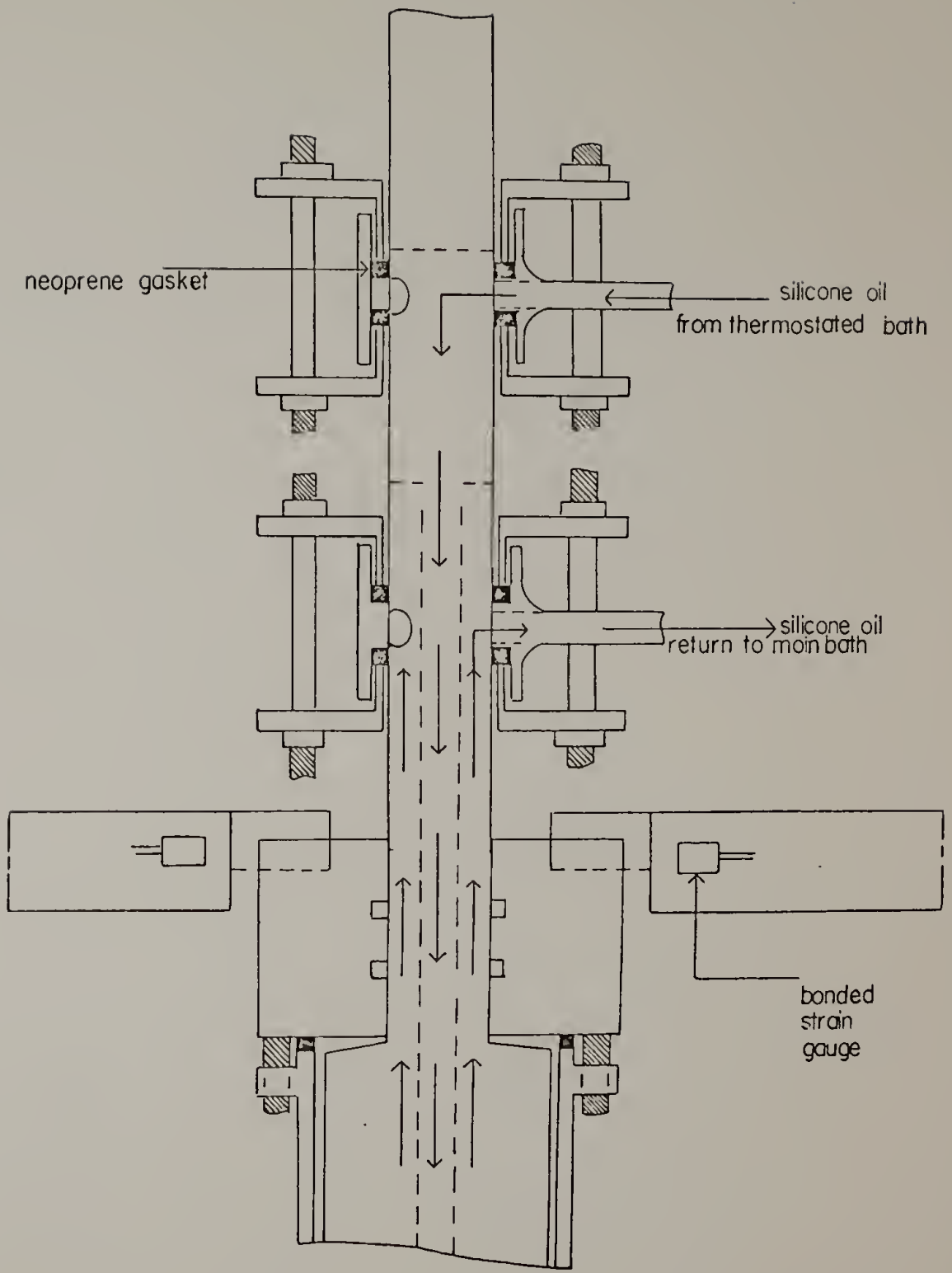
neoprene gasket
silicone oil
from thermostated bath
silicone oil
return to main bath
bonded
strain
gauge

40:1. With these reductors, the practical speed range of the instrument is from .5 rpm to 175 rpm. This corresponds to a shear rate range of 1.5 sec^{-1} to 525 sec^{-1}.

Temperature Control

In order to properly measure crystallization kinetics, the temperature of the crystallizing system must be controlled very accurately. Temperature regulation in the shearing dilatometer is accomplished using two stirred baths with silicone oil as the thermostating fluid. The main bath has a 15 gallon capacity and can be controlled to ±0.2°C using a Versatherm model 2156 proportional temperature controller with a 500 watt immersion heater. Cold water circulating through a cooling coil in the bath is used to removed heat produced by the stirrer and pump. At maximum flow rate the coil is able to cool the bath from 85°C to 55°C in twenty minutes. Two additional 500 watt heaters are used to rapidly raise the temperature of the main bath.

The second stirred bath has a capacity of two gallons and surrounds the concentric cylinders. Thermostating fluid is passed through this bath at a maximum flow rate of one gallon per minute. A 250 watt heater is installed in this bath to separately heat this resevoir.

Silicone oil is also circulated through the interior of the drive shaft and inner cylinder. This is accomplished

using two glands which fit over holes drilled in the drive shaft. Fluid enters the top gland, flows down through an interior pipe to the bottom of the inner cylinder and then out through the second gland as shown in Figure 3. With this system it is possible to maintain both surfaces of the polymer sample at the same temperature.

To monitor temperature, copper constantan thermocouples are used in conjunction with a twelve channel switching unit and a Digitec model 590 TC thermocouple thermometer. The temperature of both baths as well as the inlet and outlet streams to the inner cylinder are monitored. The temperature of the polymer sample is measured using a thermocouple inserted .016 inches from the contact surface of the polymer and outer cylinder. No reliable and functional way was found to monitor the temperature of the polymer at the inner cylinder interface.

Strain Gauges

The dilatometer was also equipped with a strain gauge network mounted on the support arms as shown in Figure 3. Two of the support bars were machined to a thickness of .063 inches to increase elastic deformation, while the remaining two bars were made .13 inches thick. One active gauge was bonded to each thin arm using a high temperature epoxy resin. In an attempt to compensate for

temperature fluctuations, a non-bonded gauge was inserted under the insulation of each thin bar. The gauges were connected to a BLH model 1225 switching and balancing unit in a four element bridge configuration. The output of this unit was read on the display of a BLH model 1200 digital strain indicator in microinches/inch of strain. To smooth out fluctuations in the strain readings, a recorder was used to read the voltage output from the strain gauge bridge.

C H A P T E R III

EXPERIMENTAL

Materials

The materials used in these experiments were obtained from Union Carbide Corporation. Two of the samples were polyethylene oxides with trade names Carbowax 6000 and WSR-N10. The other material was a low molecular weight poly-ε-caprolactone designated PCL-150.

Polyethylene oxide (PEO) is a highly crystalline material, exhibiting degrees of crystallinity greater than 50 percent. The polymer chain in the crystalline solid is twisted into a 7_2 helix along the C direction with 28 (C_2H_4O) units in the monoclinic unit cell[85]. It was chosen as a material for these studies for several reasons. It is soluble in water and has a low melting temperature which was found to be 63.6°C for PEO 6000 and 64.0°C for WSR-N10. Solubility in water is very helpful during sample changing operations. Working at low temperatures is desirable to reduce insulation problems and minimize production of highly toxic mercury vapors. In addition, a substantial amount of work has been done with PEO by this research group and others, and its crystallization behavior in dilute solution and bulk is well documented[86,87].

Polycaprolactone (PCL) also exhibits degrees of crystallinity greater than 50 percent. The crystalline polymer chains for this material are twisted in a 2_1 helix with 4 monomer units per orthorhombic unit cell[88]. The melting temperature in these experiments was found to be 54.0°C. PCL is soluble in several common aromatic solvents including toluene and benzene. In the past five years, much interest has been generated in the area of polymer blends and several authors have blended PCL with polyvinyl chloride (PVC) to produce compatible mixtures[89]. Crystallization kinetics of the PVC/PCL blends have been examined under quiescent conditions[90] and the study of PCL crystallization under shear could form a solid foundation for future shear crystallization experiments with the polymer blends.

The intrinsic viscosity of each polymer was determined initially and after several shear experiments to ascertain if degradation had occurred. The solution viscosities of the PEO samples were measured in water at 30°C with a Cannon-Ubbelohde viscometer. The PCL experiments were done in benzene at 30°C. The weight average molecular weights of PEO and PCL were calculated using the relationships given in equations 14[91] and 15[92] respectively. The number average molecular

$$[n]_{PEO} = 1.25 \times 10^{-2} \quad M_w^{0.78} \qquad (14)$$

$$[n]_{PCL} = 9.94 \times 10^{-5} \quad M_w^{0.82} \qquad (15)$$

weight of the PEO WSR-N10 samples was also measured using a membrane osmometer. The results of the molecular weight determinations are given in Table 1.

The data indicate that no significant degradation has occurred for PEO 6000. The WSR and PCL samples seem to have degraded slightly but this change did not alter the reproducibility of the crystallization kinetic data which will be discussed in a subsequent section.

Rheological Behavior and Viscous Heating

It is well known that subjecting polymeric materials to shear flows can cause heat generation through viscous dissipation. This dissipation can cause a substantial temperature profile in the sample and greatly increase the average temperature of the material. Several authors have published detailed solutions of the temperature profile in rotational Couette flow[93,94]. For the purpose of this work an approximate estimate of the temperature profile is adequate to determine the magnitude of viscous heating during crystallization. A detailed description of the analysis used to determine the temperature profile is given in Appendix I.

To calculate values of the maximum temperature rise in the sample, ΔT_{max}, it was necessary to measure the

TABLE 1

MOLECULAR WEIGHT DATA FOR EXPERIMENTAL MATERIALS

	[n] ml/g	M_w	M_n
PEO 600 unsheared	19.72	12,600	
PEO 6000 sheared	19.85	12,700	
WSR-N10 unsheared	77.00	72,150	27,000
WSR-N10 sheared	72.50	66,800	26,800
PCL-150 unsheared	18.02	9440	
PCL-150 sheared	16.60	8520	

viscosity of the materials at the different crystallization temperatures and shear rates. This was done in a Rheometrics mechanical spectrometer using a cone and plate geometry. The viscometric data are shown in Figures 4, 5, 6, and 7. PCL and PEO 6000 are Newtonian throughout the range of shear rates used in the crystallization experiments. The WSR sample exhibits non-Newtonian behavior at shear rates greater than 0.1 sec^{-1}. This non-Newtonian behavior is accounted for in the temperature analysis by substitution of the measured apparent viscosity at each shear rate.

The values for ΔT_{max} for the three materials are given in Tables 2, 3 and 4. The temperature profile for WSR sheared at 58.8°C, the lowest crystallization temperature, for isothermal and adiabatic inner walls is given in Figure 8 and 9 respectively. The actual temperature profile in the viscometer is likely to be in between that of the adiabatic and isothermal cases since the inner wall is in contact with the thermostating fluid but is probably not maintained at the exact crystallization temperature. Also, the profiles calculated are overestimates due to the assumption used that viscosity is independent of temperature. An increase in temperature would decrease the viscosity, subsequently decreasing the dissipation. In any event, the temperature rise for PEO 6000 and PCL is insignificant, but that exhibited in the WSR samples is

FIGURE 4 Viscosity versus shear rate for PEO 6000 and PCL at the temperatures used in the crystallization experiments.

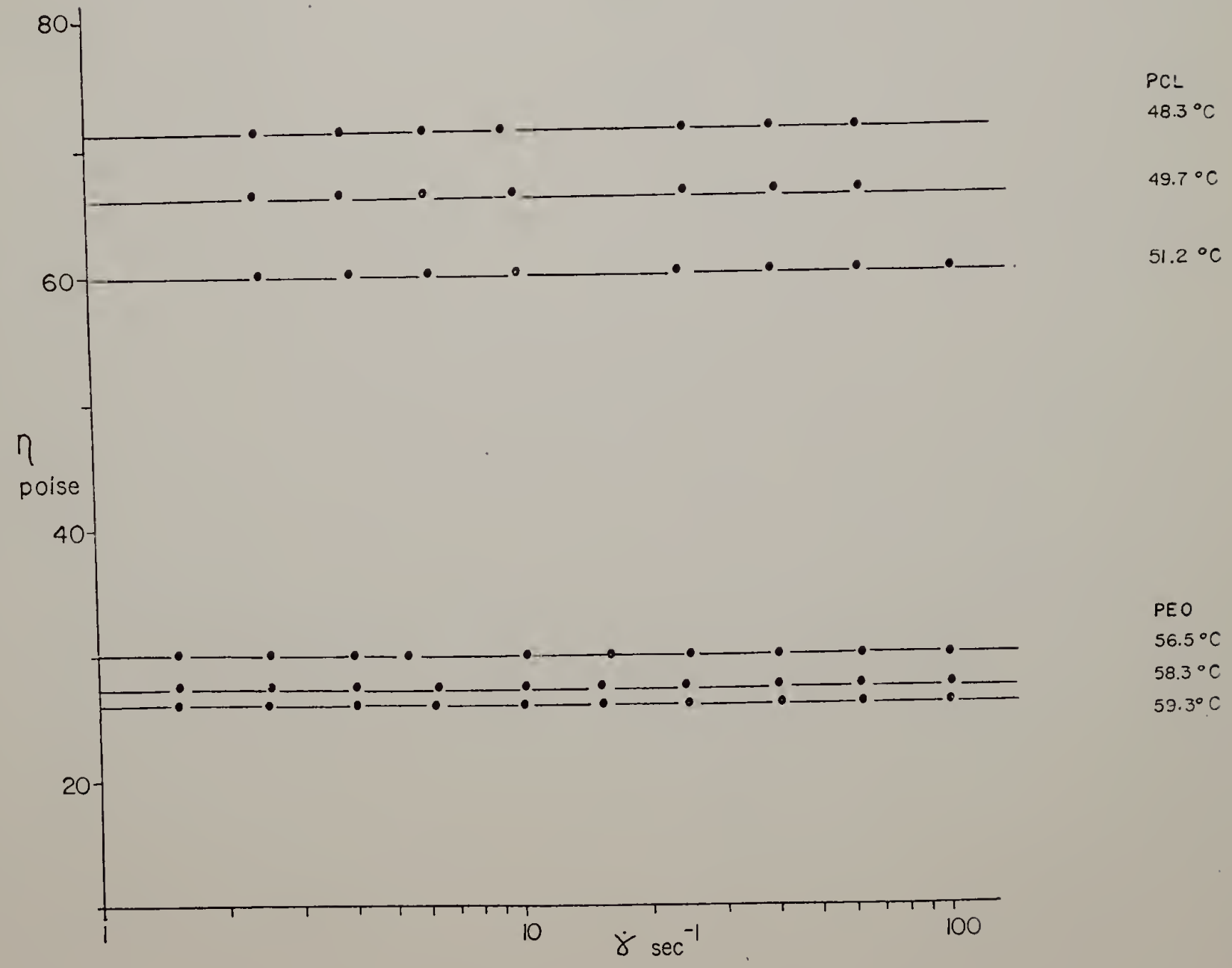
80
60
40
20
η
poise
1
10
100
γ̇ sec⁻¹
PCL
48.3 °C
49.7 °C
51.2 °C
PEO
56.5 °C
58.3 °C
59.3° C

FIGURE 5 Viscosity versus shear rate for PEO WSR-N10 at the temperatures used in the crystallization experiments.

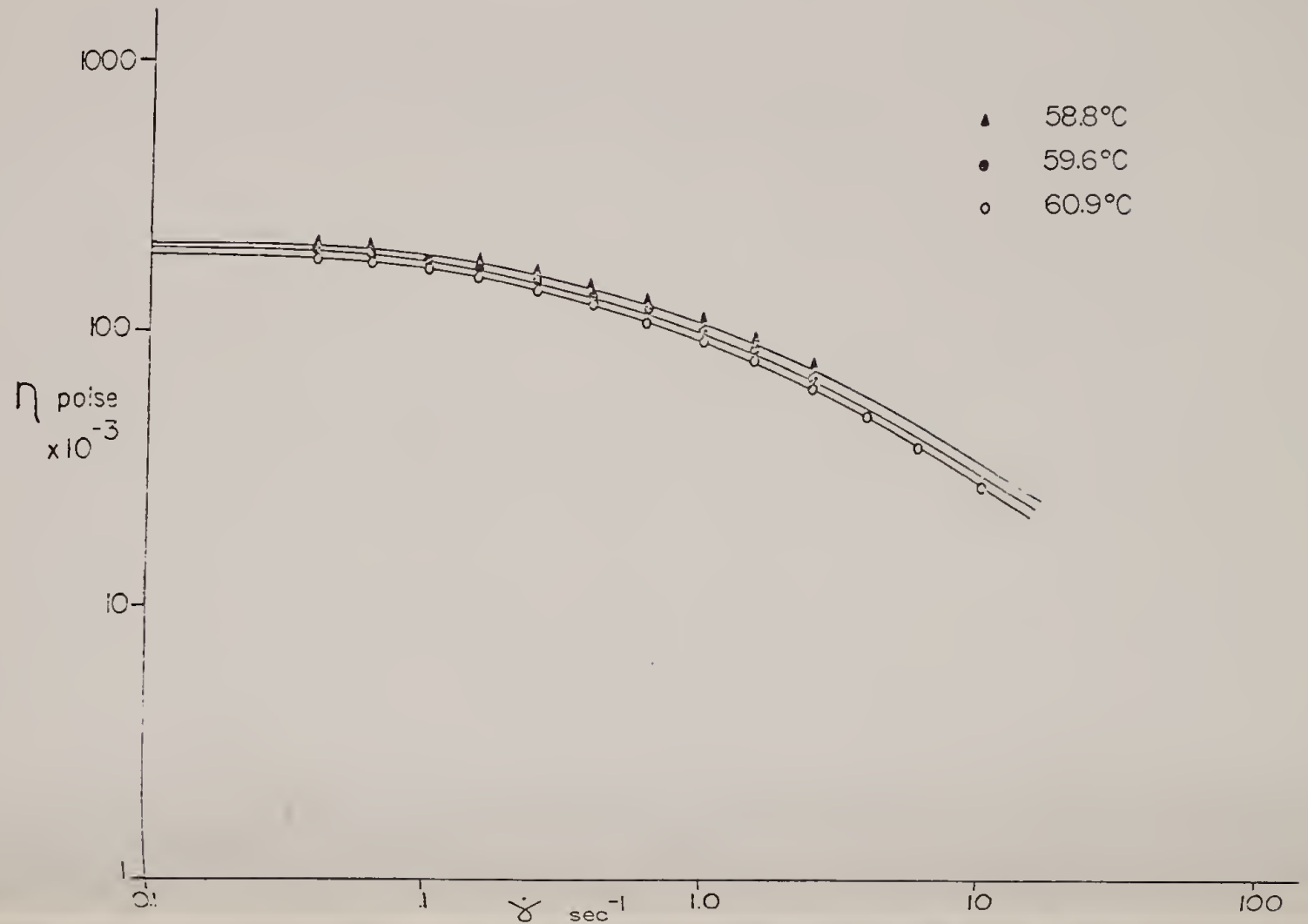
1000
100
10
1
η poise
x10^-3
58.8°C
59.6°C
60.9°C
0.1
.1
1.0
10
100
γ̇ sec^-1

FIGURE 6 Shear stress versus shear rate for PEO 6000 and PCL at the temperatures used in the crystallization experiments.

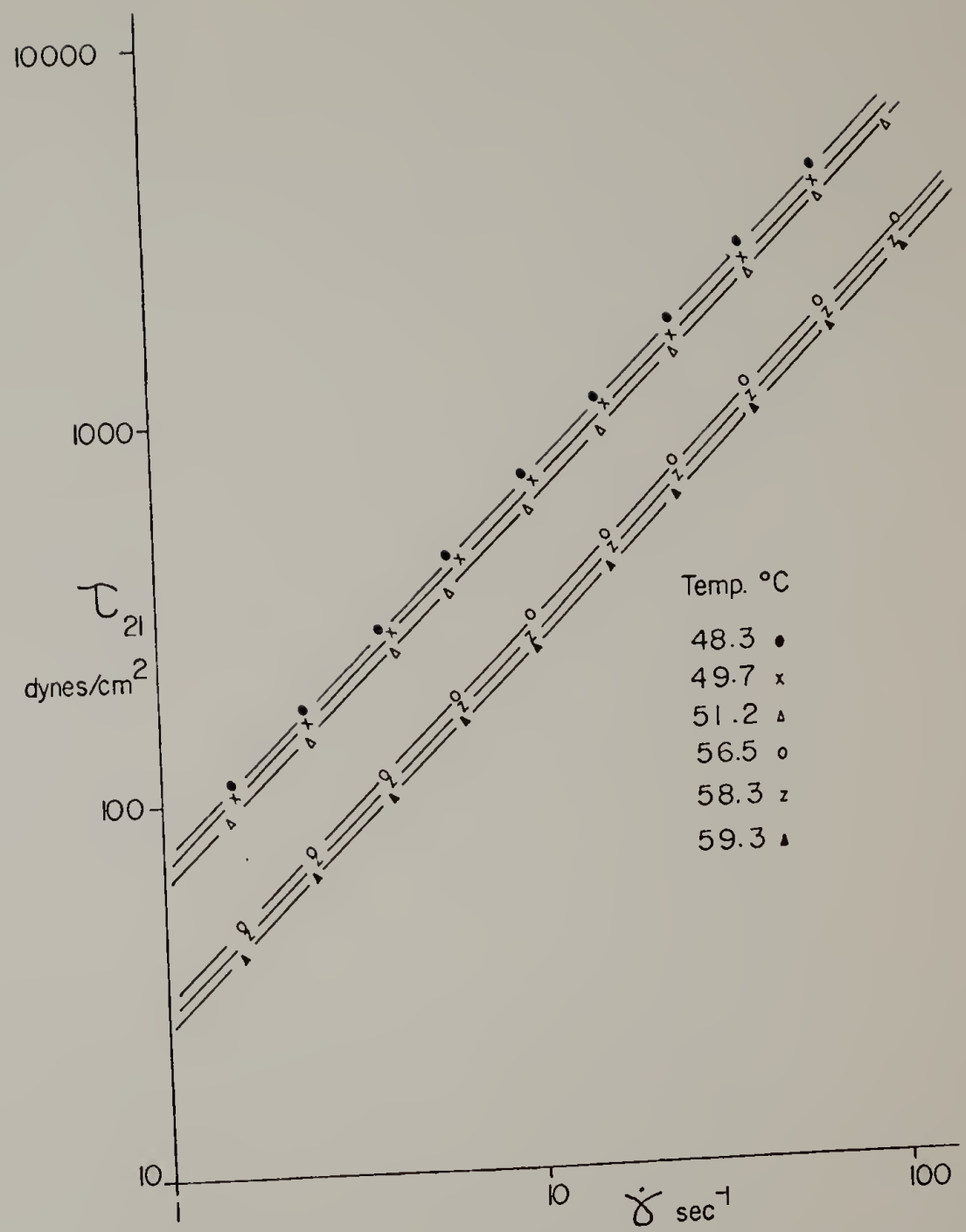
10000
1000
100
10
τ_{21}
dynes/cm^2
1
10
100
$\dot{\gamma}$ sec^{-1}
Temp. °C
48.3 •
49.7 x
51.2 Δ
56.5 o
58.3 z
59.3 ▲

FIGURE 7 Shear stress versus shear rate for PEO WSR-N10 at the temperatures used in the crystallization experiments.

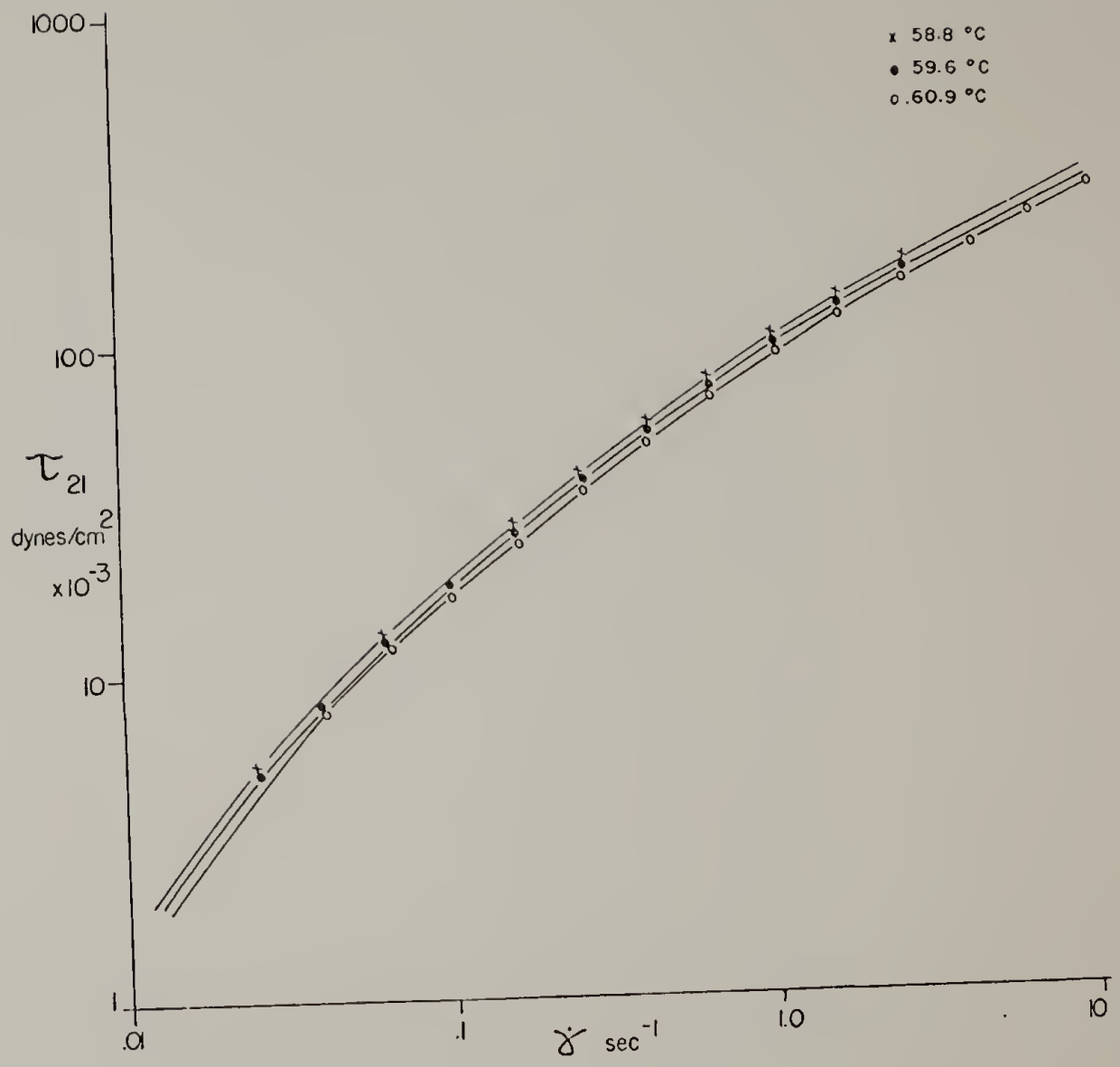
1000
100
10
1
τ_{21}
dynes/cm^2
x10^{-3}
x 58.8 °C
• 59.6 °C
o 60.9 °C
.01
.1
1.0
10
$\dot{\gamma}$ sec^{-1}

TABLE 2

VISCOUS HEATING IN PEO 6000

Temperature °C	Shear rate sec^{-1}	ΔT_{max} adiabatic inner wall	ΔT_{max} isothermal inner wall
59.3	1.6	0	0
	6.3	0	0
	15.8	0	0
	25.0	.01	0
	40.0	.01	0
	62.5	.03	.01
	99.9	.08	.02
58.3	1.6	0	0
	6.3	0	0
	15.8	0	0
	25.0	.01	0
	40.0	.01	0
	62.5	.03	.01
	99.9	.09	.02
56.6	1.6	0	0
	6.3	0	0
	15.8	0	0
	25.0	.01	0
	40.0	.02	0
	62.5	.04	.01
	99.9	.10	.02

TABLE 3

VISCOUS HEATING IN PCL-150

Temperature °C	Shear Rate sec^{-1}	ΔT_{max} adiabatic inner wall	ΔT_{max} isothermal inner wall
51.2	1.6	0	0
	6.3	0	0
	15.8	0	0
	25.0	.01	0
	40.0	.03	.01
	62.5	.07	.02
	99.9	.19	.05
49.7	1.6	0	0
	6.3	0	0
	15.8	0	0
	25.0	.01	0
	40.0	.03	.01
	62.5	.08	.02
48.3	1.6	0	0
	6.3	0	0
	15.8	.01	0
	25.0	.01	0
	40.0	.04	.01
	62.5	.09	.02

TABLE 4

VISCOUS HEATING IN WSR-N10

Temperature °C	Shear rate sec^{-1}	ΔT_{max} adiabatic inner wall	ΔT_{max} isothermal inner wall
60.9	.63	.01	0
	1.58	.07	.02
	2.5	.13	.03
	4.0	.26	.07
	6.3	.52	.13
	10.0	.99	.25
	20.0	2.59	.65
	30.0	4.56	1.14
59.6	.63	.02	0
	1.0	.07	.01
	4.0	.28	.07
	6.3	.55	.14
	10.0	1.11	.28
	20.0	2.75	.69
	30.0	4.94	1.24
58.8	.63	.01	0
	1.58	.06	0
	5.0	.42	.02
	10.0	1.13	.28
	15.0	1.99	.50
	25.0	4.06	1.02
	35.0	6.41	1.61

FIGURE 8 Isothermal temperature profile for WSR-N10 at 58.8°C and different shear rates.

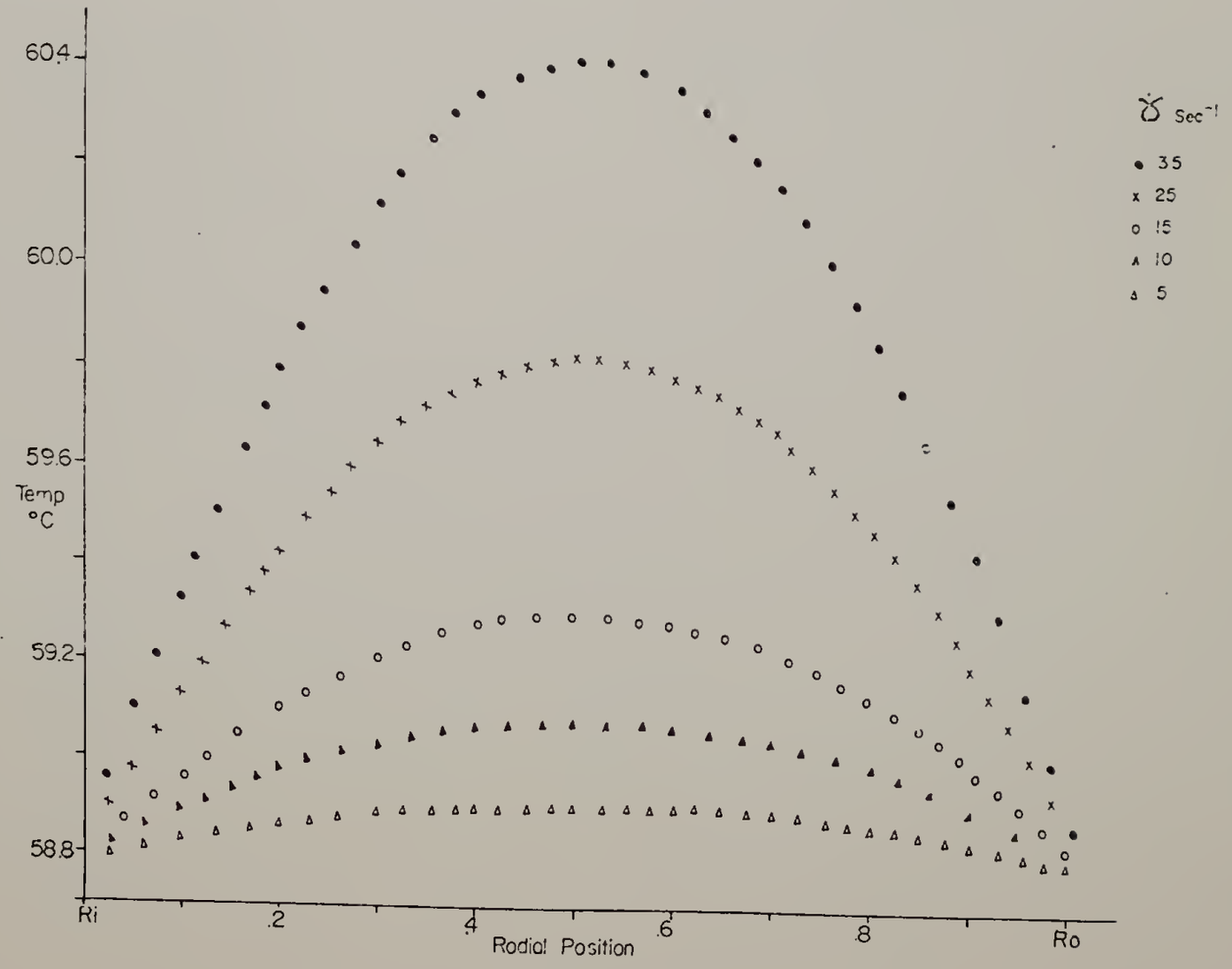
60.4
60.0
59.6
59.2
58.8
Temp °C
Ri
.2
.4
.6
.8
Ro
Radial Position
$\dot{\delta}$ Sec^{-1}
35
25
15
10
5

FIGURE 9 Adiabitic temperature profile for WSR-N10 at 58.8°C and different shear rates.

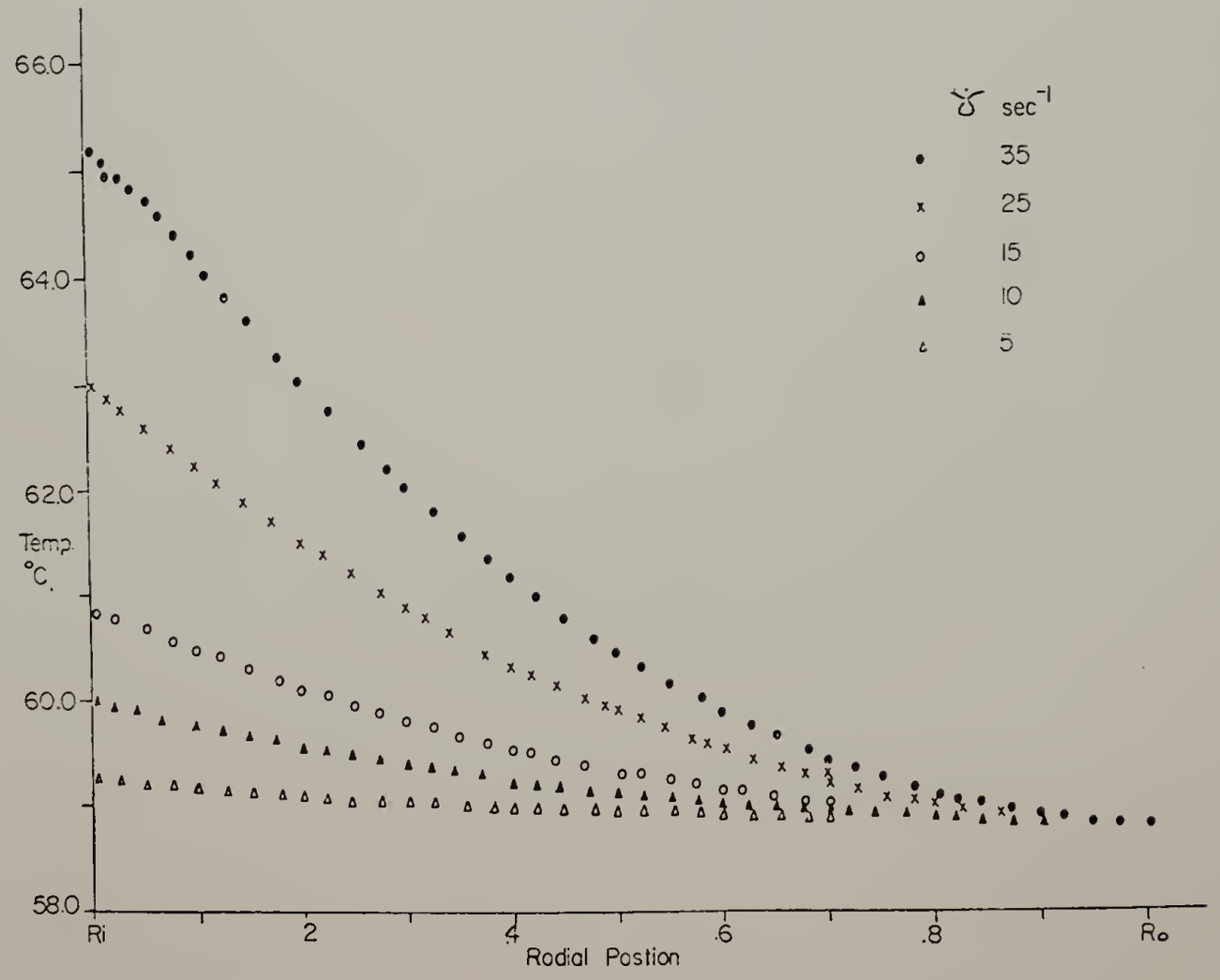
66.0
64.0
62.0
60.0
58.0
Temp. °C.
Ri
2
.4
.6
.8
Ro
Radial Postion
$\dot{\gamma}$ sec^{-1}
35
25
15
10
5

substantial and must be taken into account in the discussion of crystallization kinetics for this material.

Sample Preparation

Each polymer sample is heated to 25°C above its melting point under vacuum for 24 hours prior to introduction into the instrument. This period is necessary to remove the air bubbles produced when a fine powder of a high molecular weight polymer is melted. The shearing dilatometer is also heated to the same temperature to insure the absence of crystallization during the loading of the sample. Sufficient mercury is put in the bottom of the outer cylinder to cover the sidearm connection, the sample is put in, and the outer cylinder is raised and tightened to the brass head.

The glass sight tube is installed next making sure that the joint is sealed with high vacuum grease. Before mercury is introduced to force the sample into the annular area, a vacuum is pulled through the dry seal to remove the air in the cavity. Removal of air bubbles is critical because they can cause great fluctuations in mercury height due to the high coefficient of thermal expansion and large compressibility of air compared to the polymer sample. Mercury is introduced slowly over a five hour period forcing the polymer to flow up into the annulus. Rapid introduction of mercury with a highly viscous sample causes a

break in the flowing material resulting in mercury being trapped on top of the polymer. This is to be avoided because polymer not in the annular area is subjected to negligible shear rates which can complicate the analysis of the kinetic data.

The cavity is completely filled when polymer begins to flow into the dry seal. At this point the plug is introduced and the sample installation is complete. Preparation of the apparatus is finished with the assembly of the small bath resevoir and insulation of strain gauge and thermocouple junctions.

Run Procedure

Experiments for both quiescent and shear cases were conducted in an identical manner. Fluid at 25°C above the polymer melting point was circulated through the concentric cylinders and small bath for one hour. The pump was then shut off and the apparatus was allowed to cool. During this period of approximately 25 minutes, the main bath was cooled to the crystallization temperature. When the polymer temperature reached 5°C above the melting point, circulation of silicone oil at the crystallization temperature was begun. The motor was also turned on and the timer was activated at this point. For all conditions studied the cooling time to the crystallization temperature, as detected

by the thermocouple at the polymer-outer cylinder interface, was on the order of 15 minutes.

Measurements of mercury height, strain gauge output and temperature at various points in the apparatus were taken continuously, the frequency of measurements depending on the time scale of the transformation process. A plot of heightversus time for PEO 6000 crystallized at 56.6°C and different shear rates is shown in Figure 10. The rotational speed versus motor potentiometer setting was originally calibrated using a strobe light, but speed of rotation was checked for each run using a stopwatch. Data collection was terminated after the polymer crystallization had exceeded 15 percent.

One way to assure that the polymer sample was at the same crystallization temperature from run to run was to measure the mercury height prior to crystallization. It was found that for identical thermocouple temperatures identical heights were observed for samples with no viscous heating regardless of shear rate.

A calibration curve for each charge was obtained by heating the polymer sample from 10°C below to 10°C above its melting point in 1°C intervals. The polymer was allowed to come to equilibrium for a minimum of one hour and a maximum of eight hours (during melting) after which time the mercury height and temperature were recorded. A plot of height versus temperature was constructed showing

FIGURE 10 Height versus time for PEO 6000 at 56.6°C and different shear rates.

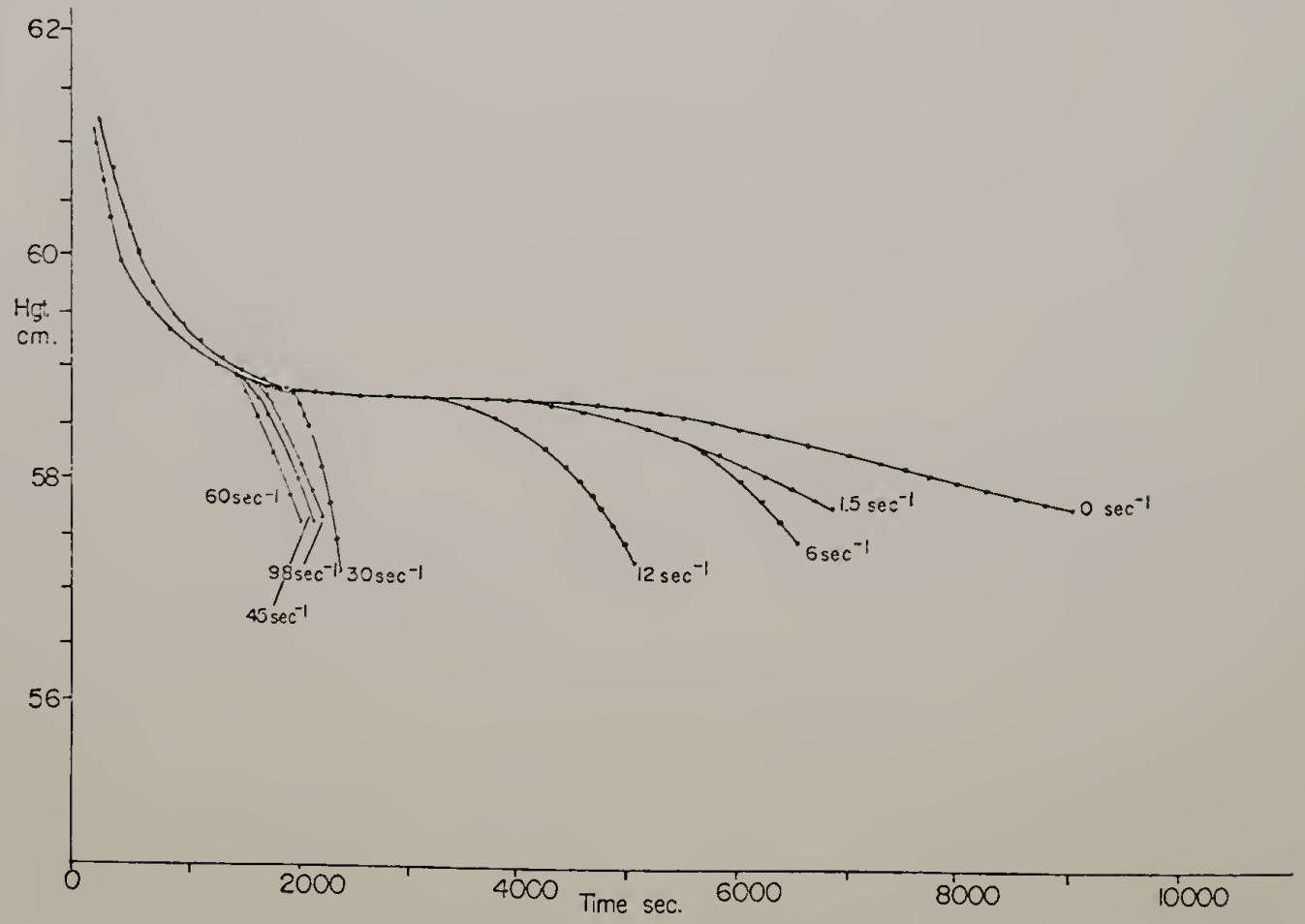
62
60
58
56
Hgt.
cm.
60sec⁻¹
98sec⁻¹
30sec⁻¹
45sec⁻¹
12 sec⁻¹
6sec⁻¹
1.5 sec⁻¹
0 sec⁻¹
0
2000
4000
6000
8000
10000
Time sec.

the typical sigmoidal shape for polydisperse macromolecules. The calibration procedure was performed after sample introduction prior to experiments and again before the sample was removed. In all cases the calibration was the same proving that there were no leaks in the system.

Data Analysis

The measured mercury height, H_t, at a given time, t, was converted into a degree of crystallinity, X_c, using equation 16.

$$X_c = \frac{H_a - H_t}{H_a - H_c} \tag{16}$$

In the equation, H_a is the height of mercury at the crystallization temperature for the pure amorphous material. This value was obtained by extrapolation of the liquidus line in the calibration curve to the proper temperature. H_c represents the mercury height for the totally crystalline material and was read directly from the calibration curve.

The value of X_c was then used in the Avrami equation given below,

$$X_c = X_\infty \left(1 - \exp\left(-\frac{k}{X_\infty}(t - t_o)^n\right)\right) \tag{17}$$

where t_o is a parameter which accounts for the time period prior to the onset of crystallization and X_∞ is a measure

of the maximum degree of crystallinity possible for the given polymer. Best fit values of n, k, and t_o in equation 17 are calculated by three methods of least squares regression explained in detail in Appendix II. The first two techniques use a linear version of the transformation equation while the third method employs a nonlinear approach.

X-ray Diffraction

The maximum degree of crystallinity, X_∞, for each sample was determined using wide angle X-ray diffraction. The instrument used was a North American Phillips wide angle diffractometer with symmetrical transmission geometry. Nickel filtered CuK_α radiation is detected by a scintillation counter, pulse height analyzer, linear rate meter arrangement. The diffractometer is interfaced with a PDP-8 computer which controls the angular motor drive and counting time.

The analysis of the data follows a technique by Peiffer[95]. A computer program fits intensities corrected for incoherent and background scattering and sample absorption to a Lorentzian shaped curve[96]. The corrected intensities are used to calculate the degree of crystallinity. The results are plotted in Figures 11, 12, and 13 as $I_c S^2$ versus S, where I_c is the corrected intensity, $S = 2\sin\theta/\lambda$, and θ is the Bragg angle. The quantity X_∞ measured in

FIGURE 11 Wide angle X-ray diffraction data for PEO 6000.

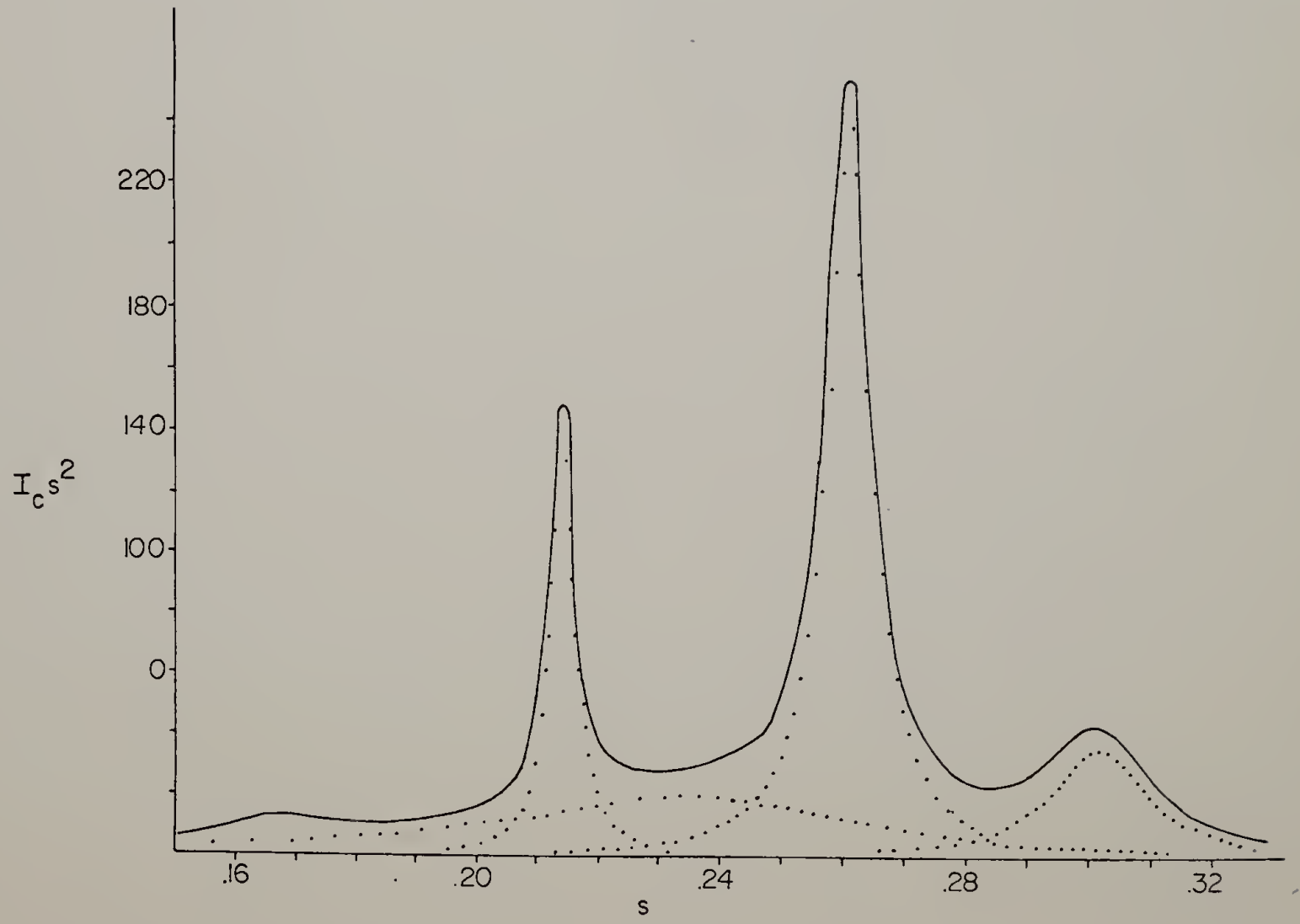
220
180
140
100
0
$I_c s^2$
.16
.20
.24
.28
.32
s

FIGURE 12 Wide angle X-ray diffraction data for PEO WSR-N10.

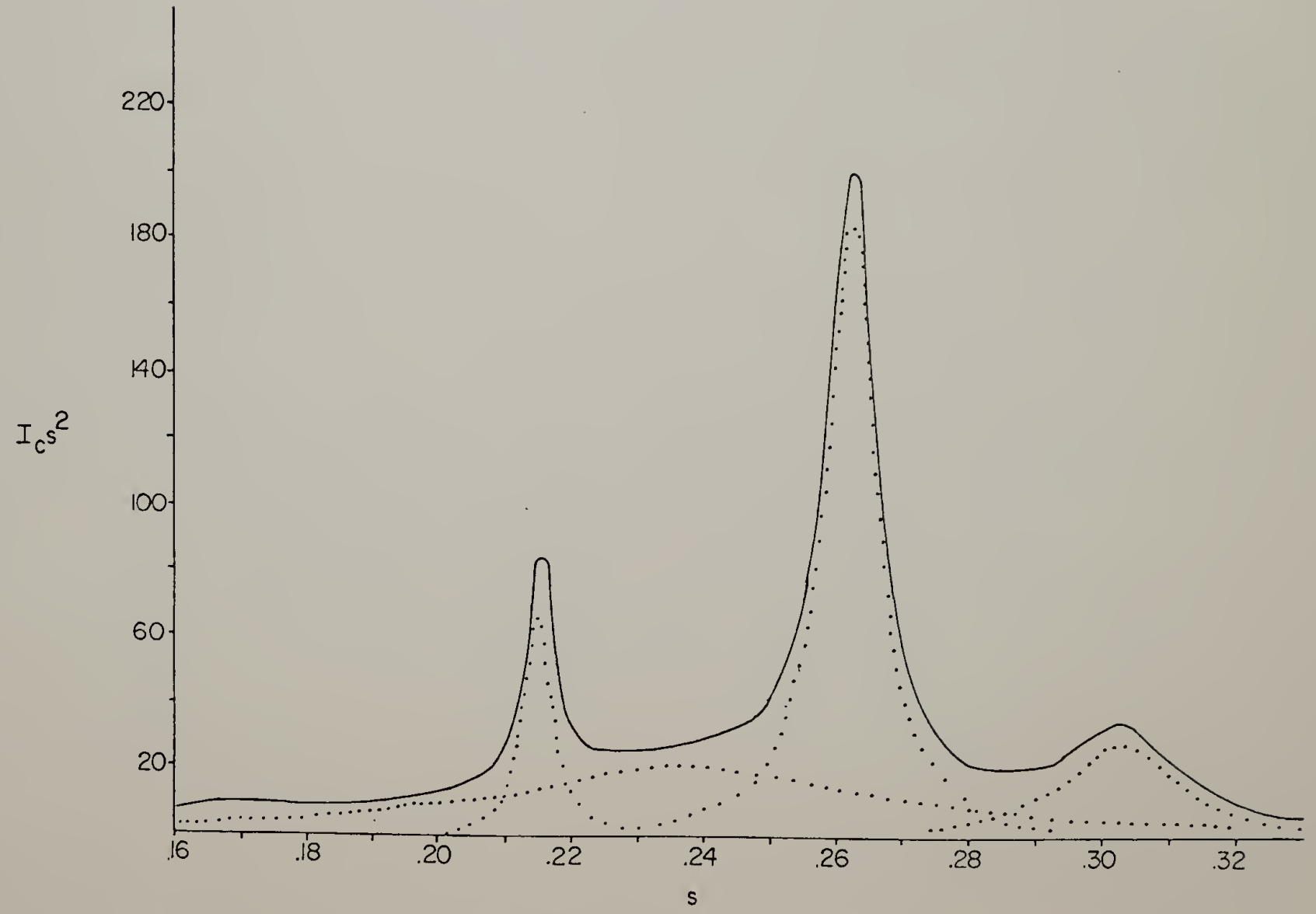
220
180
140
100
60
20
$I_c s^2$
.16
.18
.20
.22
.24
.26
.28
.30
.32
s

FIGURE 13 Wide angle X-ray diffraction data for PCL.

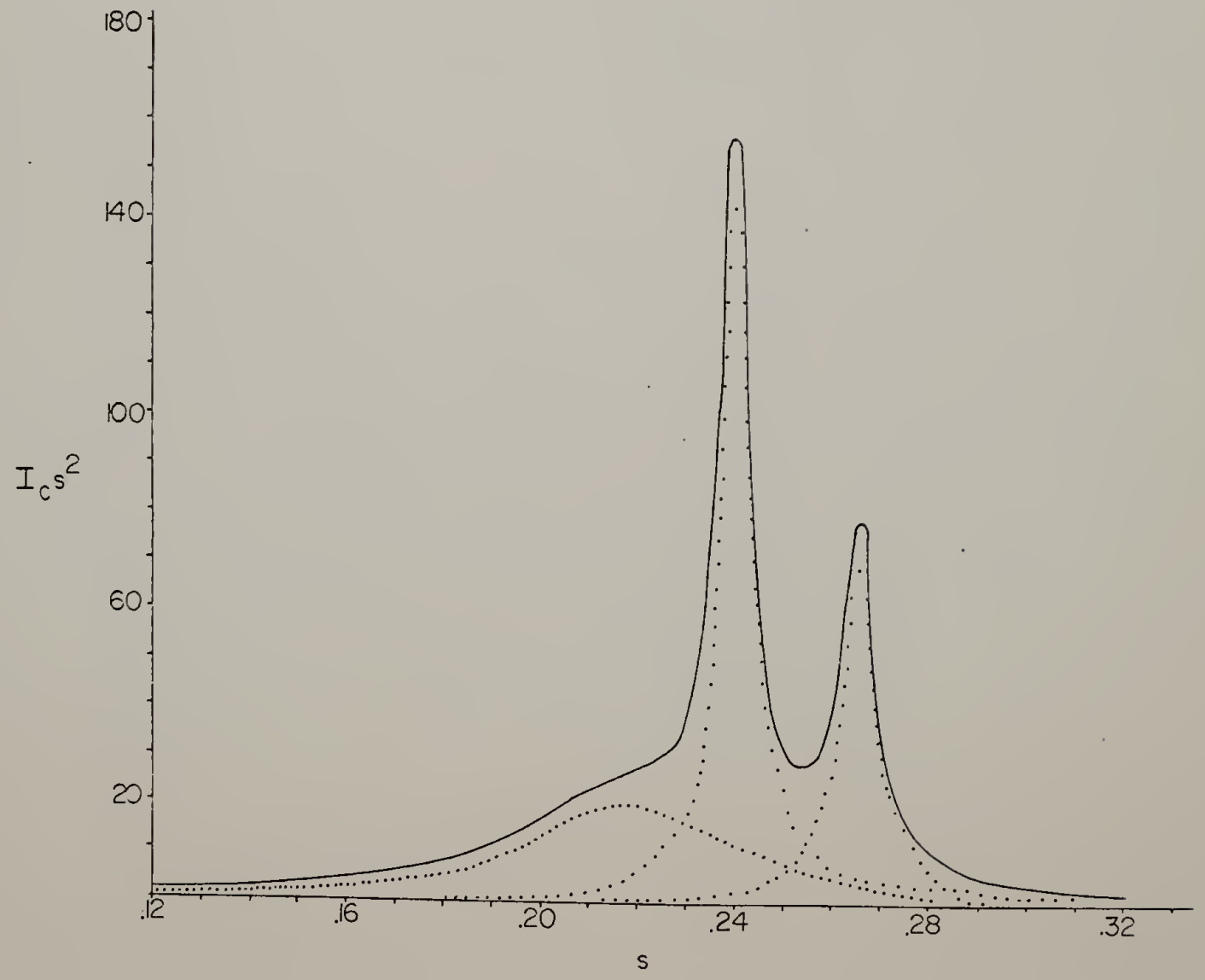
180
140
100
60
20
$I_c s^2$
.12
.16
.20
.24
.28
.32
s

these experiments was taken as a best estimate for the correction factor in the Avrami analysis.

Uncertainty in the correct value of X_∞ is introduced for several reasons. The X-ray diffraction method yields a weight average crystallinity whereas a volume average is measured in the crystallization experiments. The two results may be correlated using equation 18, where

$$\frac{1 - X_c,\text{wt.}}{X_c,\text{wt.}} = \frac{\rho_a}{\rho_c} \frac{1 - X_c, \text{vol.}}{X_c, \text{vol.}} \qquad (18)$$

ρ_a and ρ_c are the densities of the pure amorphous and pure crystalline materials. Values of ρ_a are easily obtained but a wide range of values have been reported for ρ_c leading to some doubt in the magnitude of correction necessary.

It is impossible to recover a sheared sample from the dilatometer without melting the crystalline network. The samples used for the X-ray analysis were crystallized quiescently at the lowest crystallization temperature used for each material. Two sources of error are introduced due to this approximation. An increase of as much as ten percent in the maximum degree of crystallinity, as determined by X-ray diffraction, was observed in the melt spinning of polyethylene[68]. Heat of fusion determinations showed an increase of as much as 20 percent in the degree of crystallinity for extrusion crystallized polyethylene[99].

Both extrusion and melt spinning produce extreme orientation not encountered in simple shear flow and it is assumed that degree of crystallinity is unaffected by shear rate in these experiments.

A second area of concern is the fact that temperature of crystallization has a large effect on the resulting specific volume of a crystallized polymer[100]. Polymers near their melting point achieve more perfect and complete crystallization than those transformed at lower temperatures. The difference between the maximum and minimum undercooling examined was only 5°C and the change in X_∞ over this range is assumed to be negligible.

Nucleation

In an attempt to gain some insight into the effect of shear on the nucleation process and subsequent crystallization, several experiments were performed for PEO 6000 and PCL at different undercoolings and shear rates in an instrument built by Ulrich[87]. The apparatus is a thermostated parallel plate shearing device mounted on the stage of a polarizing microscope. Numbers of nuclei in the field were counted from photographs taken at different times to determine the nucleation rate. Ulrich found a linear dependence of nucleation rate on shear rate[87]. Thus it was necessary to collect data at only two values of shear rate to produce the curve over the desired shear

rate range. This was done for PCL at each of the three crystallization temperatures used in the shearing dilatometer experiments.

Data was taken at one temperature for PEO 6000 and compared to that of Ulrich for PEO 20M, a polyethylene oxide of slightly higher molecular weight than PEO 6000. At the same undercooling, the nucleation results were very similar for both materials. It was concluded that Ulrich's data would be a satisfactory measure of the nucleation behavior for the PEO used in this study.

Data collection in the parallel plate apparatus was done in a similar fashion to the method used in the dilatometric experiments with one exception. Heat time was reduced from one hour to 15 minutes due to the smaller thermal mass of the parallel plate instrument. The time necessary to cool to the crystallization temperature was found to be around ten minutes, a decrease of 50 percent from the previous experiments. A photograph of the field of nuclei for a PCL sample shear crystallized at 15 sec^{-1} and 49.9°C is shown in Figure 14. The nucleation results for PEO 6000 and PCL appear in Figures 15 and 16.

Rheometrics Crystallization

Calibration of the strain gauges on the shearing dilatometer with known viscosity Newtonian fluids showed that the sensitivity of the gauges was not as large as

FIGURE 14 Photograph of nuclei formed in PCL sample, magnification 200X.

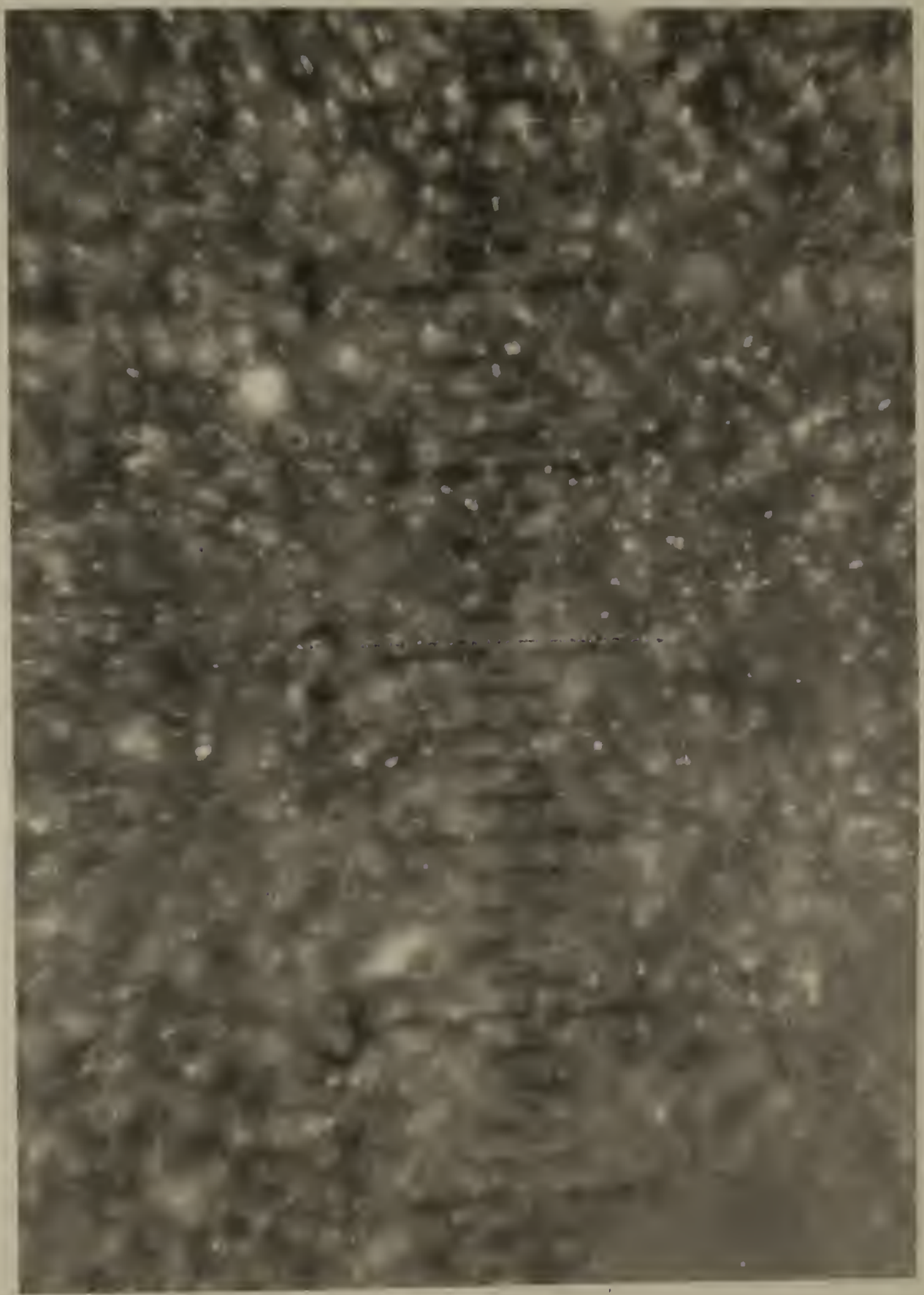

FIGURE 15 Nucleation rate versus shear rate for PEO 6000 at different crystallization temperatures.

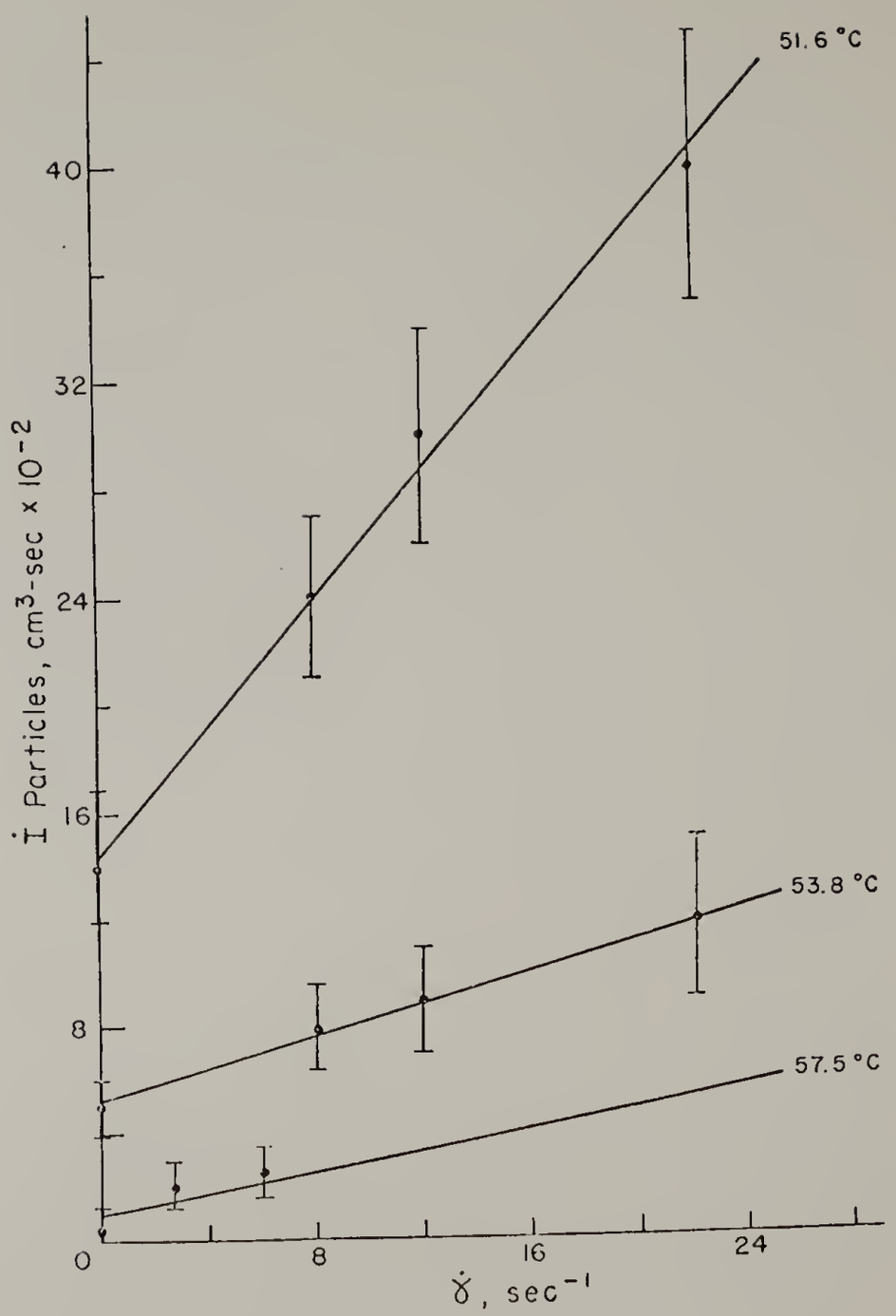
51.6 °C
53.8 °C
57.5 °C
40
32
24
16
8
0
8
16
24
İ Particles, cm³-sec x 10⁻²
γ̇, sec⁻¹

FIGURE 16 Nucleation rate versus shear rate for PCL at different crystallization temperatures.

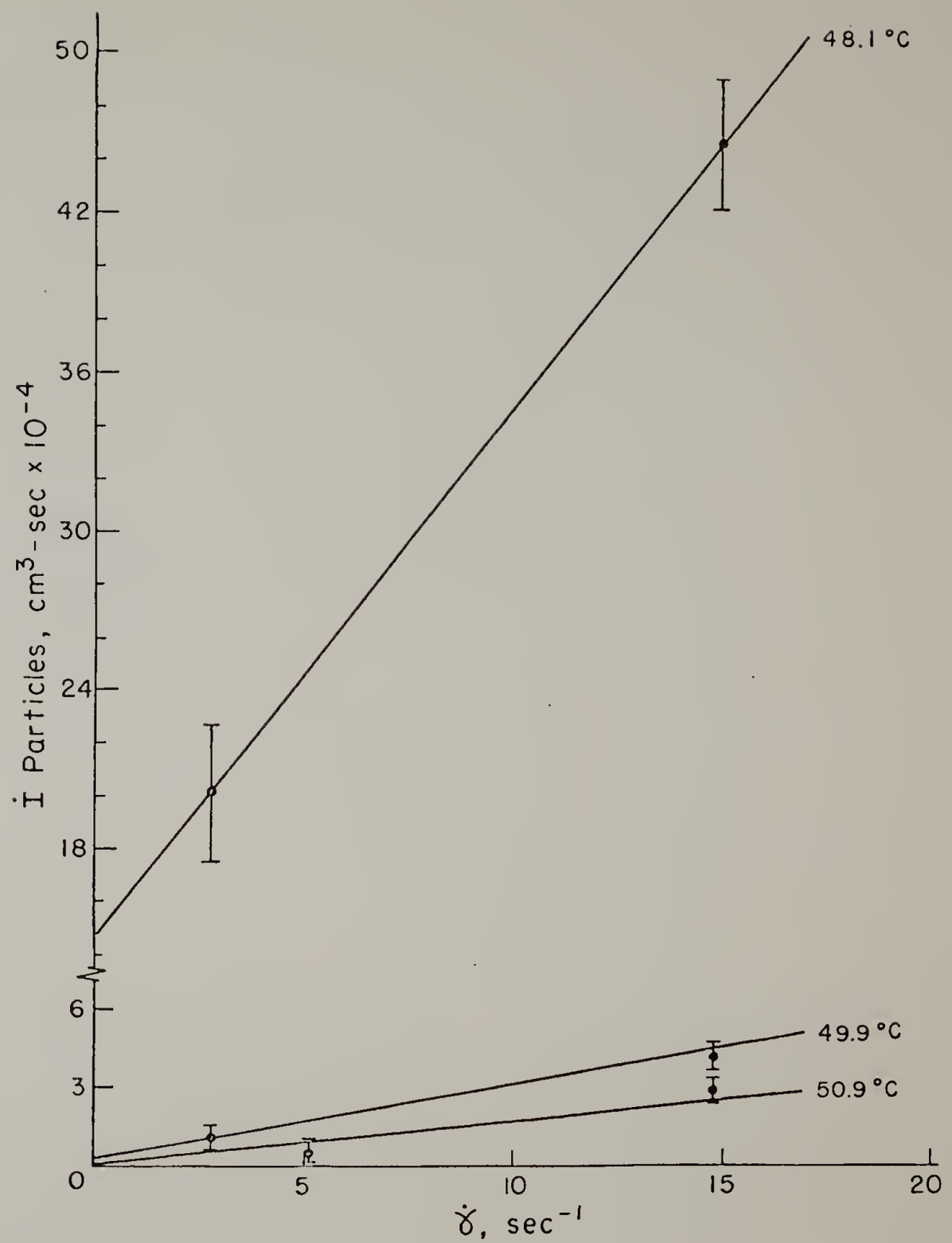
48.1 °C
49.9 °C
50.9 °C
50
42
36
30
24
18
6
3
0
5
10
15
20
İ Particles, cm³-sec x 10⁻⁴
γ̇, sec⁻¹

expected from design estimates. To obtain a sensitive measure of the increasing shear stress and viscosity with increasing crystallinity at the initial stages of the transformation, the Rheometrics mechanical spectrometer with cone and plate geometry was used. Samples of PEO 6000 and PCL were studied at selected temperatures and shear rates. The torque and temperature were recorded as a function of time for each sample until extensive crystallization caused sample slip and subsequent failure.

It was found that the temperature control was accurate to ±.5°C in the hot air heated sample chamber. This is somewhat worse than that achieved in the shearing dilatometer but the elapsed times to onset of crystallization under identical experimental conditions were comparable for both experiments. The shear stress measurements were also comparable for both techniques but the Rheometrics data was found to be much more accurate during the initial stages of transformation.

C H A P T E R IV

RESULTS

The purpose of this study was to measure the effect of shear on the kinetics of the crystallization process. To aid in the interpretation of these data some experiments examining nuclei formation and stress increase as a function of undercooling and shear rate were also performed.

Kinetics

It was very difficult to accurately determine the time at which crystallization first began in these experiments. To solve this problem, model curves with different values of Avrami exponent and starting time were constructed and compared to the data. The region between 1 and 5 percent crystallinity was fit to these models. The starting time obtained from the appropriate model was then used in the regression procedure detailed in Appendix II to determine values for the Avrami coefficients.

The Avrami parameters for PEO 6000 are given in Table 5. Each exponent value is listed with an associated error estimated from the regression. The relationship between the magnitude of this error and the goodness of

TABLE 5

AVRAMI CONSTANTS FOR PEO 6000

Temperature °C	Shear rate sec^{-1}	n	k
55.6	0	2.9 ± .1	3.9×10^{-6}
56.7	0	3.2 ± .2	1.5×10^{-8}
56.7	1.4	3.7 ± .1	4.8×10^{-9}
56.7	5.4	5.0 ± .1	3.9×10^{-10}
56.8	10.9	5.1 ± .2	1.9×10^{-10}
56.5	28.0	4.8 ± .3	3.0×10^{-7}
56.3	45.7	6.1 ± .2	1.1×10^{-8}
56.9	56.1	6.2 ± .5	3.6×10^{-9}
56.6	93.4	6.4 ± .2	1.1×10^{-9}
58.1	0	2.6 ± .1	3.7×10^{-8}
58.0	1.3	3.7 ± .2	1.5×10^{-9}
58.1	5.3	4.0 ± .1	2.6×10^{-9}
58.1	10.8	5.0 ± .4	1.1×10^{-10}
58.2	11.0	4.7 ± .2	1.6×10^{-10}
58.2	19.4	5.0 ± .4	8.2×10^{-8}
58.1	32.5	6.7 ± .3	4.1×10^{-10}
58.1	54.8	6.6 ± .3	2.8×10^{-10}
58.5	84.1	6.2 ± .2	1.0×10^{-10}
59.0	0	2.2 ± .1	2.6×10^{-7}
59.8	0	2.9 ± .1	1.7×10^{-10}
59.5	3.0	4.4 ± .1	7.7×10^{-13}
59.4	5.3	4.3 ± .1	9.0×10^{-12}
59.0	8.6	5.2 ± .2	8.0×10^{-11}
59.0	9.3	5.2 ± .3	5.3×10^{-11}
59.4	10.8	5.6 ± .2	3.7×10^{-14}
59.6	11.0	5.8 ± .2	6.2×10^{-14}
59.0	20.2	6.0 ± .2	1.5×10^{-12}
50.0	35.7	6.3 ± .2	6.1×10^{-12}
59.1	40.0	6.1 ± .2	2.3×10^{-12}
59.6	44.6	6.7 ± .4	8.0×10^{-14}
60.0	68.9	6.6 ± .1	1.8×10^{-14}

the fit is shown in Figure 17 where the regression values of degree of crystallinity are given by the solid lines. It can be seen that the data is described extremely well by exponents with errors approaching 5 percent. The rate constant, k, was determined by extrapolation and errors in this parameter can be as large as two orders of magnitude.

The values of the Avrami coefficients for PEO 6000 crystallized quiescently lie within the range of reported values for this material[8,12,84]. The value of n in the sheared cases is higher than the quiescent value and generally increases with increasing shear rate. These results are in reasonable agreement with those reported by Fritzsche[84]. Higher values of n were seen in that work. This may be explained by the higher range of shear rates studied (30 sec^{-1} to 168 sec^{-1}). The increase in n with increasing shear rate trend was not reported by Fritzsche. This can be attributed to the lower shear rate range of this study and to the fact that his experiments were not conducted at preset crystallization temperatures which made it difficult to isolate the effect of shear rate. Fritzsche noted a substantial increase in values of n with increasing temperature at constant shear rate. This behavior was observed in these experiments, but to a much smaller degree and only at higher shear rates.

As previously discussed, the quiescently obtained values of the rate constant are in good agreement with

FIGURE 17 Degree of crystallinity versus time for three different PEO 6000 experiments.

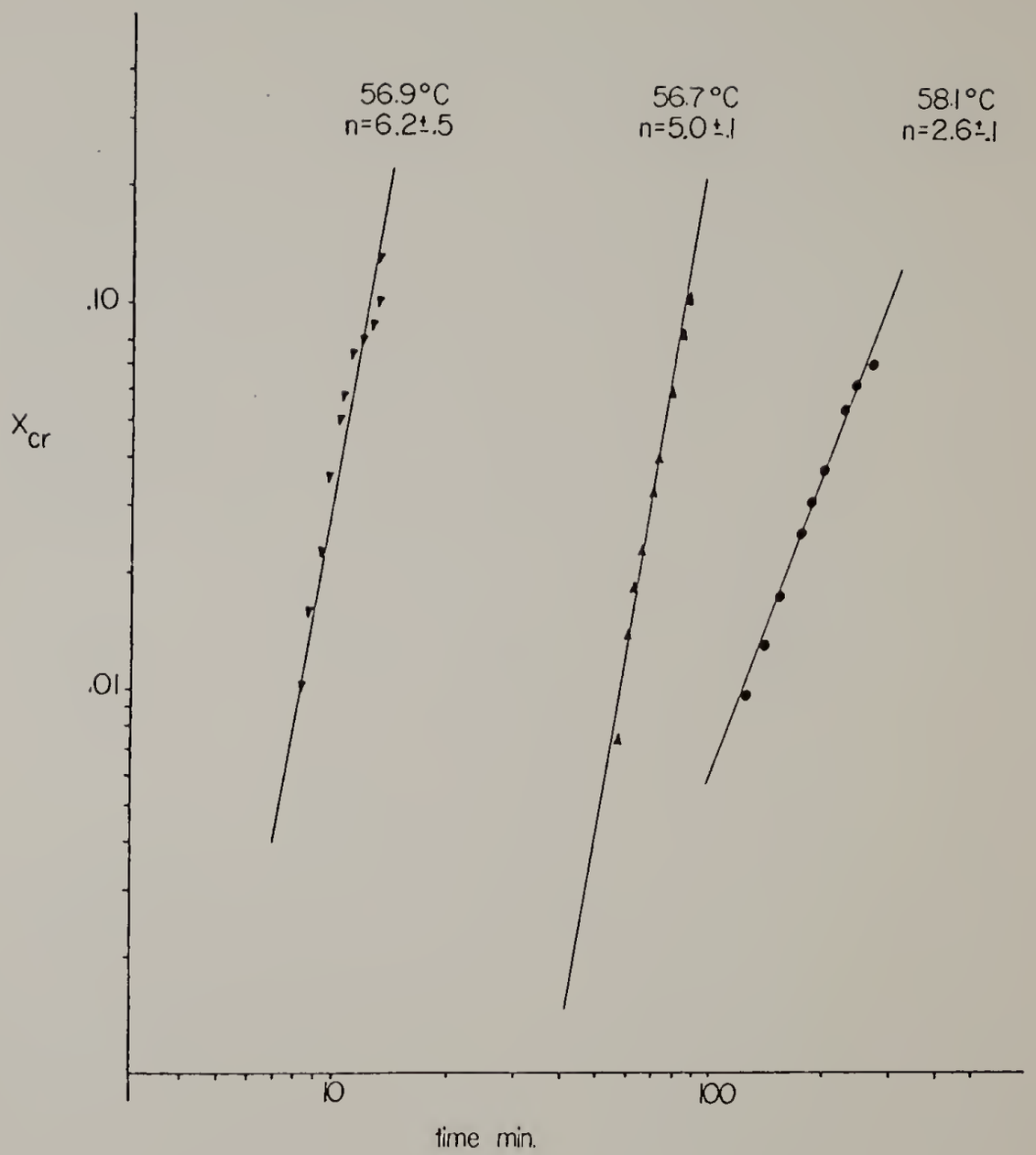
56.9°C
n=6.2±.5
56.7°C
n=5.0±.1
58.1°C
n=2.6±.1
.10
.01
X_{cr}
10
100
time min.

published results and show the proper temperature dependence. The values obtained at constant shear rate exhibit the expected temperature dependence, namely decreasing in value with increasing temperature. At constant temperature, the value of k decreases with increasing shear rate. This is in agreement with Fritzsche[84] but contradicts the findings of Ulrich[87]. He observed a slight increase in k with shear in his experiments which were confined to very low shear rates and Avrami exponent values less than 3.5. The form of the equation for k in the Avrami treatment contains nucleation and growth rate terms, which are assumed to have a constant value, along with geometric parameters describing the shape of the growing crystal. Data collected in these experiments and in those performed by Ulrich indicate that nucleation rate and possibly growth rate change during shear crystallization. The deviation of these parameters from a constant value becomes more pronounced with increasing shear rate. This information indicates that interpretation of the value of k in terms of the Avrami analysis is not applicable for highly accelerated shear crystallization experiments.

The kinetic results for PEO WSR-N10 are listed in Table 6 and are in good agreement with those reported for this material in the quiescent case[101-103]. The shear experiments are characterized by high values of n and

TABLE 6

AVRAMI CONSTANTS FOR PEO WSR-N10

Temperature °C	Shear rate sec^{-1}	n	k
58.5	0	3.2 ± .1	2.6×10^{-6}
58.0	0	3.0 ± .2	2.4×10^{-5}
57.8	0	3.3 ± .1	2.9×10^{-6}
58.6	5.4	3.9 ± .3	5.6×10^{-8}
58.8	7.6	5.2 ± .1	1.2×10^{-9}
59.1	17.0	5.3 ± .3	2.8×10^{-8}
59.2	25.2	6.7 ± .7	1.0×10^{-10}
57.8	37.6	5.5 ± .5	1.8×10^{-7}
59.2	36.5	5.8 ± .2	4.4×10^{-10}
59.6	0	3.2 ± .1	3.6×10^{-7}
59.8	0	2.9 ± .2	4.5×10^{-6}
59.5	0	3.0 ± .1	2.4×10^{-7}
59.6	1.4	3.9 ± .2	3.9×10^{-8}
59.6	3.0	3.3 ± .1	2.1×10^{-7}
59.5	5.4	3.5 ± .2	9.7×10^{-8}
59.2	8.4	4.5 ± .4	6.0×10^{-9}
59.6	9.6	4.4 ± .2	4.6×10^{-8}
59.6	10.8	3.5 ± .4	7.5×10^{-8}
59.6	17.1	5.9 ± .2	1.4×10^{-12}
59.9	19.8	5.0 ± .2	5.2×10^{-8}
59.6	27.1	4.1 ± .1	3.6×10^{-8}
59.8	38.9	3.9 ± .2	1.6×10^{-7}
61.1	0	2.9 ± .2	6.5×10^{-8}
61.0	0	3.1 ± .2	4.1×10^{-8}
61.0	1.4	4.1 ± .1	1.7×10^{-9}
60.9	3.1	4.8 ± .4	2.3×10^{-10}
61.0	5.4	4.9 ± .3	1.5×10^{-11}
61.0	9.1	5.0 ± .5	1.6×10^{-10}
61.8	9.2	5.1 ± .4	1.6×10^{-11}
61.3	28.5	5.1 ± .4	6.1×10^{-9}

reduced values of k similar to those found for PEO 6000. The kinetic data was restricted to lower degrees of transformation due to erratic height readings in the range of 8 percent crystallinity. This irregularity resulted from the inability of the mercury head to force the melt, with rapidly increasing viscosity caused by crystallization, to space fill the annular volume. This behavior was not observed for the lower molecular weight PEO and PCL materials.

The value of n in Table 6 rises with shear rate up to a maximum and then decreases slightly. Viscous dissipation is thought to contribute to this behavior. All of the experiments shown in the first group in Table 6 with the exception of the one at 57.8°C were run at essentially the same temperature. The experimental temperature was recorded at the onset of crystallization and should contain little if any contribution due to crystallization increased viscosity. It can be seen that there is a detectable temperature increase, measured at the polymer-inner cylinder interface, as the shear rate increases. These readings are assumed to be minimum temperature values in the system as shown by the model studies which predicted local ΔT values as high as 6°C in the interior of the samples for the adiabatic approximation with a shear rate of 35 sec^{-1}. This increase in melt temperature decreases

the driving force for crystallization and results in a slower crystallization process. The enhancement of the crystallization process produced by increasing shear is thus partially negated by rising temperatures due to viscous heating.

The Avrami coefficients for PCL are given in Table 7. Both n and k exhibit the same type of behavior with increasing shear rate seen in the experiments with the other two materials studied. The maximum value of n is approximately the same as it was for the polyethylene oxide samples. The value of k at constant shear rate was found to decrease with increasing temperatures but at a much slower rate than for PEO. The quiescent value of k decreases with increasing temperature which is opposite to the expected trend. This is most likely explained by the error in the result since the highest and lowest values differ by a factor of 10 and the value of k can vary by as much as two orders of magnitude.

The results for all materials show that the Avrami exponent, which is indicative of the speed of the crystallization process, increases with increasing shear rate. Values of n are around 3 for the quiescent cases and increase to values greater than 5 with shear. Viscous heating at high shear rates in WSR-N10 samples result in slightly reduced values of n. Values of the rate constant

TABLE 7

AVRAMI CONSTANTS FOR PCL

Temperature °C	Shear rate sec^{-1}	n	k
48.1	0	3.0 ± .1	9.8×10^{-10}
48.0	1.4	3.7 ± .2	7.2×10^{-10}
48.0	2.9	3.9 ± .1	1.4×10^{-9}
48.3	5.2	3.7 ± .3	5.8×10^{-9}
48.1	10.9	3.7 ± .1	1.2×10^{-7}
48.1	14.6	4.0 ± .2	1.3×10^{-8}
48.6	16.0	5.0 ± .3	2.0×10^{-10}
48.4	26.9	5.5 ± .4	4.6×10^{-11}
49.8	0	2.9 ± .1	1.4×10^{-9}
49.8	1.3	2.9 ± .2	2.4×10^{-8}
49.8	2.8	3.1 ± .1	1.8×10^{-8}
49.8	5.1	4.5 ± .2	1.6×10^{-11}
49.8	8.9	4.2 ± .5	8.9×10^{-10}
49.8	10.8	4.3 ± .1	1.3×10^{-9}
49.5	11.2	4.7 ± .2	9.3×10^{-11}
49.8	14.9	4.9 ± .2	1.8×10^{-11}
49.8	26.6	5.1 ± .2	1.6×10^{-11}
49.9	48.0	5.0 ± .3	2.8×10^{-11}
50.9	3.0	2.9 ± .1	1.0×10^{-8}
50.9	5.5	3.2 ± .2	5.0×10^{-9}
50.8	11.0	4.0 ± .3	2.0×10^{-10}
50.8	14.3	4.1 ± .1	5.8×10^{-10}
50.8	16.0	4.8 ± .3	6.4×10^{-12}
50.8	24.9	4.8 ± .1	1.8×10^{-11}
50.9	47.2	5.0 ± .3	1.8×10^{-11}
51.6	15.3	4.1 ± .1	1.6×10^{-10}

k exhibit the expected temperature behavior in the quiescent systems studied, but values of k in sheared systems behave in a manner opposite to that expected and cannot be interpreted in terms of classical Avrami theory.

Stress Measurements

It has been postulated by many researchers that shear stress rather than shear rate is the important parameter controlling accelerated crystallization. To measure stress in the melt, strain gauges were installed on the support bars of the instrument as discussed in Chapter II.

Typical data taken for PCL at 5.7°C undercooling and shear rates of 15 sec^{-1} and 0 sec^{-1} are shown in Figure 18. The top curves represent the change in height with cooling and subsequent crystallization. In the time period of the experiment, quiescent crystallization does not take place. The strain gauge in this case follows the cooling of the melt, as reflected by a change in height, extremely well. The strain gauge output shown for the stressed system also follows the height curve well. Unfortunately, the curve shown represents an average reading in an output where the signal to noise ratio is 3 to 4. It was not possible to remove these fluctuations electronically and it was therefore assumed that the problem was due to eccentricity in the concentric cylinders. Repeated realignment attempts also failed to remove the noise. The

FIGURE 18 Height and strain gauge output versus time for PCL.

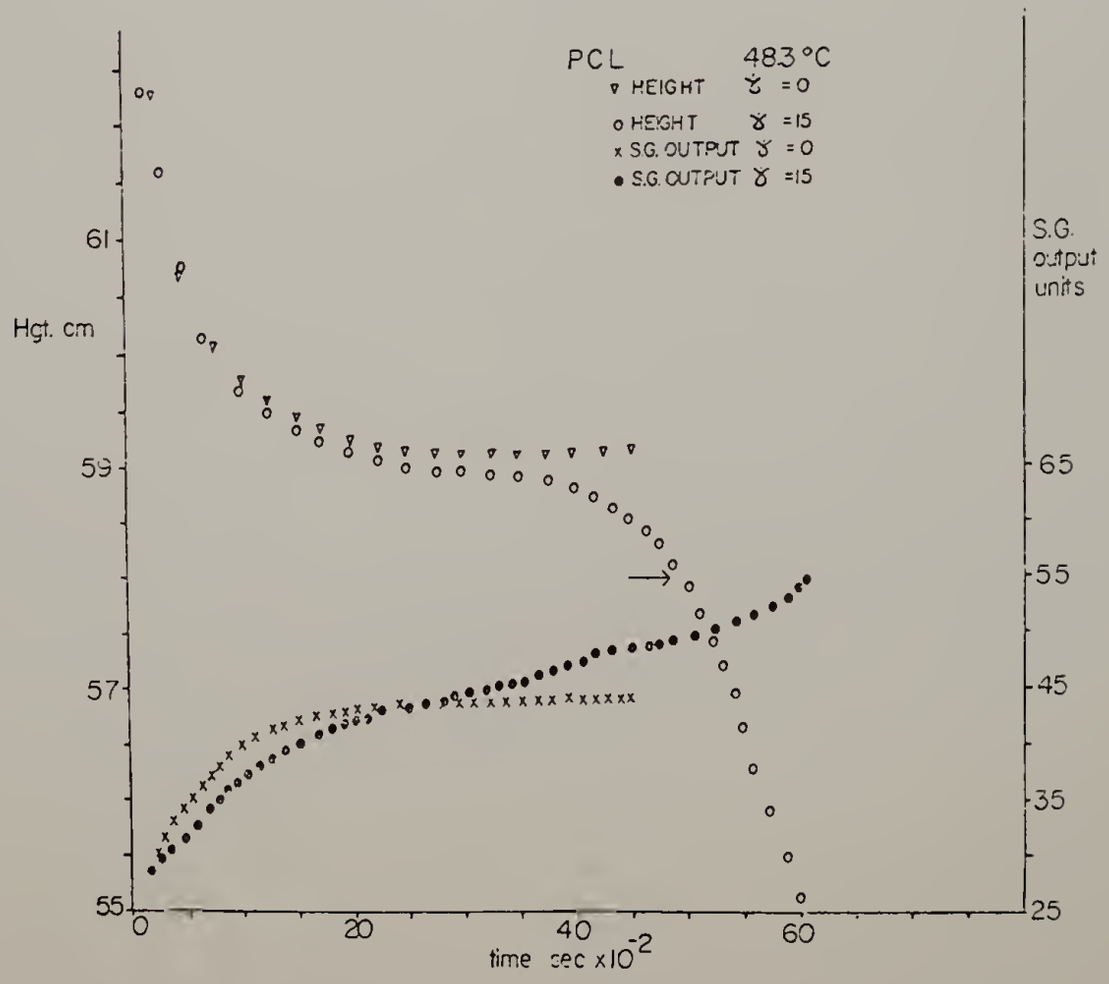
PCL 483 °C
▿ HEIGHT ϑ = 0
o HEIGHT ϑ = 15
x S.G. OUTPUT ϑ = 0
• S.G. OUTPUT ϑ = 15
Hgt. cm
61
59
57
55
S.G. output units
65
55
45
35
25
0
20
40
60
time sec x10-2

noise problem coupled with the fact that the output at 10 percent crystallinity, indicated by the arrow in Figure 18, is very small led to the decision that the reliability of data taken in this system would be too low to draw any significant quantitative conclusions.

It became obvious during the course of the rheological studies undertaken in this work that the Rheometrics mechanical spectrometer could be a useful tool to study the increase in shear stress in a crystallizing melt. Several experiments were attempted with PCL and PEO 6000 at the shear rates and crystallization temperatures used in the shearing dilatometer system. The WSR-N10 samples would not stay in the sample cavity at shear rates above 5 sec^{-1} and were therefore not investigated.

Plots of shear stress versus time for two samples of PEO 6000 are shown in Figure 19. The large fluctuations in stress after the onset of crystallization have also been noted by Tan and Gogos[104] who attributed them to a "slip-stick" mechanism of the melt acting in a rubber-like fashion. In subsequent figures these fluctuations have been averaged to give a point value of shear stress.

Additional runs with PEO 6000 are shown in Figure 20. Temperature control in the Rheometrics was possible to approximately ±.5°C but cooling time for the melt 15 degrees above T_m to the crystallization temperature was extremely variable. Elapsed time to onset of crystalliza-

FIGURE 19 Shear stress versus time for crystallizing PEO 6000.

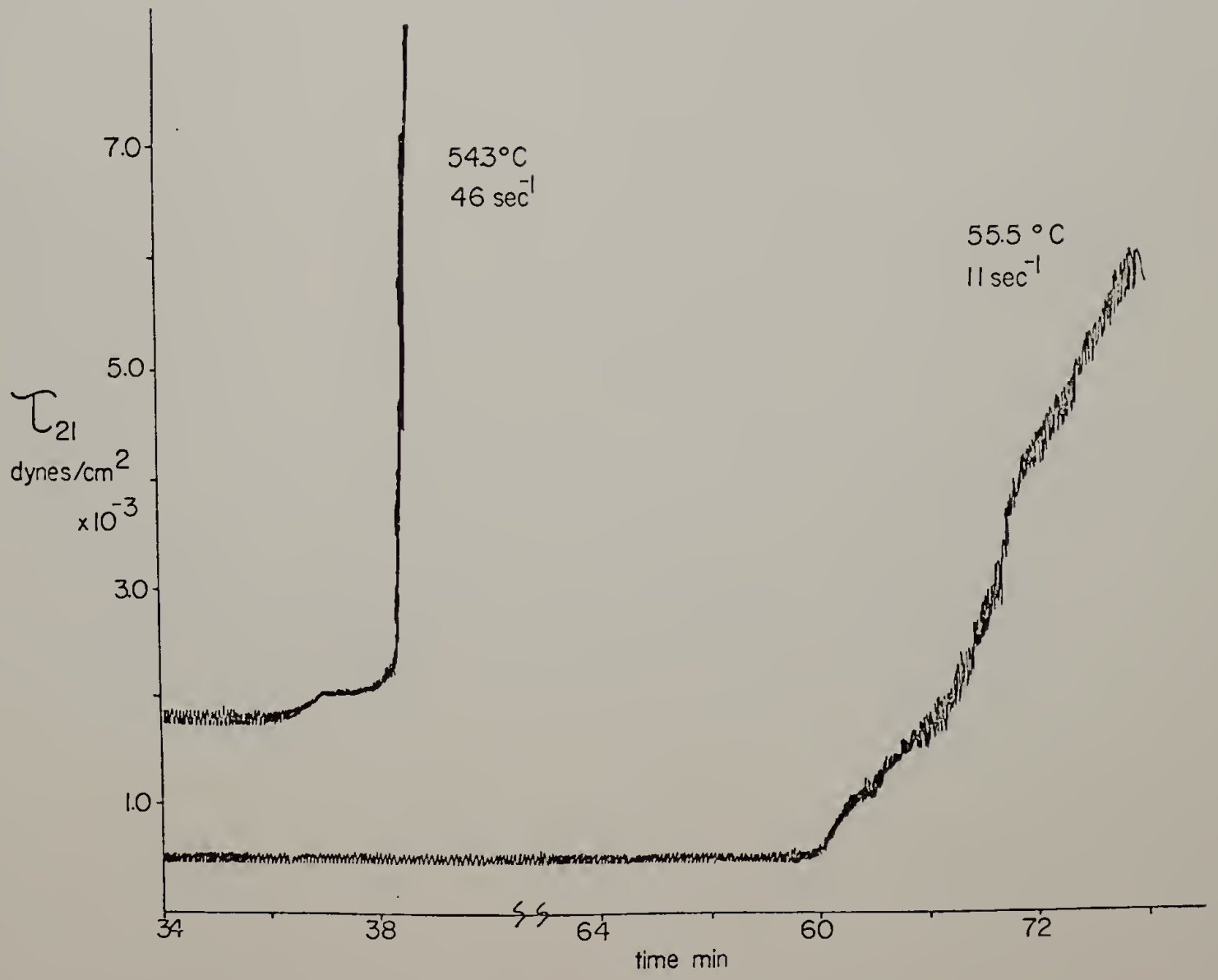
7.0
5.0
3.0
1.0
τ_{21}
dynes/cm^2
x10^{-3}
543°C
46 sec^{-1}
55.5 °C
11 sec^{-1}
34
38
64
60
72
time min

FIGURE 20 Shear stress versus time for crystallizing PEO 6000 at different temperatures and shear rates.

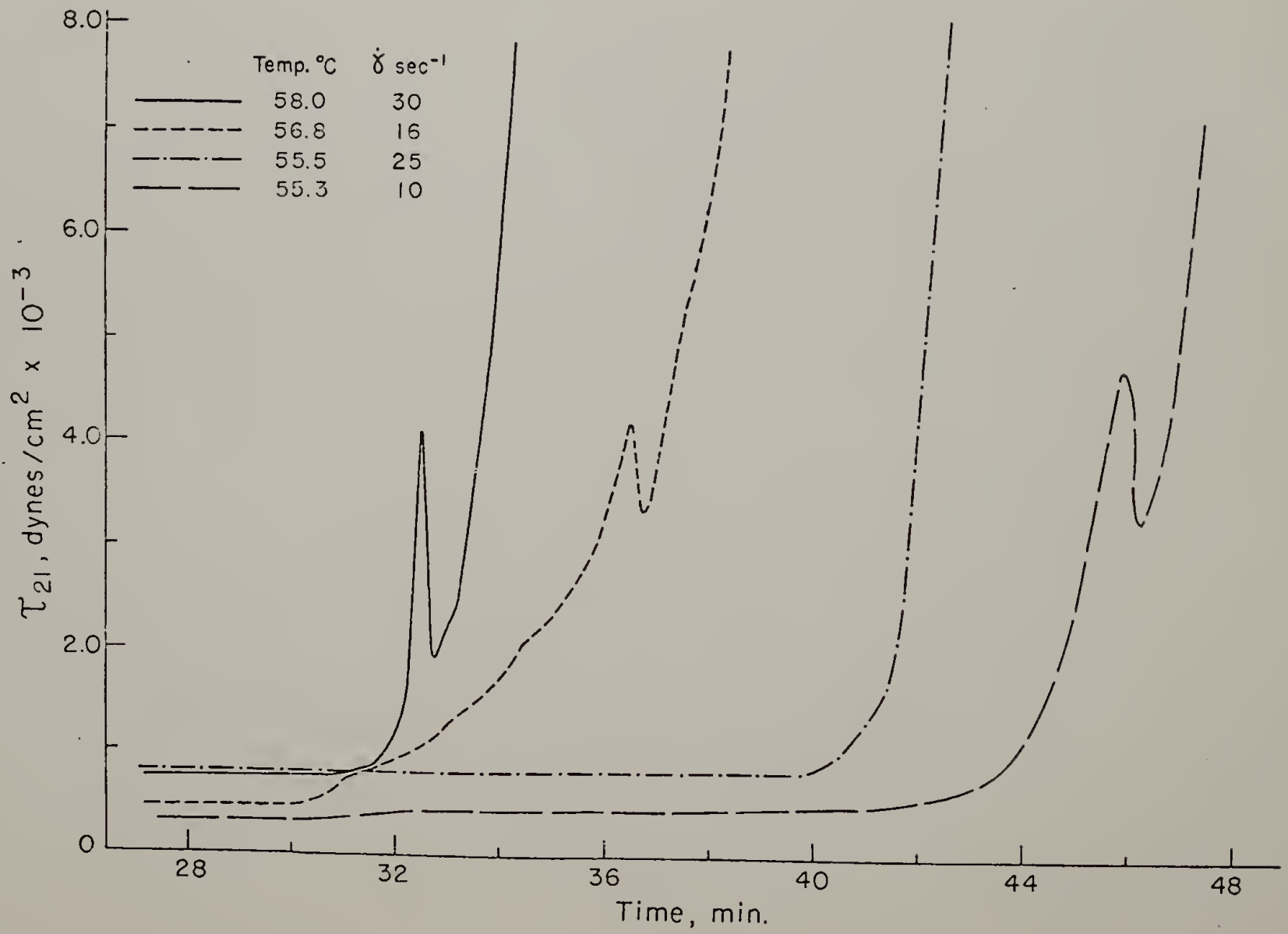
Temp. °C
$\dot{\delta}$ sec^{-1}
58.0 30
56.8 16
55.5 25
55.3 10
τ_{21}, dynes/cm^2 x 10^{-3}
8.0
6.0
4.0
2.0
0
28
32
36
40
44
48
Time, min.

tion for samples crystallized below 56°C is much longer than for samples at higher crystallization temperatures at corresponding shear rates. This is not a function of the crystallization process and hence must be due to the increased cooling time necessary to reach the lower temperatures. Large discrepancies were also observed between oven setting and resulting temperatures. Consequently, the data are at a number of different crystallization temperatures, only a few of which correspond to those in the dilatometric studies. The two runs which are in the proper temperature range have approximately the same incubation time as seen in the shearing dilatometer experiments. Incubation time is defined as the period between the time the polymer reaches thermal equilibrium and the time at which the onset of crystallization is observed.

To compare stress and degree of crystallinity the following procedure was adopted. The degree of crystallinity at given times after the onset of crystallization in the dilatometric experiments was compared to the rise in stress for the same time periods in the Rheometric experiments for similar values of shear rate and temperature. It was necessary to interpolate between crystallinity time curves to obtain data at the appropriate shear rates. In some cases it was also necessary to make assumptions concerning incubation times at the shear stress experiment temperatures which fell between the crystallization

temperatures in the dilatometric experiments. Finally, after the incubation time was determined, a value of n was assumed which determined the shape of the crystallinity time curve. The data for PEO 6000 are given in Table 8.

The shear stress data for PCL are given in Figure 21. The incubation times for these runs coincide reasonably well with those measured in the kinetic experiments. An identical procedure was followed to study shear stress as a function of crystallinity and the results for this material are also shown in Table 8.

The change in shear stress per fractional degree of crystallinity seems to be reasonably constant for each material although the data is rather scarce. This is not surprising if one considers the crystallites as dispersed particles increasing the viscosity of the flowing melt. It is not clear why the stress increase in PEO 6000 is greater per volume fraction transformed than it is in PCL. It is possible that the larger PEO crystallites interact and serve as crosslinks forming regions of network structures in the melt.

The greatest error in the analysis is introduced through incubation time assumptions. No assumptions of this kind were made for PEO and this data is thought to be fairly accurate. Extrapolations of incubation time had to be made in each case for PCL and it is difficult to

TABLE 8

STRESS INCREASE AS A FUNCTION OF DEGREE OF CRYSTALLINITY FOR PEO 6000 AND PCL

Sample	Temperature °C	Shear rate sec^{-1}	$\Delta\tau_{21}$ $dynes/cm^2$	X_{cr}
PEO	56.8	30	7000	.025
PEO	57.8	16	6500	.024
PCL	48.5	27	3650	.042
PCL	49.0	11	2800	.027
PCL	48.5	14	2600	.025
PCL	49.0	5	2200	.020

FIGURE 21 Shear stress versus time for crystallizing PCL at different temperatures and shear rates.

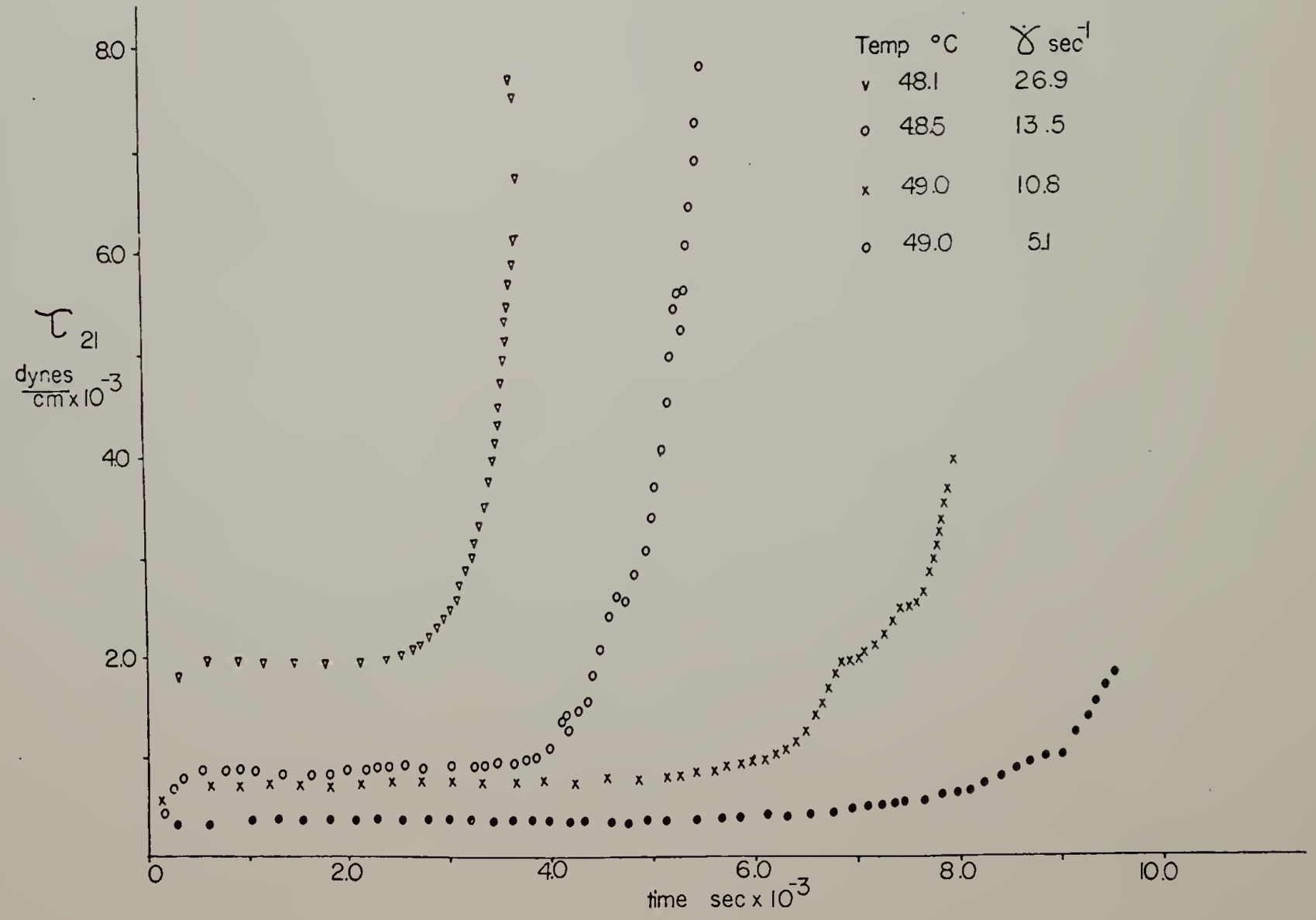
Temp °C
48.1
48.5
49.0
49.0
$\dot{\gamma}$ sec^{-1}
26.9
13.5
10.8
5.1
τ_{21}
dynes/cm x 10^{-3}
8.0
6.0
4.0
2.0
0
2.0
4.0
6.0
8.0
10.0
time sec x 10^{-3}

assess the effect these assumptions had on the stress increase values for this material. The output from the strain gauges monitored during the crystallization process indicated a higher stress increase as a function of crystallinity for PEO in support of the Rheometrics data. However, no consistent value for the ratio of these stress increases could be determined. The experiments have produced some interesting results but more data must be taken in order to draw any definite quantitative conclusions.

Several qualitative conclusions may be drawn from the shear stress experiments. The data at all temperatures show that stress increases more rapidly for higher shear rates at a given temperature. It was also found that at a given shear rate stress increases faster at a lower temperature. These results substantiate the findings in the crystallization kinetics experiments.

Induction Time

Degree of crystallinity is shown as a function of time for different shear rates at the three crystallization temperatures for PEO 6000 in Figures 22-24. The shape of these curves is indicative of the speed of transformation, steeper lines signifying larger exponent values and a more rapid crystallization. A measurement of the elapsed time to onset of crystallization may be determined from these plots. The zero time in all graphs shown

corresponds to the time at which the polymer sample has reached the crystallization temperature. The measurement of time at the onset of crystallization is subject to some uncertainty. To alleviate this error, elapsed time was measured to a fractional degree of transformation of .005. This time is defined as the induction time.

The results for the lowest crystallization temperature, 56.7°C, are shown in Figure 22. The induction time decreases with increasing shear rate. There appears to be a saturation effect with shear at the two highest shear rate values, similar to the results reported by Fritzsche[84]. The similarity of these two induction times is due in part to the different experimental temperatures. Reducing the temperature in the highest shear rate experiment would reduce the induction time slightly but would not remove the saturation effect.

The experiments conducted at 58.1°C are shown in Figure 23. Again there seems to be a saturation effect at the higher shear rates, the difference in induction times being only three minutes. The differences between the quiescent and low shear rate experiments are more pronounced at this temperature than at 56.7°C.

The results for the highest crystallization temperature, 59.6°C, are shown in Figure 24. There appears to be a trend toward saturation at the higher shear rates, although the actual time difference between the highest

FIGURE 22 Degree of crystallinity versus ln time for PEO 6000 at 56.7°C.

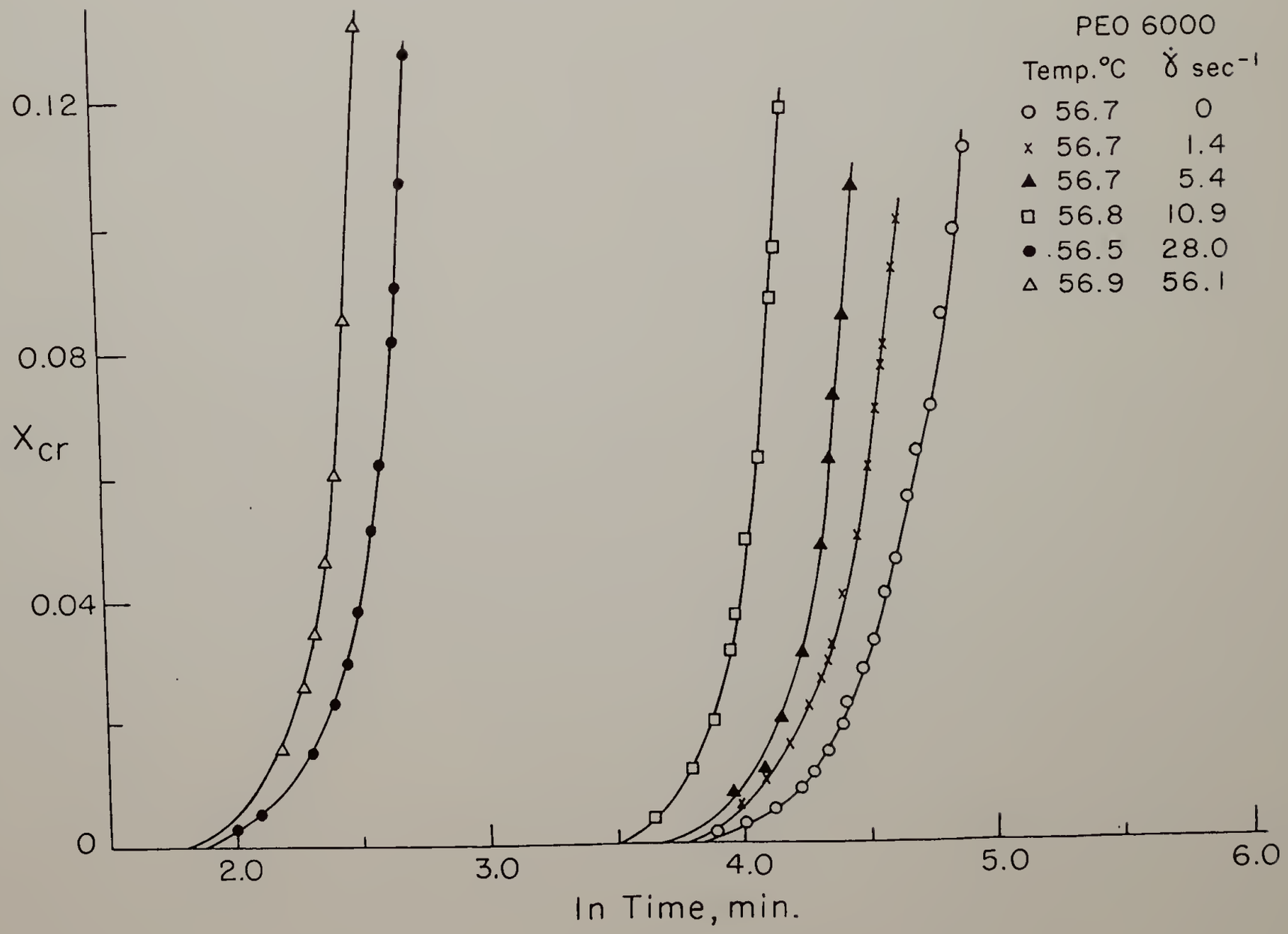
PEO 6000
Temp.°C
$\dot{\delta}$ sec^{-1}
56.7 0
56.7 1.4
56.7 5.4
56.8 10.9
56.5 28.0
56.9 56.1
0.12
0.08
0.04
0
X_{cr}
2.0
3.0
4.0
5.0
6.0
ln Time, min.

FIGURE 23 Degree of crystallinity versus ln time for PEO 6000 at 58.1°C.

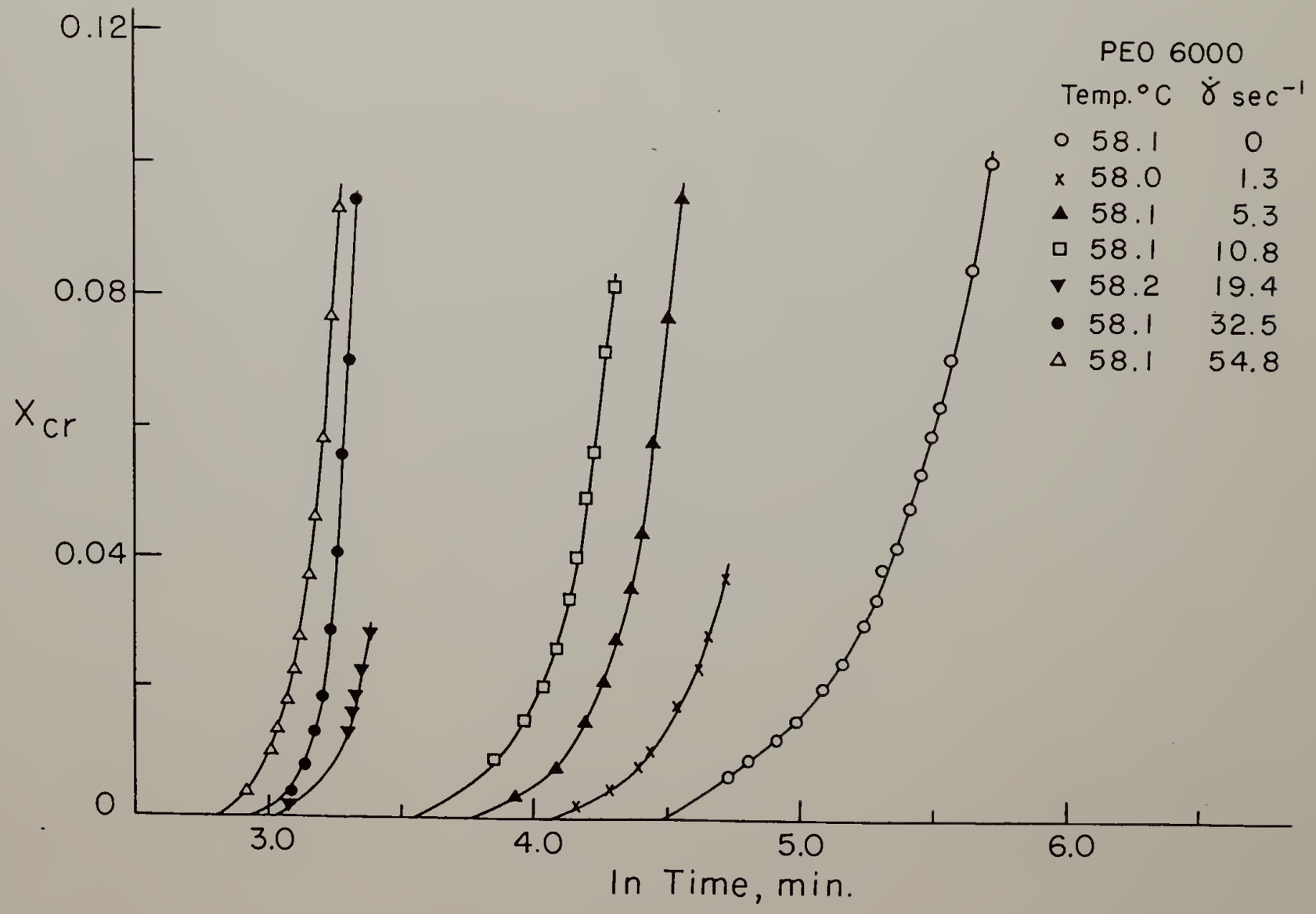
0.12
0.08
0.04
0
X_{cr}
3.0
4.0
5.0
6.0
ln Time, min.
PEO 6000
Temp.°C
$\dot{\gamma}$ sec^{-1}
58.1 0
58.0 1.3
58.1 5.3
58.1 10.8
58.2 19.4
58.1 32.5
58.1 54.8

FIGURE 24 Degree of crystallinity versus ln time for PEO 6000 at 59.6°C.

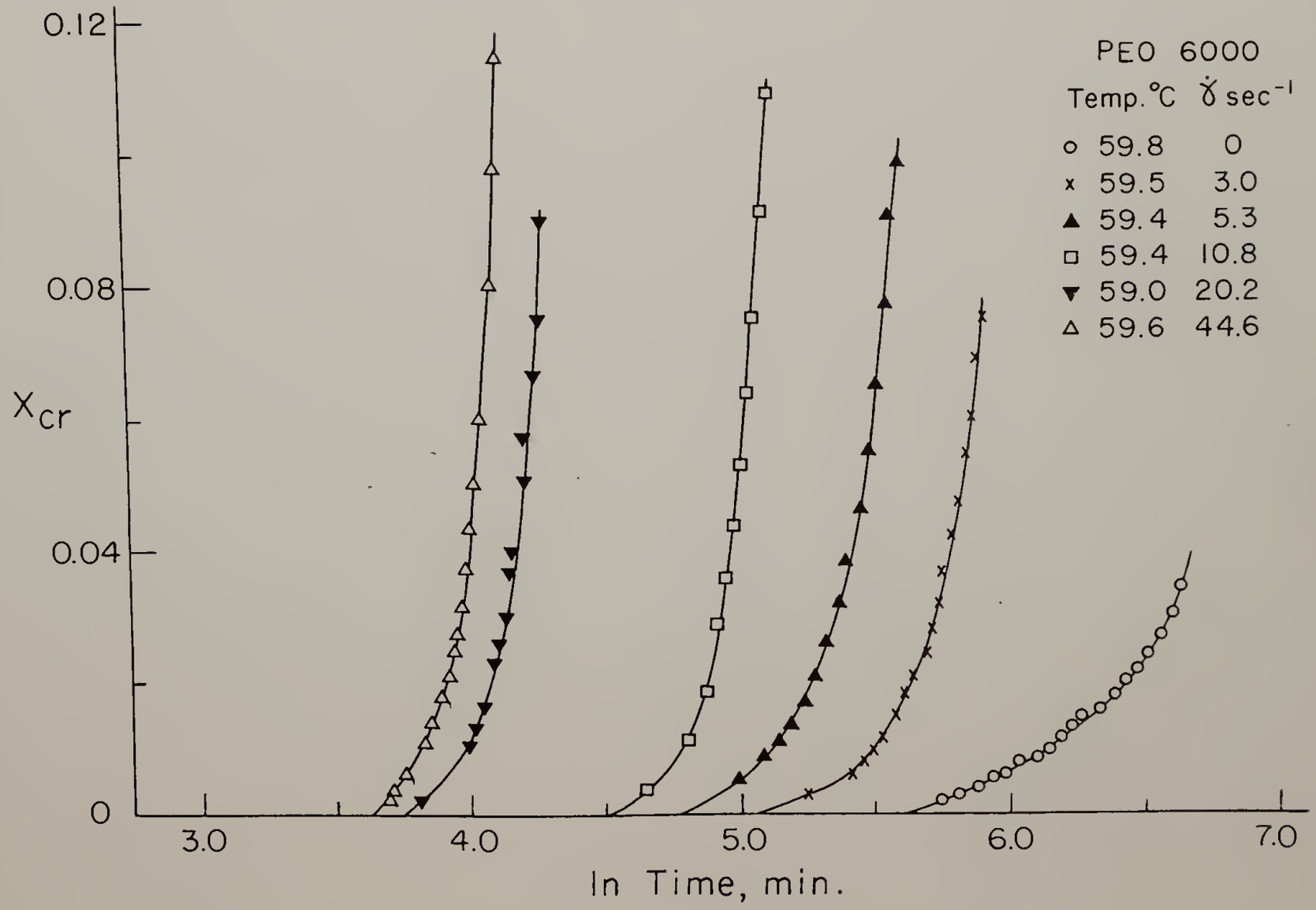
0.12
0.08
0.04
0
X_{cr}
3.0
4.0
5.0
6.0
7.0
ln Time, min.
PEO 6000
Temp. °C
$\dot{\gamma}$ sec^{-1}
59.8 0
59.5 3.0
59.4 5.3
59.4 10.8
59.0 20.2
59.6 44.6

shear rate runs is seven minutes. The effect of even small amounts of shear at this temperature produces a large effect as manifested in the difference in induction times for the quiescent and 3.0 sec^{-1} curves.

The induction time curves for WSR-N10 are given in Figures 25-27. The lowest crystallization temperature data are shown in Figure 25. The induction times at all shear rates are reasonably close together, the difference between the highest and lowest value is on the order of 11 minutes. It can be seen that the induction for 7.6 sec^{-1} is higher than that for 5.4 sec^{-1}. This must be attributed to the higher crystallization temperature due in part to increased viscous dissipation.

The data at 59.6°C are shown in Figure 26. Unlike the experiments at the lower temperature, these samples were cooled to different crystallization temperatures. The result was that with viscous heating, the measured temperatures at different shear rates were approximately equal. The induction times fall into two groups, a high shear rate group with shorter induction times, and a low shear rate group. The order within each group seems to depend on temperature but the induction times are so similar in value that no definite conclusions can be drawn. However, the reduction in induction time between the highest and lowest shear rates is significant.

FIGURE 25 Degree of crystallinity versus ln time for PEO WSR-N10 at 58.5°C.

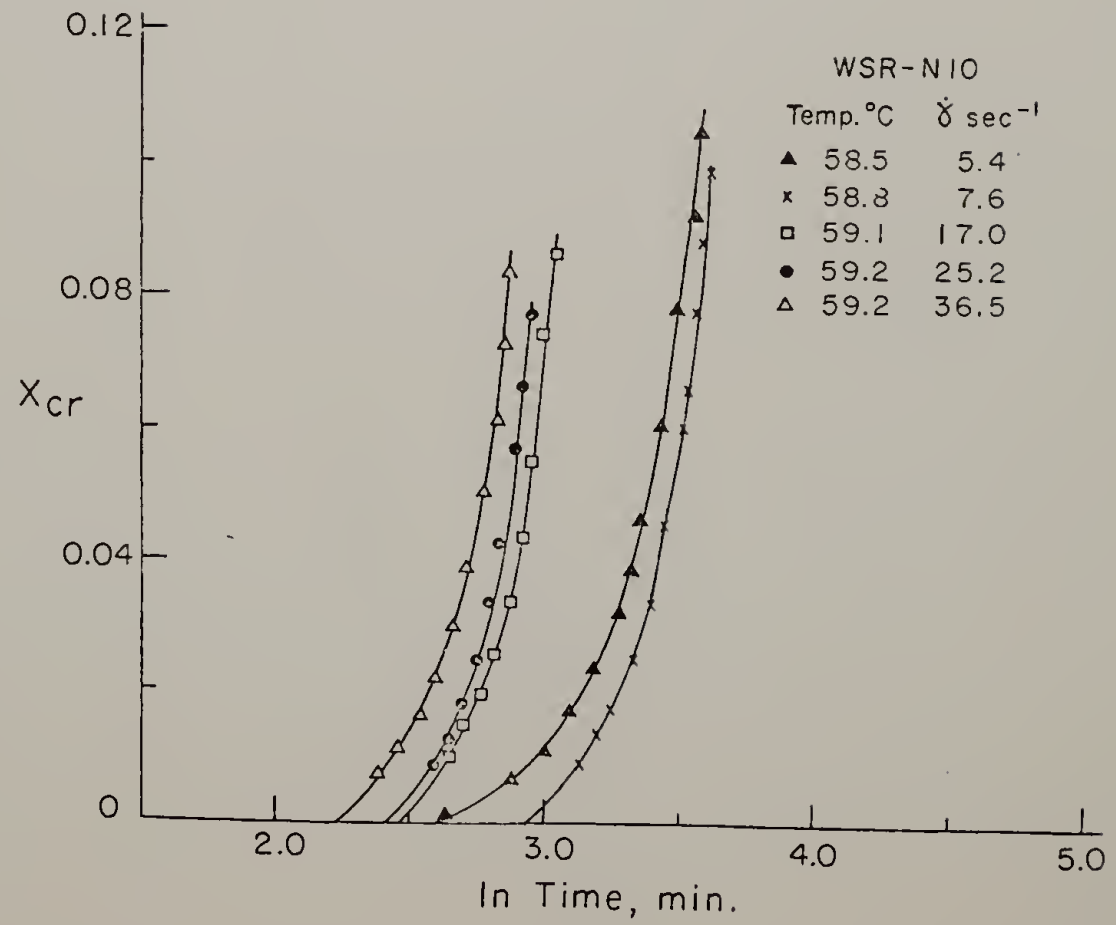
0.12
0.08
0.04
0
X_{cr}
WSR-N10
Temp. °C
$\dot{\delta}$ sec^{-1}
▲ 58.5 5.4
× 58.8 7.6
□ 59.1 17.0
● 59.2 25.2
△ 59.2 36.5
2.0
3.0
4.0
5.0
ln Time, min.

FIGURE 26 Degree of crystallinity versus ln time for PEO WSR-N10 at 59.6°C.

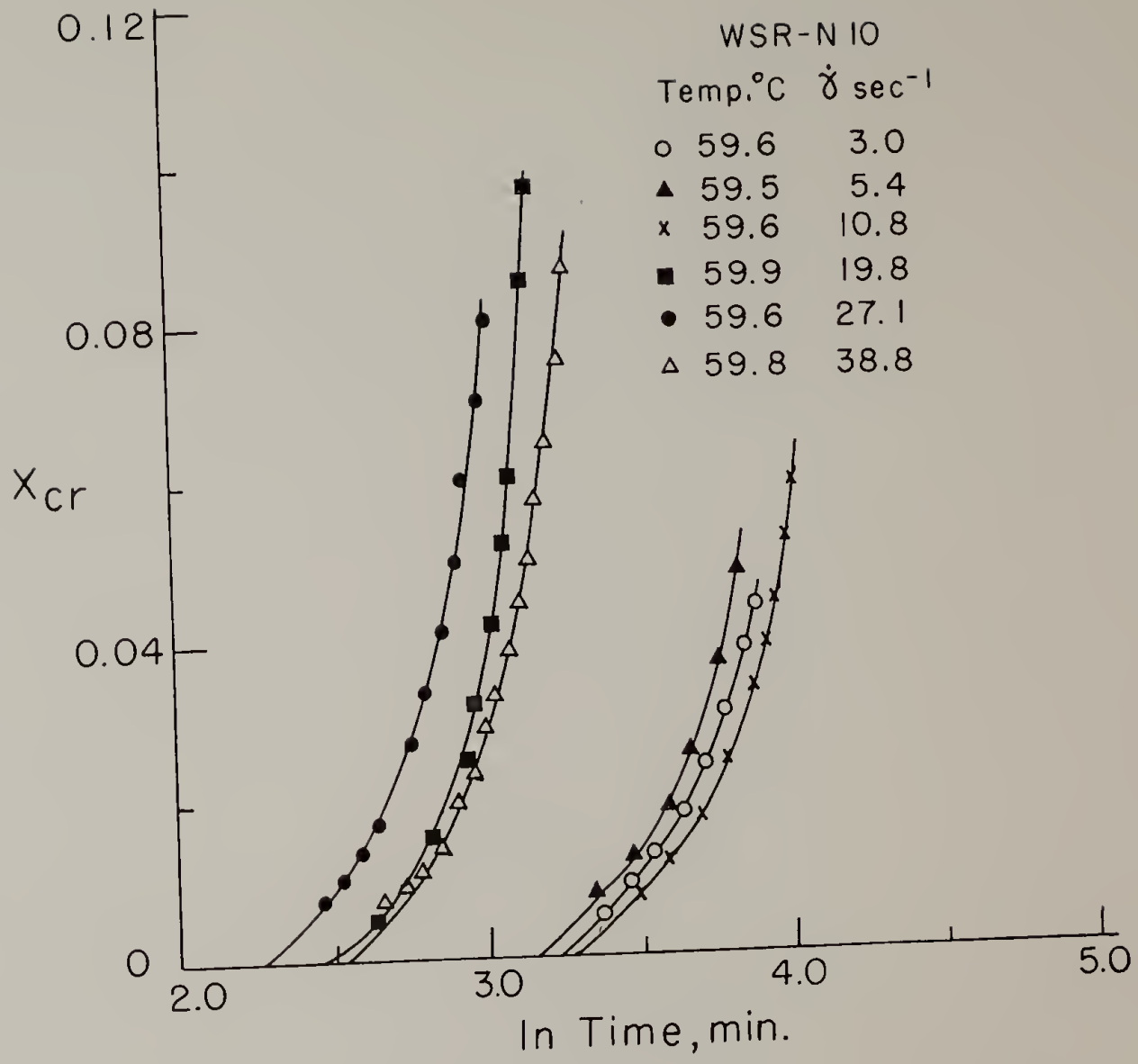
WSR-N 10
Temp.°C
$\dot{\delta}$ sec^{-1}
59.6 3.0
59.5 5.4
59.6 10.8
59.9 19.8
59.6 27.1
59.8 38.8
0.12
0.08
0.04
0
X_{cr}
2.0
3.0
4.0
5.0
ln Time, min.

Crystallization data at 61.0°C are shown in Figure 27. As expected the times are substantially longer than those for similar shear rates at lower temperatures. The induction times at this temperature show a decrease with increasing shear rate even with slightly increasing temperatures.

It is difficult to compare data for WSR-N10 due to the existence of an unknown temperature gradient across the sample prior to and during crystallization. On the basis of the temperature measurements at the outer cylinder-polymer interface, it appears that at constant temperature, shear rate has the same qualitative effect on induction time as it did in the PEO 6000 samples.

The crystallinity-time data for PCL are given in Figures 28-30. It can be seen that the induction times for experiments at any of the three crystallization temperatures decrease with increasing shear rate. The induction times at constant shear rate decrease with decreasing temperatures in all cases. Both results are similar to those found in the previous experiments. One interesting difference between PCL and the two PEO materials is that the range of induction times as a function of shear rate remains relatively constant for PCL as the crystallization temperature is increased, while the range for the other polymers increases with increasing temperatures.

FIGURE 27 Degree of crystallinity versus ln time for PEO WSR-N10 at 61.0°C.

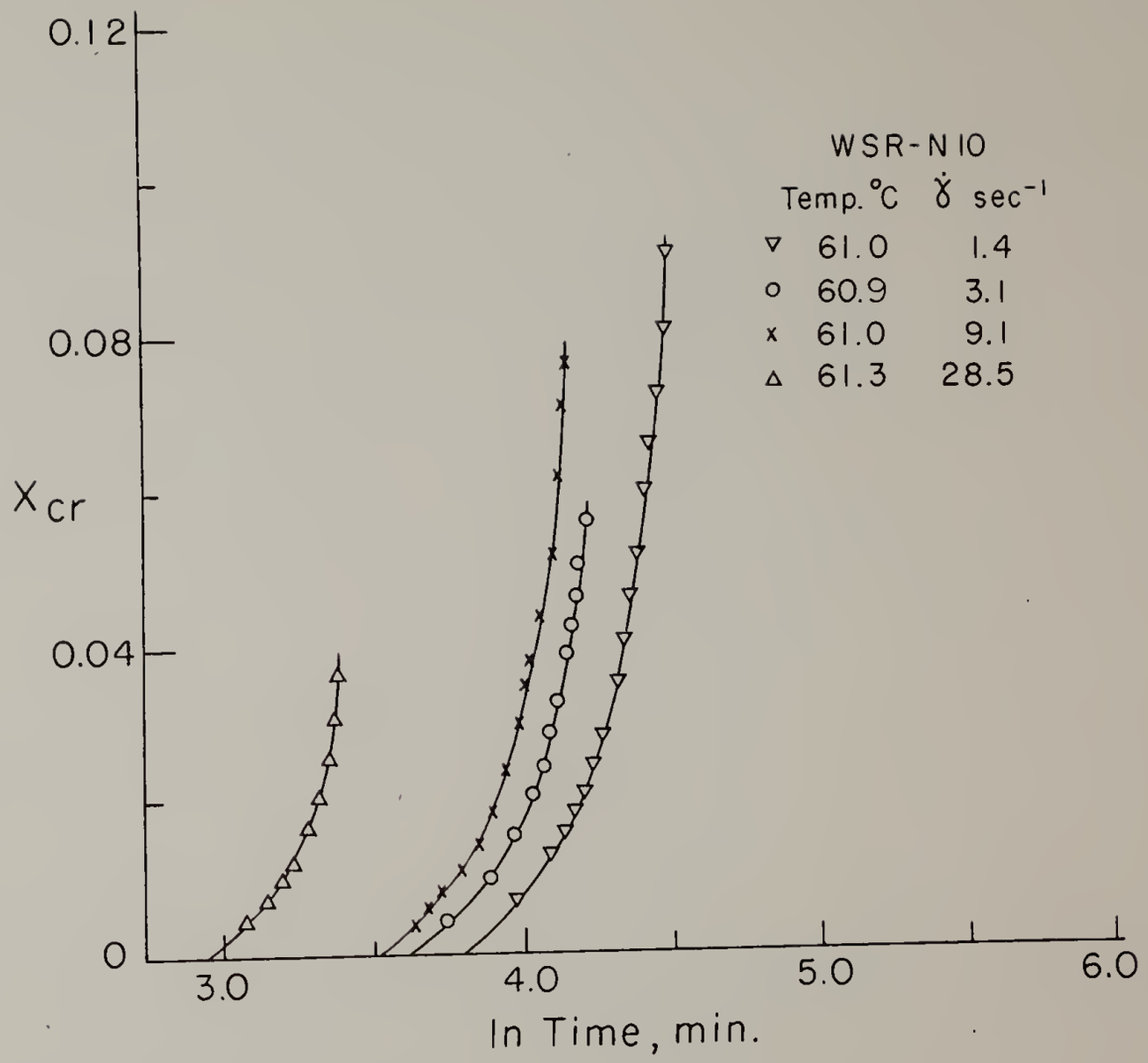
0.12
0.08
0.04
0
X_{cr}
3.0
4.0
5.0
6.0
ln Time, min.
WSR-N10
Temp. °C
$\dot{\gamma}$ sec^{-1}
61.0 1.4
60.9 3.1
61.0 9.1
61.3 28.5

FIGURE 28 Degree of crystallinity versus ln time for PCL at 48.1°C.

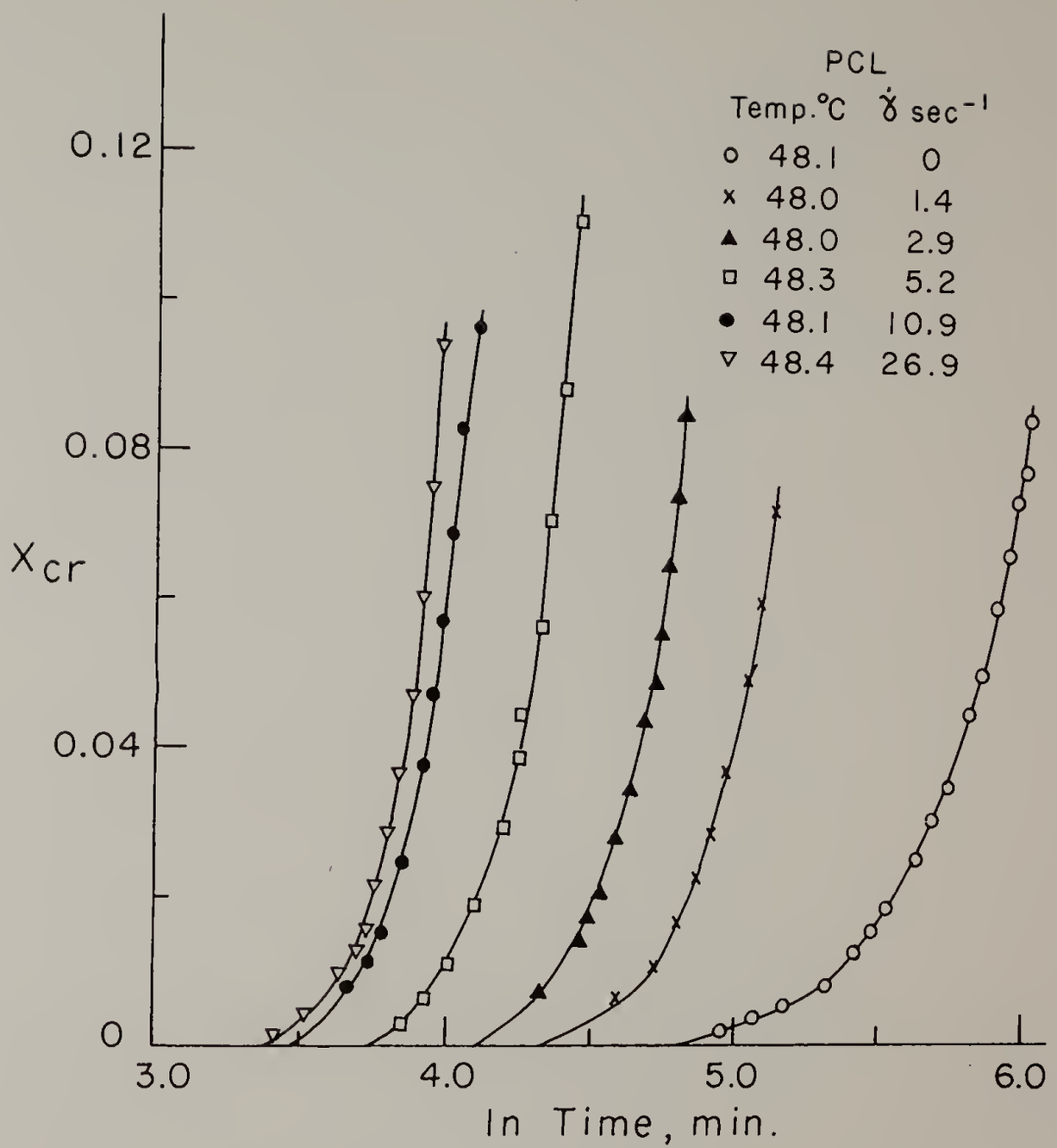
PCL
Temp.°C
$\dot{\gamma}$ sec^{-1}
48.1 0
48.0 1.4
48.0 2.9
48.3 5.2
48.1 10.9
48.4 26.9
0.12
0.08
0.04
0
X_{cr}
3.0
4.0
5.0
6.0
In Time, min.

FIGURE 29 Degree of crystallinity versus ln time for PCL at 49.8°C.

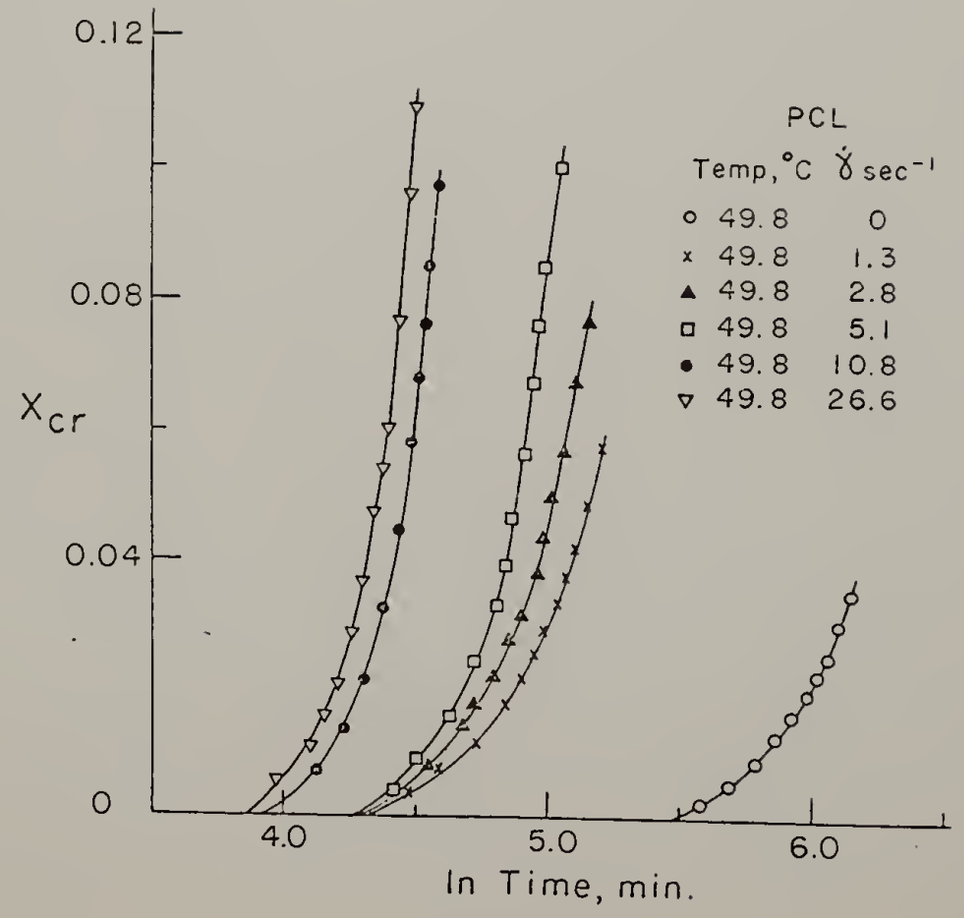
0.12
0.08
0.04
0
X_{cr}
4.0
5.0
6.0
ln Time, min.
PCL
Temp, °C
$\dot{\gamma}$ sec^{-1}
49.8 0
49.8 1.3
49.8 2.8
49.8 5.1
49.8 10.8
49.8 26.6

FIGURE 30 Degree of crystallinity versus ln time for PCL at 50.8°C.

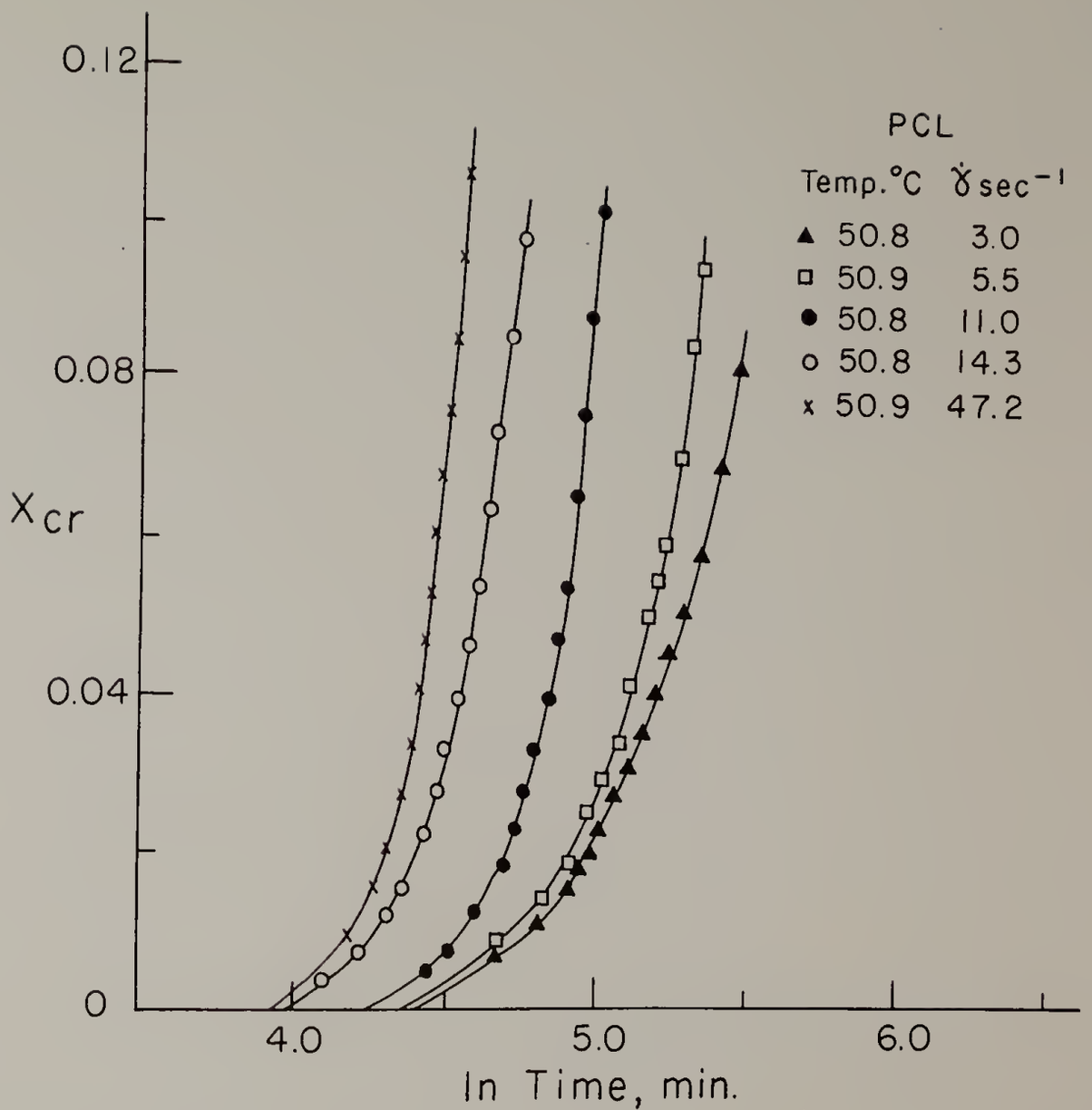
0.12
0.08
0.04
0
X_{cr}
4.0
5.0
6.0
ln Time, min.
PCL
Temp.°C
$\dot{\gamma}$ sec^{-1}
▲ 50.8 3.0
□ 50.9 5.5
● 50.8 11.0
○ 50.8 14.3
× 50.9 47.2

The saturation effect exhibited by these experiments suggests the existence of a limiting value of shear stress in the melt capable of enhancing crystallization. PCL has a higher zero shear viscosity and may reach this limiting value of stress at a lower shear rate. This could explain the narrower range of induction times. Ulrich[87] tested this concept by adding a small amount of high molecular weight material to the polyethylene oxide samples used in his experiments. The results for all shear rates tested were nearly identical indicating there is an effective shear stress limit.

Nucleation

Nucleation rate as a function of shear rate and crystallization temperature is plotted for PEO 6000 and PCL in Figures 15 and 16 respectively. The nucleation rate is seen to be very dependent on shear rate, especially at greater undercoolings. The dependence on shear is similar for both materials but the absolute value of nucleation rate in the PCL system is a factor of 100 larger than in the PEO 6000 samples.

The term nucleation rate can be somewhat misleading as shown in Figure 31. The data in this figure were taken from the work of Ulrich[87] and replotted to show nuclei formation as a function of time in PEO 20M, a polyethylene oxide sample with a molecular weight of approximately

FIGURE 31 Number of nuclei versus time for PEO 20M at 53.8°C and different shear rates.

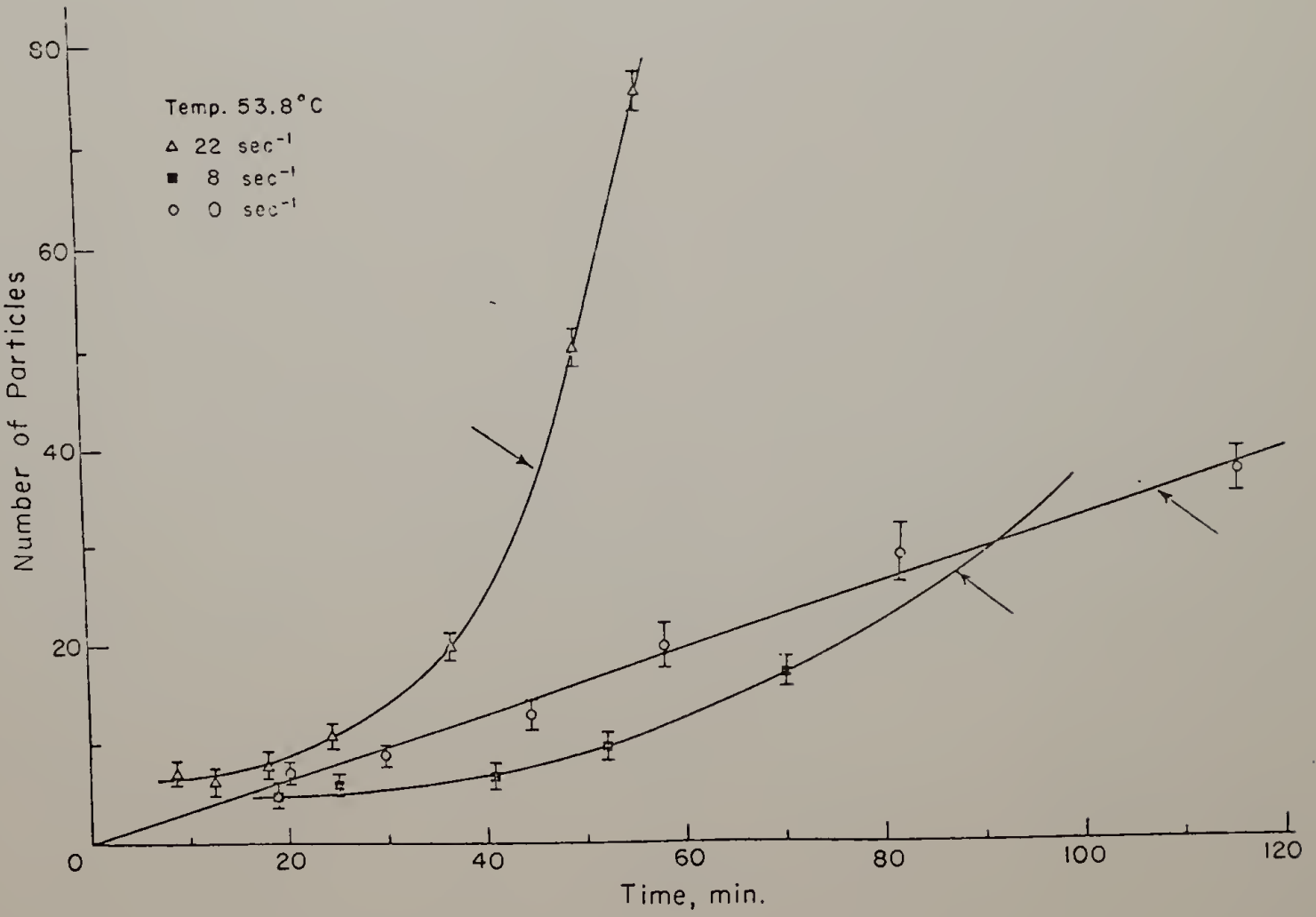
Temp. 53.8°C
△ 22 sec⁻¹
■ 8 sec⁻¹
○ 0 sec⁻¹
Number of Particles
0
20
40
60
80
0
20
40
60
80
100
120
Time, min.

20,000. The quiescent case shows a constant change in the number of nuclei per unit time and consequently has a single value of nucleation rate. The sheared cases are not linear and nucleation rate is changing with time. Single values for the nucleation rate in his work were calculated from the slope of the steepest portion of the curve. Ulrich originally expressed the data as number of particles versus fractional degree of conversion and the arrows in Figure 31 indicate the points where X_{cr} has reached a value of .0022.

Similar data are shown for PCL at 48.3°C for two different shear rates in Figure 32. At this temperature the higher shear rate run nucleates sooner and has a steeper slope throughout. Even for the low shear rate, the number of nuclei increases very rapidly at this temperature. Data at 49.9°C are shown in Figure 33. In this case a distinct difference is seen in the nucleation behavior for different shear rates, the higher shear rate case nucleating much more rapidly. Unfortunately, no data are available for the quiescent case at either temperature.

The results of these studies show that the nucleation process in sheared polymer melts is quite different from that found in the quiescent case. As shear rate is increased, the nucleation behavior becomes increasingly divergent from quiescent conditions as shown in Figure 31.

FIGURE 32 Number of nuclei versus time for PCL at 48.2°C and different shear rates.

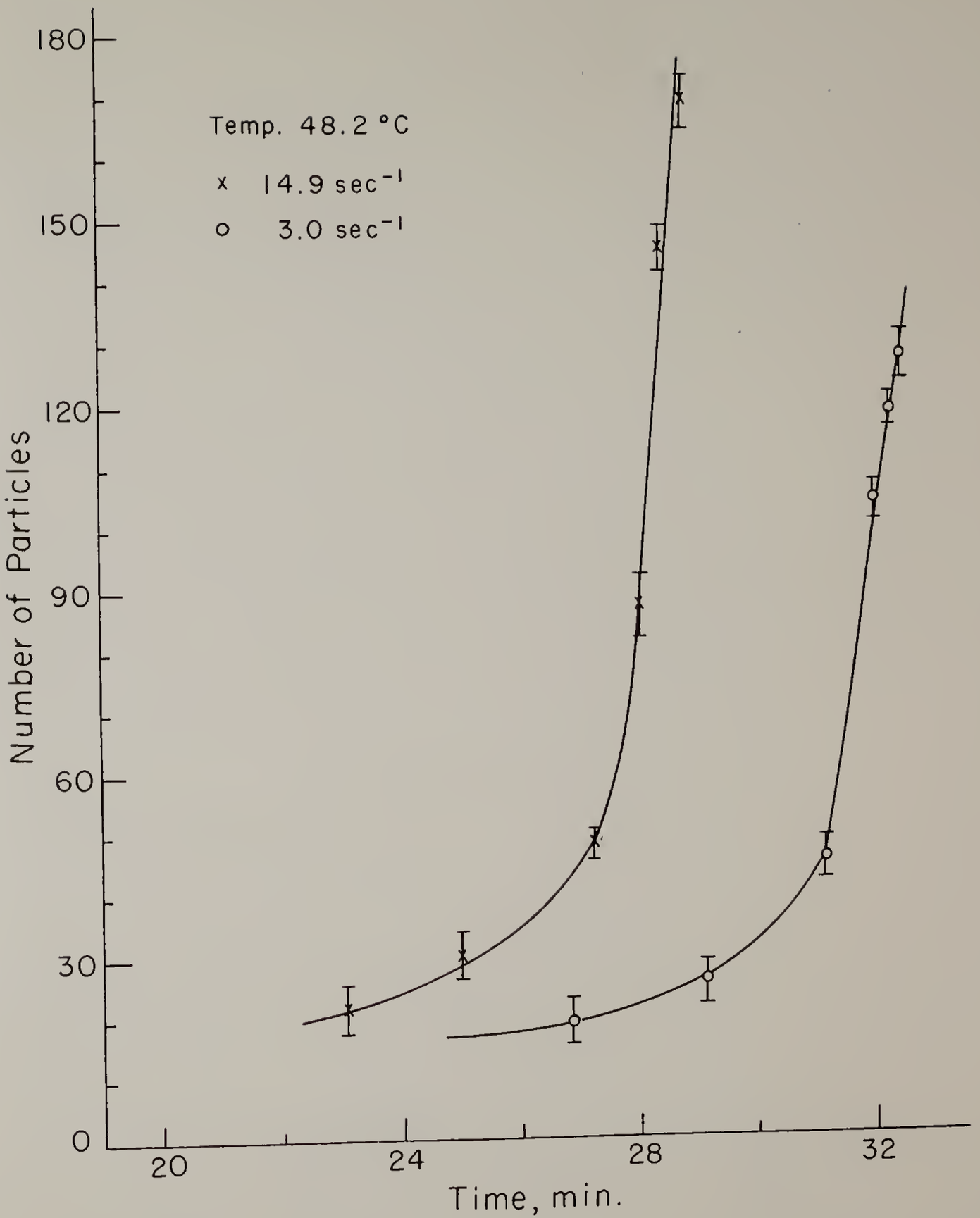
Temp. 48.2 °C
x 14.9 sec⁻¹
o 3.0 sec⁻¹
Number of Particles
180
150
120
90
60
30
0
20
24
28
32
Time, min.

FIGURE 33 Number of nuclei versus time for PCL at 49.9°C and different shear rates.

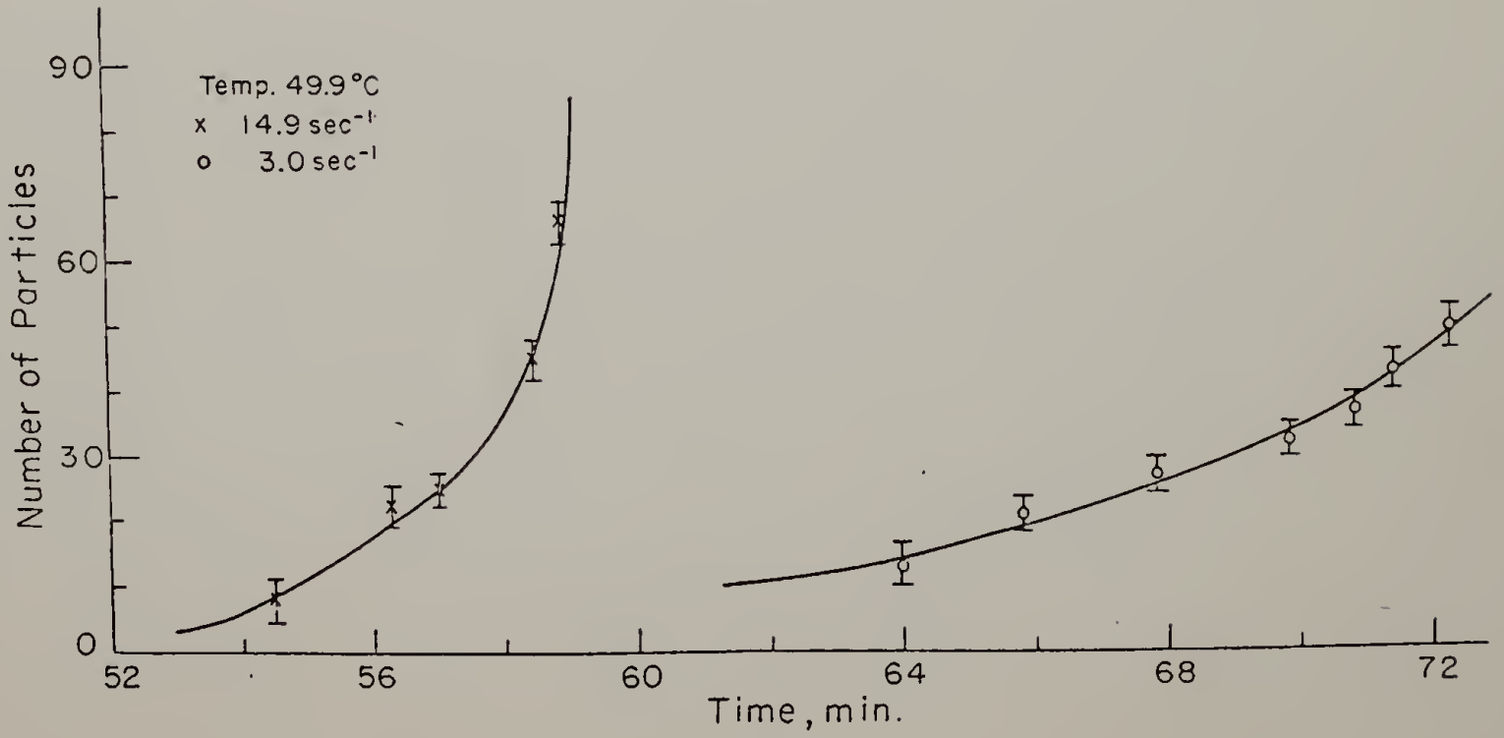
Temp. 49.9°C
x 14.9 sec⁻¹
o 3.0 sec⁻¹
Number of Particles
0
30
60
90
52
56
60
64
68
72
Time, min.

This fact clearly indicates that nucleation plays an important role in shear induced crystallization.

C H A P T E R V

DISCUSSION

Induction Shear Strain

The concept of induction shear strain has been discussed by Krueger and Yeh[77] and Lagasse and Maxwell[54]. It is defined in equation 19 where $\dot{\gamma}$ is the shear rate and t_i is the induction time. The induction

$$\gamma_i = t_i \dot{\gamma} \tag{19}$$

shear strain is dimensionless and the data are plotted in relative units. The findings of Krueger and Yeh show an induction strain dependent on temperature but independent of shear rate. The experiments in this case were conducted with a high density polyethylene sample at shear rates of 0.4 sec^{-1} to 10 sec^{-1}. The experiments of Lagasse and Maxwell show values of γ_i which are dependent on temperature, molecular weight and shear rate. Over the entire shear rate range of .01 sec^{-1} to 20 sec^{-1} the highest molecular weight polyethylene (M_w = 1.8 x 10^6) exhibited a constant induction shear strain. The lowest molecular weight material (M_w=1.9x10^5) approached a constant value of γ_i at the higher shear rates. This levelling

off could be seen at lower values of $\dot{\gamma}$ when temperature was reduced.

The results for induction shear strain in the PCL samples crystallized in the shearing dilatometer are shown in Figure 34. The value of γ_i is reduced with decreasing temperature as noted by the other researchers but is not independent of shear rate at any temperature.

The data for the PEO samples are shown in Figure 35. The solid lines represent data taken for PEO 6000 while the dotted lines are data from the WSR-N10 system. The same temperature dependence seen in the previous experiments is shown by these materials. The value of γ_i seems to approach a limit in the higher molecular weight fraction as the shear rate is reduced. At lower temperatures, this constant value persists to higher values of shear rate. The low molecular weight PEO behaves in a fashion similar to the PCL samples.

Lagasse and Maxwell have concluded that the controlling mechanism of shear accelerated crystallization is chain extension in the polymer melt. This extension has been attributed to the existence of chain entanglements acting as temporary crosslinks[106]. The reduction in density of crosslinks has been put forth to explain the decrease in melt viscosity with increasing shear rate[107]. The molecular weight necessary for entanglements to occur is customarily taken as that value at which the slope of

FIGURE 34 Induction shear strain versus shear rate for PCL at different crystallization temperatures.

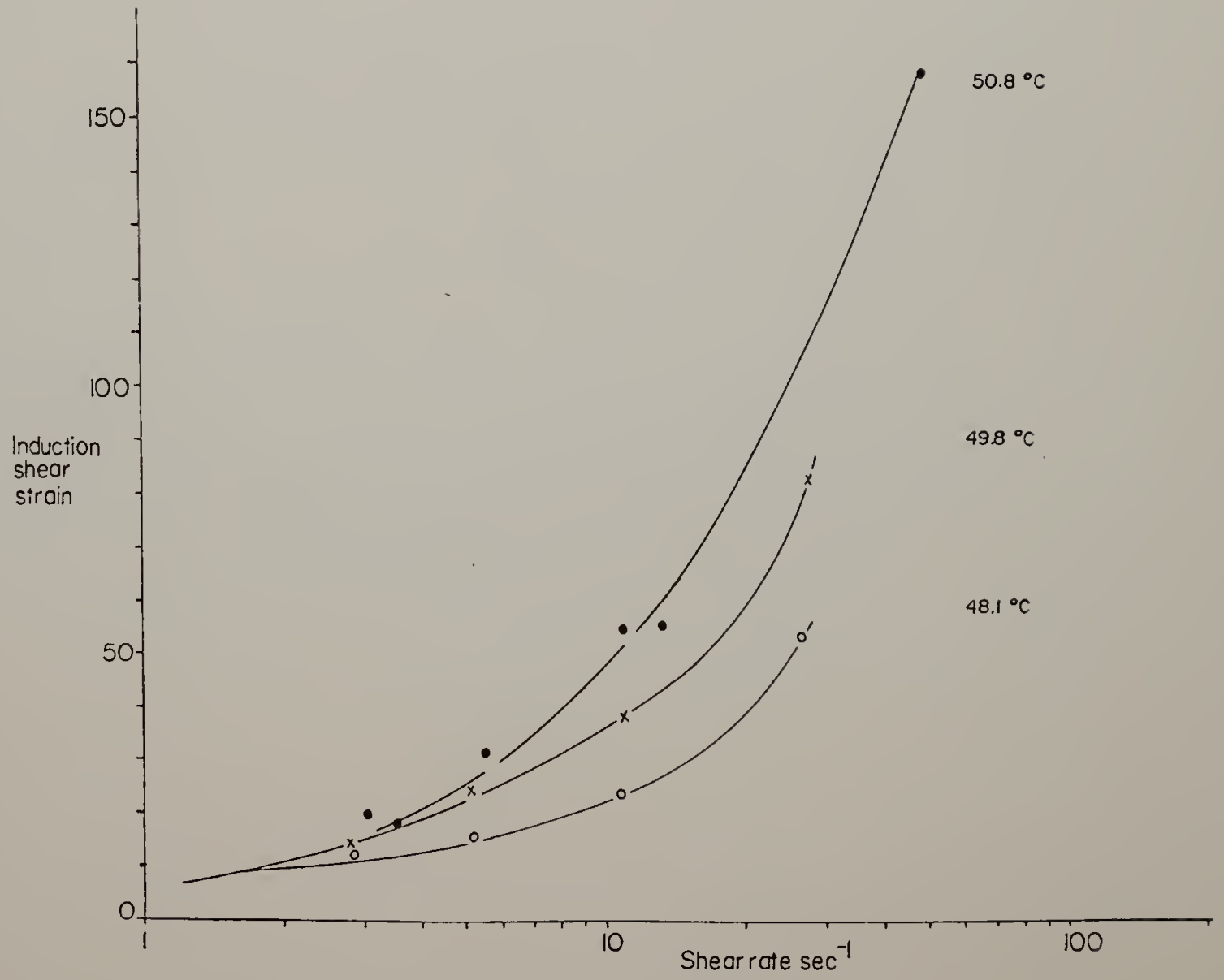
150
100
50
0
Induction shear strain
1
10
100
Shear rate sec⁻¹
50.8 °C
49.8 °C
48.1 °C

FIGURE 35 Induction shear strain versus shear rate for PEO at different crystallization temperatures.

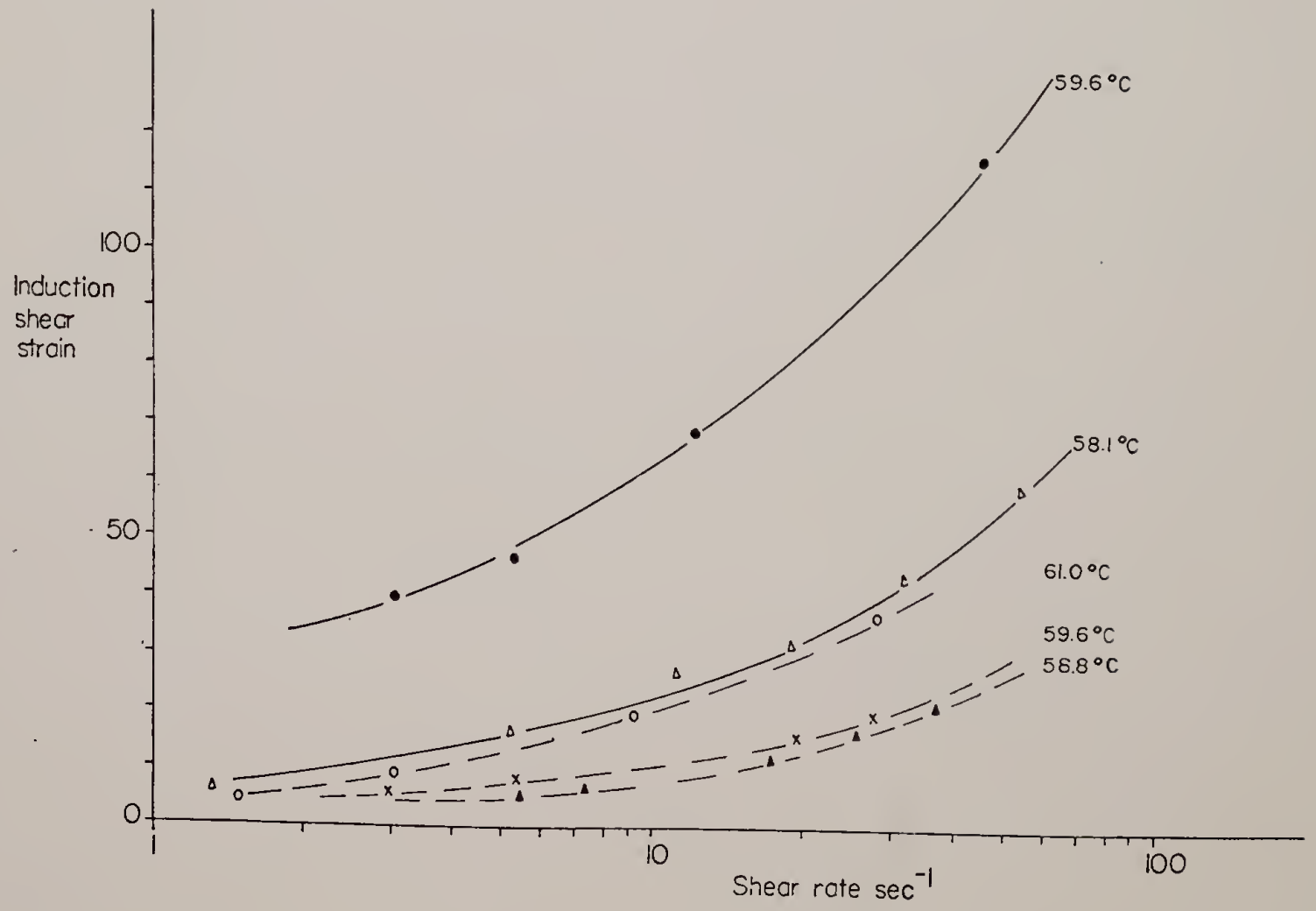
59.6 °C
58.1 °C
61.0 °C
59.6 °C
56.8 °C
100
50
0
Induction shear strain
1
10
100
Shear rate sec⁻¹

the viscosity versus molecular weight curve changes abruptly from 1 to 3.4[108]. Porter and Johnson[109] and Teramoto and Fujita[110] have measured the viscosity as a function of molecular weight for polyethylene oxide. Their results show the change in slope to occur over a molecular weight range whose intermediate value is around 10,000.

The induction shear strain results may be interpreted in light of the entanglement concept. Increasing shear rate would serve to increase the occurrence of disentanglement limiting the ultimate amount of chain segment extension achieved in steady shear flow. Therefore, if more rapid crystallization were due to chain extension, it would be expected that shear rate would become increasingly less effective in accelerating the crystallization process. Alternatively, as shear rate is increased by a given factor, the non-Newtonian behavior of the melt, described by an equation such as 20

$$\tau_{21} = K \dot{\gamma}^{n} \qquad \text{where } n < 1 \tag{20}$$

results in a smaller increase in τ_{21}, the shear stress. If one can consider the molecular chain extension in a first approximation to be roughly proportional to imposed shear stress, then the same conclusion concerning the decreasing effectiveness of shear rate is reached. This decreasing effectiveness of increasing shear rate is observed in

WSR-N10 samples as increased values of induction shear strain.

The constant value of γ_i in the experiments of Lagasse and Maxwell may in part be due to the time scale of the experiment which was in the range of .1 to 100 seconds. The authors' conclusion that transient effects in shear flow startup control accelerated crystallization seems to be valid in their experiments but does not appear to be applicable in this work.

Shear enhancement of crystallization also occurs for the PEO 6000 and PCL samples which have molecular weights very similar to the critical entanglement values. The induction shear strain never exhibits a plateau value for the shear rates studied and the effect of shear rate has an increasingly diminished effect in accelerating the transformation process. Both of these materials were found to be Newtonian and follow equation 20 with a value of n equal to 1. Hence, an increase in shear rate yields a proportional increase in shear stress. It may be concluded that in these systems an increase in melt stress does not result in a proportional increase in chain extension. Chain extension must also reach some limiting value as shown by the inability of high shear rates to further decrease the induction time.

Nucleation Rate and Temperature Analysis

An expression for the kinetics of polymer nucleation was originally formulated by Turnbull and Fisher[1] and given in equation 1. Hoffman and Lauritzen have also theoretically treated the kinetics of nucleation[111,112] and have derived expressions for the work required to form a critical size nucleus, ΔG^*, in the Fisher-Turnbull equation. These expressions are given below where W contains lateral and surface free energy

$$\dot{I} = I_o \exp\left(\frac{-\Delta F^*}{RT}\right) \exp\left(\frac{-W(T_m^o)^2}{T(\Delta T)^2}\right) \tag{21}$$

$$\dot{I} = I_o \exp\left(\frac{-\Delta F^*}{RT}\right) \exp\left(\frac{-W\, T_m^o}{T\, \Delta T}\right) \tag{22}$$

contributions as well as the heat of fusion and geometric and Boltzman's constant. The form given in equation 21 describes the case for a three dimensional nucleus while equation 22 applies to two dimensional nucleus formation. The natural logarithm of nucleation rate plotted versus $(T_m^o)^2/T(\Delta T)^2$ or $T_m^o/T\Delta T$ should yield a straight line with a slope of -W. It has been found by some researchers that a given set of data may fit each equation equally well[7] or the fit may be better for one form than the other[7,10]. Barnes et al.[8] used equation 22 with success to describe several molecular weight fractions of polyethylene oxide

and this will be the form of the equation used in this analysis.

Tan and Gogos[104] have formulated a treatment of crystallization kinetics in terms of the observed induction time. It is assumed that the nucleation rate, $\dot{I}$, is proportional to the reciprocal of the induction time. Equation 22 may then be recast as equation 23. It should be noted here that

$$\frac{1}{t_i} = I_o \exp\left(\frac{-\Delta F^*}{RT}\right) \exp\left(\frac{-W\ T_m^o}{T\Delta T}\right) \qquad (23)$$

Tan and Gogos employed equation 21 to describe the temperature dependence in their treatment. The formulation of equation 23 assumes that the nucleation behavior in sheared systems has this form and does not contain any additional terms. Theoretical treatments describing nucleation in sheared solutions have included additional terms[21].

The energy required for interfaced transport, ΔF^*, was evaluated by Tan and Gogos after a method formulated by Hoffman[113]. The resulting nucleation equation is given below. The value of

$$\ln \frac{1}{t_i} = \ln I_o - \frac{4120}{R(51.6+T-T_g)} - \frac{W\ T_m^o}{T\Delta T} \qquad (24)$$

the glass transition temperature, T_g, is around 200°K for PEO[98] and 213°K for PCL[90]. The changes in Tg with molecular weight and the resulting effect on the transport term

will be discussed later. The differences in undercooling used in these experiments are not expected to influence ΔF^* for a given material. Plots of $\ln \frac{1}{t_i}$ versus $T_m^o/T\Delta T$ for the three materials studied are given in Figures 36-38. It is sometimes necessary to adjust the value of T_m^o to produce linear plots[104,10] but this was not needed in this data.

The parallel straight lines for each shear rate agree with the results found by Tan and Gogos. It was possible to shift these lines into coincidence in their work using a correction factor of 1.5 $\ln \dot{\gamma}$ as shown in equation 25. This

$$\ln \frac{1}{t_i} - 1.5 \ln \dot{\gamma} + \frac{4120}{R(T-Tg+51.6)} = \ln I_o - \frac{W T_m^o}{T\Delta T} \qquad (25)$$

exact correction term does not produce the desired shift in this work but the $\ln \dot{\gamma}$ dependence seems to be valid for all sets of data in these experiments. Ulrich[87] attempted a similar analysis using measured experimental values of the nucleation rate. It was found that the plots produced were not straight lines for the sheared cases. The deviations from linearity were assumed to be due to uncertainties in the data.

Several interesting results may be derived from Figures 36-38. The parallel slopes at different shear rates indicate that the parameters in W are constants for

FIGURE 36 Ln $1/t_i$ versus $T_m^{\circ}/T(\Delta T)$ for PEO 6000 at different shear rates.

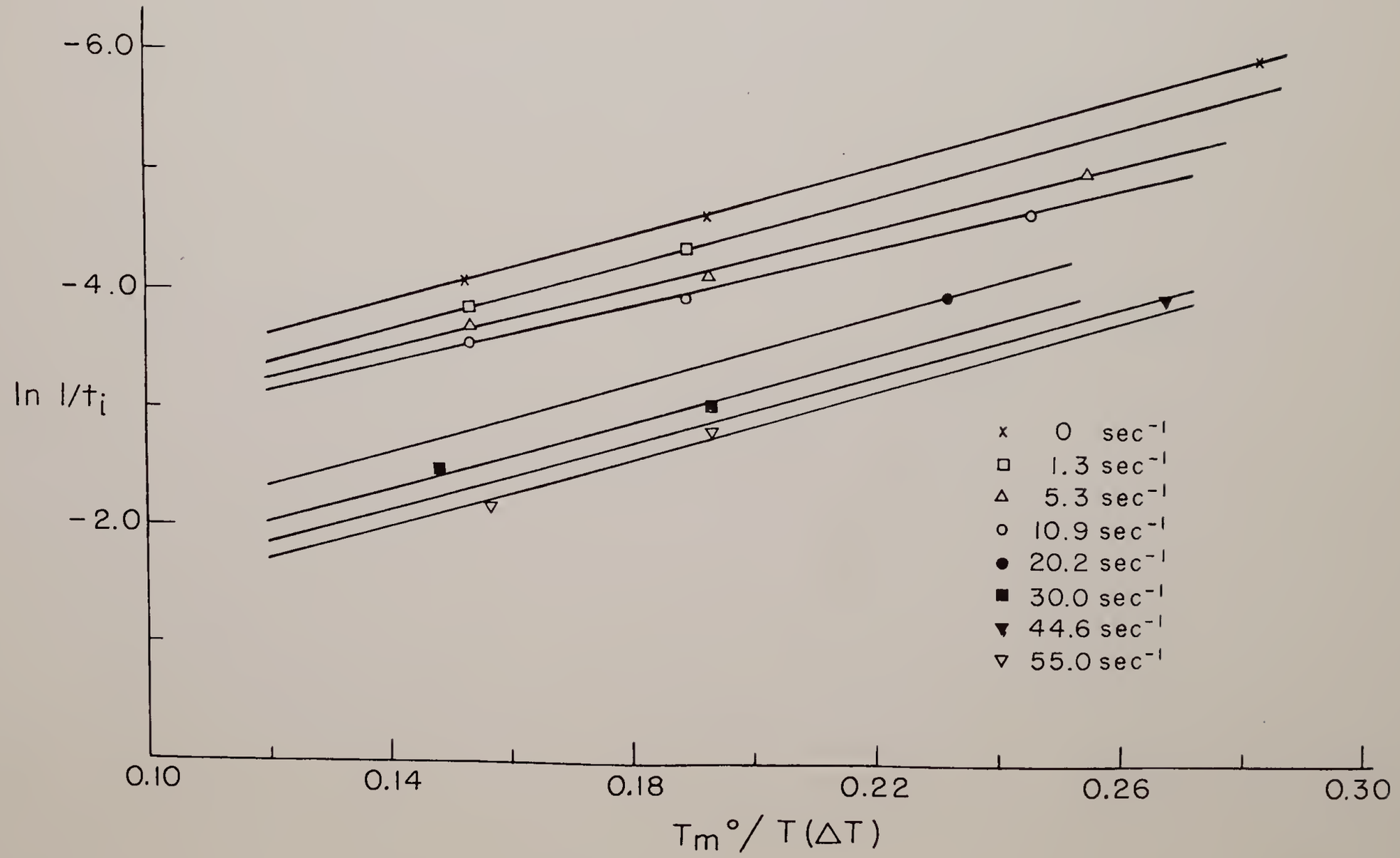
-6.0
-4.0
-2.0
ln 1/t_i
0.10
0.14
0.18
0.22
0.26
0.30
$T_m°/\ T(\Delta T)$
x 0 sec^{-1}
□ 1.3 sec^{-1}
△ 5.3 sec^{-1}
○ 10.9 sec^{-1}
● 20.2 sec^{-1}
■ 30.0 sec^{-1}
▼ 44.6 sec^{-1}
▽ 55.0 sec^{-1}

FIGURE 37 Ln $1/t_i$ versus $T_m^o/T(\Delta T)$ for PEO WSR-N10 at different shear rates.

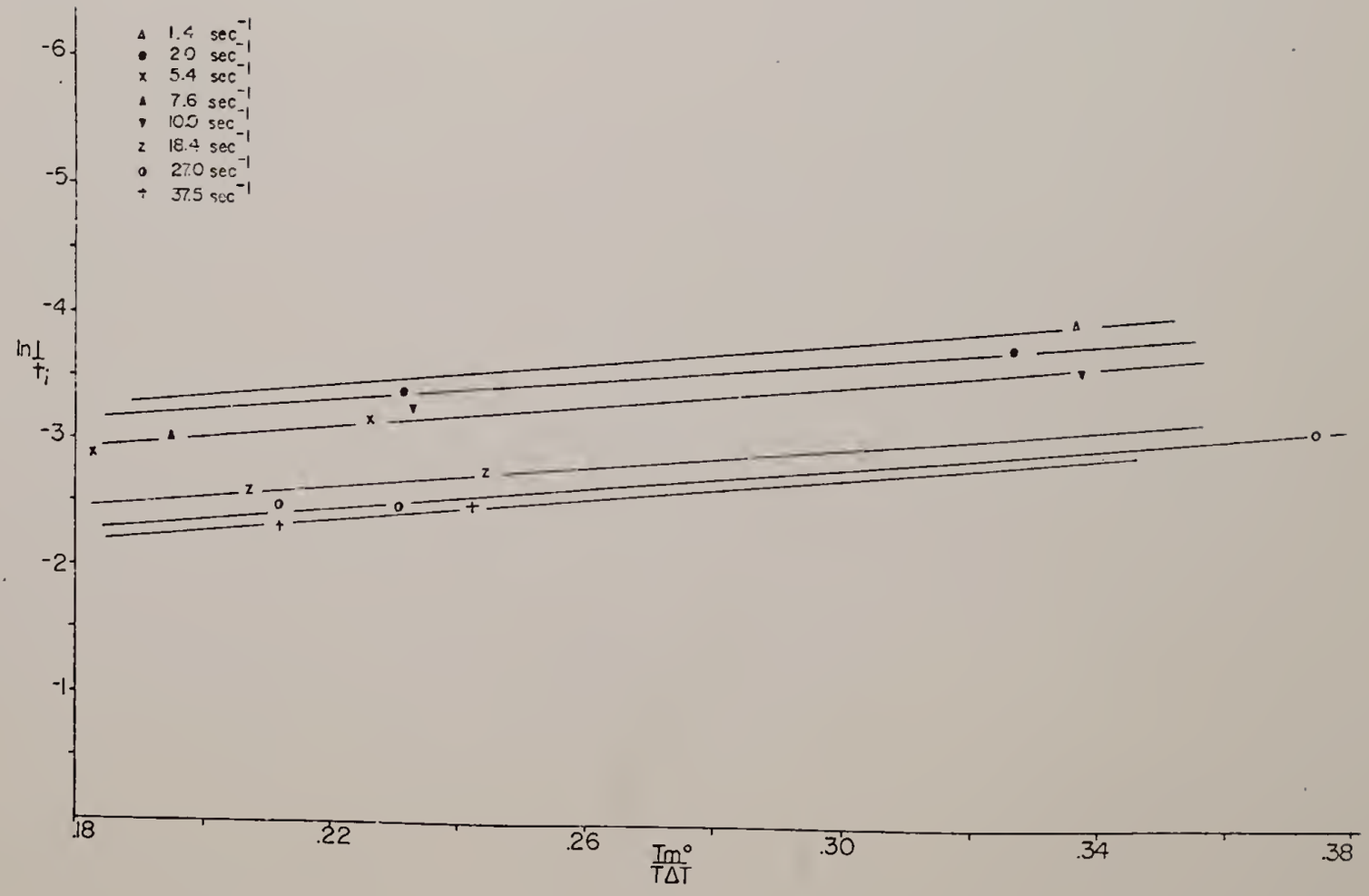
Δ 1.4 sec⁻¹
● 2.0 sec⁻¹
x 5.4 sec⁻¹
▲ 7.6 sec⁻¹
▼ 10.0 sec⁻¹
z 18.4 sec⁻¹
o 27.0 sec⁻¹
+ 37.5 sec⁻¹
-6
-5
-4
-3
-2
-1
ln 1/t_i
.18
.22
.26
.30
.34
.38
Tm°/TΔT

FIGURE 38 Ln $1/t_i$ versus $T_m^o/T(\Delta T)$ for PCL at different shear rates.

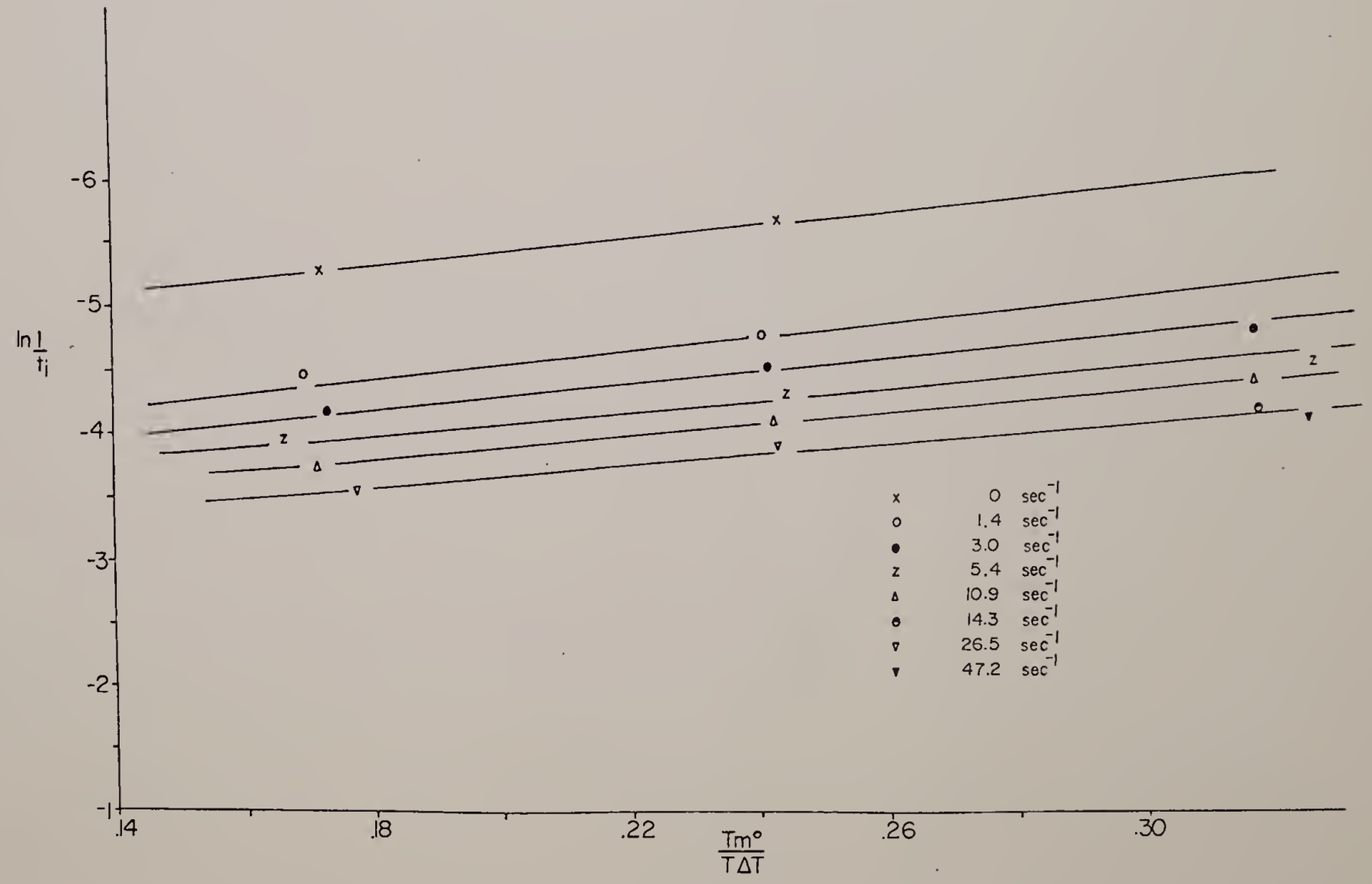
-6
-5
-4
-3
-2
-1
ln 1/t_i
.14
.18
.22
.26
.30
Tm°/TΔT
x 0 sec⁻¹
o 1.4 sec⁻¹
● 3.0 sec⁻¹
z 5.4 sec⁻¹
Δ 10.9 sec⁻¹
⊖ 14.3 sec⁻¹
▽ 26.5 sec⁻¹
▼ 47.2 sec⁻¹

a given material. It is not expected that shear would substantially alter these terms. The difference in values of slope manifested for the two PEO materials is likely due to the contribution of two terms in equation 25. The T_g for PEO 6000, which has a molecular weight close to the entanglement value, should be substantially higher than that of the high molecular weight WSR-N10. Consequently, the correction term for interfacial transport would be expected to have different values for the two materials. This contribution should be small unless the value of T_g is very high. The second contribution to the change in slope is due to the factors in W. It is not unreasonable to assume that the heat of fusion could be altered by the incorporation in the growing crystal of a large number of chain ends for the lower molecular weight material. Certain geometric terms could also be slightly influenced by molecular weight changes.

The difference in slopes for the three materials leads to some interesting consequences. Many authors have thought of shear stress (or for the purposes of this work shear rate) in the melt as producing additional undercooling termed "stress induced supercooling"[87,20,52]. Estimates of this quantity may be made in Figures 36-38 by shifting from one shear rate curve to another at the same induction time. If the quiescent case is used as a reference, the

additional undercooling that would be seen by a quiescent melt with the same induction time as that in a sheared melt at the same imposed crystallization temperature can be calculated.

It is difficult to obtain quantitative data for WSR-N10 due to the long extrapolations which must be made and the lack of reliable quiescent data. Two sets of sheared runs were compared at two similar rate values for PEO 6000 and WSR-N10. For WSR-N10, increasing the shear rate from 7.6 sec^{-1} to 27 sec^{-1} increased the crystallization temperature at the same induction time from 58.8°C to 61.0°C. An increase in shear rate from 5.3 sec^{-1} to 30 sec^{-1} for PEO 6000 only changed the temperature from 57.7°C to 58.5°C. This demonstrates that the stress induced undercooling is substantially greater in the high molecular weight material. The slope of the curve in Figure 38 indicates that the stress induced undercooling in PCL is greater than that in PEO 6000 but not equal to that in WSR-N10.

Ulrich[87] examined his nucleation data in a similar fashion and compared the calculated ΔT to a value obtained from a modified version of a theory by Krigbaum and Roe[20] proposed by Haas and Maxwell[52]. The results were found to correlate reasonably well at small imposed undercoolings and low shear rates. The value of the first normal stress difference in the melt is necessary to calculate the appropriate induced undercooling from the theory. This data is

not available at this time but could be easily obtained. The comparison of the two predictions would be quite interesting.

Conclusions

The results of this research have shown that the imposition of shear on a crystallizing polymer melt greatly accelerates the crystallization process and reduces the characteristic induction time. The Avrami exponent, indicative of the speed of the transformation process, was found to increase with increasing shear rate and approach a limiting value in some cases for the high molecular weight material.

Shear stress rather than shear rate appears to be the more important parameter affecting the crystallization process. It is thought that the entanglements present in the polymer melt serve as temporary crosslinks forcing chain segments between them in a stressed system to be extended. This chain orientation facilitates the nucleation process which effectively produces more crosslinks leading to accelerated crystallization. The entanglements in the melt are transitory in nature and are affected by the temperature of the system and the imposed shear.

It was found that the effect of shear on induction time approached a limit in the low entanglement density

systems. This indicates that, due to relaxation processes and other factors, the chains can only be oriented a certain amount. If this conclusion is sound, nucleation behavior should also show saturation effects at high shear levels and this trend has been observed by Wolkowicz[114] for sheared polybutene-1 melts. Nucleation behavior, as manifested by induction time, is somewhat obscure in the higher entanglement density system. The high shear rates cause substantial viscous dissipation which increases the temperature of the system and retards nucleation. This is counteracted by increasing orientation due to increased imposed stress. The data indicate there is a point above which the temperature effect dominates and the transformation is no longer accelerated with increasing shear.

The gross transformation kinetics can also be analyzed as a function of stress in terms of the Avrami parameter. At high shear rates in the low molecular weight systems, the orientation is limited and nucleation behavior is similar. As nuclei formation increases, the crosslinking effect will increase. The melt then approximates a higher entanglement density system which may be oriented more fully by higher shear. This explains the observation that the transformation process is accelerated more at higher shear rates (higher Avrami n) even though induction times are similar. This increased acceleration is not a large effect in most cases.

In conclusion, it appears that the predominant factor affecting accelerated crystallization in sheared systems is the increase in nucleation rate due to orientation in the melt. The higher molecular weight polyethylene oxide subjected to the same shear conditions and undercooling as a lower molecular weight material exhibited a substantially smaller induction time, indicating a more rapid nucleation process. It is difficult to separate the growth process from the nucleation process which proceeds it but gross transformation data indicate that the growth process is not significantly affected by increased shear.

C H A P T E R VI

FURTHER RESEARCH

Instrument Modifications

These experiments have produced some interesting results which indicate that very small amounts of shear are sufficient to accelerate the transformation process. This fact coupled with the viscous heating problem and the shear saturation effect suggest a further reduction in the shear rate capabilities of the instrument to the range .1 sec^{-1} to 10 sec^{-1} would be desirable. This could easily be accomplished by the addition of the appropriate gear reductor.

The study of polyethylene oxide produced valuable information but it is thought that the study of more industrially significant materials would be appropriate. It is quite possible that these materials would have substantially greater viscosities that PEO WSR-N10. Reduction of gap thickness may then be necessary to reduce viscous dissipation.

It is now impossible to recover a crystallized sample from the dilatometer without melting it and this is seen as a severe limitation of the instrument. If the outer cylinder was appropriately modified to facilitate

this process, experimental techniques such as X-ray diffraction, electron microscopy, light scattering and thermal analysis could be employed to study the crystallite orientation and size and final degree of crystallinity in the samples as a function of shear rate and undercooling.

The limited correlations of shear stress versus degree of crystallinity lead to some interesting conclusions. To remove uncertainty inherent in the correlation technique, the stress increase and degree of crystallinity should be measured concurrently and not in two separate experiments. The strain gauge network should be redesigned to produce a more sensitive output. This could be accomplished in several ways with minimal difficulty. Realignment and possible remachining may be necessary to reduce the noise fluctuations in the system.

New Experiments

Shear has been shown to have a dramatic effect on the nucleation process. The basic mechanism of this enhanced nucleation still remains unclear at this time. Some experiments have been conducted to assess the effect of dispersed inert impurities on nucleation but the results are nebulous. This type of investigation with size and volume fraction of particles as variables bears repeating.

Molecular orientation under shear has been postulated as a source of increased nucleation. It should be

possible to determine orientation using birefringence measurements in the melt before and during crystallization. The apparatus used in this study to measure nuclei formation could be adapted for this purpose. This technique along with the use of monodisperse molecular weight materials could provide useful information to explain shear saturation and other effects.

LITERATURE CITED

1. J. C. Fisher and D. Turnbull, J. Chem. Phys., 17, 71 (1949).
2. F. VonGoler and G. Sachs, Z. Physik, 77, 281 (1932).
3. M. Avrami, J. Chem. Phys., 7, 1103 (1939).
4. M. Avrami, J. Chem. Phys., 8, 212 (1940).
5. M. Avrami, J. Chem. Phys., 9, 177 (1941).
6. U. R. Evans, Trans. Faraday Soc., 41, 365 (1945).
7. L. Mandelkern, Crystallization of Polymers, McGraw-Hill, New York, 1963.
8. W. J. Barnes, W. G. Leutzel, and F. P. Price, J. Phys. Chem., 65, 1742 (1961).
9. A. Sharples, Polymer, 3, 250 (1962).
10. L. Mandelkern, J. Appl. Phys., 25, 830 (1954).
11. W. Banks and A. Sharples, J. Polymer Sci. A, 2, 4059 (1964).
12. H. G. Kim and L. Mandelkern, J. Polymer Sci. A2, 6, 181 (1968).
13. J. W. Stafford, J. Polymer Sci. C, 42, 837 (1973).
14. J. N. Hay, J. Polymer Sci. Polymer Letters, 14, 543 (1976).
15. P. J. Flory, J. Chem. Phys., 15, 397 (1947).
16. M. V. Volkenstein, Configurational Statistics of Polymer Chains, John Wiley, New York, 1963.
17. K. J. Smith, Polym. Eng. Sci., 16, 168 (1976).

18. R. J. Gaylord and D. J. Lohse, Polym. Eng. Sci., 16, 163 (1976).

19. R. J. Gaylord, J. Polymer Sci. A2, 14, 1827 (1976).

20. W. R. Krigbaum and R. J. Roe, J. Polymer Sci. A, 2, 4391 (1964).

21. A. J. McHugh, J. Appl. Polymer Sci., 19, 125 (1975).

22. A. Peterlin, Pure Appl. Chem., 12, 563 (1966).

23. L. Mandelkern, J. Appl. Phys., 26, 443 (1955).

24. L. R. G. Treloar, Trans. Faraday Soc., 37, 84 (1941).

25. A. N. Gent, Trans. Faraday Soc., 50, 521 (1954).

26. E. H. Andrews, Proc. Royal Soc., A277, 562 (1964).

27. H. G. Kim and L. Mandelkern, J. Polymer Sci. A2, 6, 181 (1968).

28. J. T. Judge and R. S. Stein, J. Appl. Phys., 32, 2357 (1961).

29. T. Kawai, M. Iguchi, and H. Tonami, Kolloid Z. and Z. Polym., 221, 28 (1967).

30. A. J. Pennings and A. M. Kiel, Kolloid Z. and Z. Polym. 205, 160 (1965).

31. K. Yamaura, S. Matsuzawa, and K. Ide, J. Macromol. Sci. B, 4, 761 (1970).

32. S. Matsuzawa, K. Yamaura, and H. Yanagisawa, Kolloid Z. and Z. Polym., 250, 20 (1972).

33. A. G. Wikjord and R. St. John Manley, J. Macromol. Sci. B, 4, 397 (1970).

34. Z. Pelzbauer and R. St. John Manley, J. Macromol. Sci. B, 4, 761 (1970).

35. P. H. Lindenmeyer, SPE Trans., 4, 1 (1964).

36. A. Keller and M. J. Machin, J. Macromol. Sci. B, 1, 41 (1967).

37. A. G. Wikjord and R. St. John Manley, J. Macromol. Sci B, 2, 501 (1968).

38. M. R. Mackley, Colloid and Polymer Sci., 253, 261 (1975).

39. D. Krueger and G. S. Y. Yeh, J. Macromol. Sci. B, 6, 431 (1972).

40. A. J. Pennings, J. M. A. van der Mark, and H. C. Booij, Kolloid Z. and Z. Polym., 236, 99 (1970).

41. G. I. Taylor, Proc. Royal Soc. London, A146, 501 (1934).

42. G. I. Taylor, Phil. Trans. Royal Soc. London, A223, 289 (1923).

43. A. J. Pennings and M. F. J. Pijpers, Macromolecules, 3, 261 (1970).

44. A. J. Pennings, A. Zwijnenburg, and R. Lageveen, Kolloid Z. and Z. Polym., 251, 500 (1973).

45. M. R. Mackley, Colloid and Polymer Sci., 251, 373, (1973).

46. B. Hlavacek and F. A. Seyer, Kolloid Z. and Z. Polym., 243, 32 (1971).

47. F. A. Seyer and B. Hlavacek, Kolloid Z. and Z. Polym., 251, 108 (1973).

48. S. Torza, J. Polymer Sci. A2, 13, 43 (1975).

49. A. J. McHugh and J. M. Schultz, Kolloid Z. and Z. Polym., 251, 13 (1973).

50. M. R. Mackley and A. Keller, Phil. Trans. Royal Soc. London, A278, 29 (1975).

51. M. J. Hill and A. Keller, J. Macromol. Sci. B, 3, 153 (1969).

52. T. W. Haas and B. Maxwell, Polym. Eng. Sci., 9, 225 (1969).

53. A. Werata and C. G. Gogos, Polym. Eng. Sci., 11, 19 (1971).

54. R. R. Lagasse and B. Maxwell, Polym. Eng. Sci., 16, 189 (1976).

55. R. B. Williamson and W. F. Busse, J. Appl. Phys., 38, 4187 (1967).

56. H. D. Keith, F. J. Padden and R. G. Vadimsky, J. Appl. Phys., 37, 4027 (1966).

57. A. K. Van der Vegt and P. P. A. Smit, Soc. Chem. Ind. London, Monograph 25, 313 (1967).

58. C. L. Sieglaff and K. J. O'Leary, J. Macromol. Sci. B, 2, 793 (1968).

59. V. Folt, Rubber Chem. Tech., 44, 12 (1971).

60. J. H. Southern and R. S. Porter, J. Macromol. Sci. B, 4, 541 (1970).

61. P. D. Griswold and J. A. Cuculo, ACS Polymer Preprints, 16, 481 (1975).

62. J. R. Collier, Y. T. Tam, J. Newcome, and N. Dinos, Polym. Eng. Sci., 16, 204 (1976).

63. E. S. Clark, SPE Journal, 23, 46 (1967).

64. K. Nakamura, T. Watanabe, K. Katayama, and T. Amano, J. Appl. Polymer Sci., 16, 1077 (1972).

65. A. Ziabicki, J. Appl. Polymer Sci., 2, 24 (1959).

66. A. Ziabicki and K. Kedzierska, J. Appl. Polymer Sci., 2, 14 (1959).

67. J. R. Dees and J. E. Spruiell, J. Appl. Polymer Sci., 18, 1053 (1974).

68. K. Katayama, T. Amano, and K. Nakamura, Kolloid Z. and Z. Polym., 226, 125 (1968).

69. D. Y. Fund, E. Orlando, and S. H. Carr, Polym. Eng. Sci., 13, 295 (1973).

70. P. G. Anderson and S. H. Carr, Polym. Eng. Sci., 16, 217 (1976).

71. M. R. Mackley and A. Keller, Polymer, 14, 16 (1973).

72. M. R. Mackley, F. C. Frank, and A. Keller, J. Material Sci., 10, 501 (1975).

73. V. Tan and C. G. Gogos, Polym. Eng. Sci., 16, 512 (1976).

74. T, Kawai, T. Matsumoto, M. Kato, and H. Maeda, Kolloid Z. and Z. Polym., 222, 1 (1968).

75. K. Kobayashi and T. Nagasawa, J. Macromol. Sci. B, 4, 331 (1970).

76. L. A. Manrique and R. S. Porter, ACS Polymer Preprints, 16, 471 (1975).

77. D. Krueger and G. S. Y. Yeh, J. Appl. Phys., 43, 4339 (1972).

78. A. K. Fritzsche and F. P. Price, Polym. Eng. Sci., 14, 401 (1974).

79. A. K. Fritzsche, F. P. Price, and R. D. Ulrich, Polym. Eng. Sci., 16, 182 (1976).

80. D. Luch and G. S. Y. Yeh, J. Polymer Sci. A2, 11, 467 (1973).

81. G. S. Y. Yeh, Polym. Eng. Sci., 16, 138 (1976).

82. G. S. Y. Yeh, Polym. Eng. Sci., 16, 145 (1976).

83. M. Hashiyama, Doctoral Thesis, University of Massachusetts, 1976.

84. A. K. Fritzsche, Doctoral Thesis, University of Massachusetts, 1972.

85. F. P. Price and R. W. Kilb, J. Polymer Sci., 57, 395 (1962).

86. S. Buckser and L. H. Tung, J. Phys. Chem., 63, 763 (1958).

87. R. D. Ulrich, Doctoral Thesis, University of Massachusetts, 1972.

88. Y. Chatani, Y. Okita, H. Tadokoro, and Y. Yamashita, Polymer J., 1, 555 (1970).

89. J. V. Koleske and R. D. Lundberg, J. Polymer Sci A2, 7, 795 (1969).

90. C. J. Ong, Doctoral Thesis, University of Massachusetts, 1973.

91. F. E. Bailey, J. Polymer Sci., 32, 517 (1968).

92. J. V. Koleske and R. D. Lundberg, J. Polymer Sci. A2, 7, 897 (1969).

93. J. Gavis and R. L. Laurence, Indus. and Eng. Chem. Fundamentals, 7, 232 (1968).

94. R. M. Turian and R. B. Bird, Chem. Eng. Sci., 18, 689 (1963).

95. D. Peiffer, S. D. Hong, and R. S. Stein, J. Polymer Sci A2, 13, 1945 (1975).

96. R. Cembrola, incomplete Doctoral Thesis, University of Massachusetts.

97. L. E. Alexander, X-Ray Diffraction Methods in Polymer Science, Wiley-Interscience, New York, 1969.

98. J. Brandrup and E. H. Immergut, Eds., Polymer Handbook, 2nd edition, Wiley-Interscience, New York, 1975.

99. W. G. Perkins, N. J. Capiati and R. S. Porter, Polym. Eng. Sci., 16, 200 (1976).

100. L. Mandelkern, A. S. Posner, A. F. Diori, and D. E. Roberts, J. Appl. Phys., 32, 1509 (1961).

101. N. L. Jain and F. L. Swinton, Europ. Polym. J., 3, 371 (1967).

102. J. N. Hay, M. Sabir, and R. L. T. Steven, Polymer, 10, 187 (1969).

103. J. N. Hay and M. Sabir, Polymer, 10, 203 (1969).

104. V. Tan and C. G. Gogos, Polym. Eng. Sci., 16, 512 (1976).

105. G. M. Martin and L. Mandelkern, J. Appl. Phys., 34, 2312 (1963).

106. J. J. Benbow and E. R. Howells, Polymer, 2, 429 (1961).

107. W. W. Graessley, J. Chem. Phys., 43, 2696 (1965).

108. S. Middleman, The Flow of High Polymers, Wiley-Interscience, New York, 1968.

109. R. S. Porter and J. F. Johnson, Trans. Soc. Rheology, 6, 107 (1962).

110. A. Teramoto and H. Fujita, Macromol. Chemie, 85, 261 (1965).

111. J. D. Hoffman and J. I. Lauritzen, J. Res. Nat. Bureau Stds., 65A, 297 (1961).

112. J. I. Lauritzen and J. D. Hoffman, J. Res. Nat. Bureau Stds., 64A, 73 (1959).

113. J. D. Hoffman, SPE Trans., 4(4), 1 (1964).

114. M. D. Wolkowicz, incomplete Doctoral Thesis, University of Massachusetts.

APPENDIX I

CALCULATION OF TEMPERATURE RISE IN CIRCULAR COUETTE FLOW

The assumptions in this analysis are that the fluid is incompressible and Newtonian, and that the density, ρ, the thermal conductivity, k, and viscosity, η, are independent of temperature. A better approximation would be to assume an exponential dependence for viscosity and temperature but this complicates the solution beyond the scope of this simple analysis[1].

Assuming laminar flow, the dynamic equations for this system may be solved to determine the velocity profile

$$0 = \frac{d}{dr}\left(\frac{1}{r}\frac{d}{dr}(rV_\theta)\right) \tag{1}$$

subject to the following boundary conditions,

$$V_\theta = \underline{V} \quad \text{at} \quad r = \bar{k}R$$
$$V_\theta = 0 \quad \text{at} \quad r = R$$

where R is the outer radius, $\bar{k}$ is the ratio of inner and outer radii, and $\underline{V}$ is the linear speed of the rotating inner cylinder. The solution is given in equation 2.

$$V_\theta = \frac{\Omega_o \bar{k} R}{(\bar{k} - 1/\bar{k})}\left(\frac{r}{R} - \frac{R}{r}\right) \tag{2}$$

The energy equation may then be solved substituting the

$$0 = k\frac{1}{r}\frac{d}{dr}\left(r\frac{dT}{dr}\right) + \eta\left[r\frac{d}{dr}\left(\frac{V_\theta}{r}\right)\right]^2 \tag{3}$$

appropriate velocity profile.

$$0 = K \frac{1}{r} \frac{d}{dr} \left(r \frac{dT}{dr}\right) + \eta \frac{\Omega_o^2 \bar{k}^2 R^4}{(\bar{k}-1/\bar{k})^2 r^4} \tag{4}$$

Defining a set of dimensionless parameters

$$\S = r/R \qquad \text{dimensionless radial component}$$

$$\theta = \frac{T - T_{cr}}{T_{cr}} \qquad \text{dimensionless temperature}$$

$$N = \frac{\eta\, \Omega_o^2\, R^2\, \bar{k}^2}{k\, T_{cr}\, (\bar{k}-1/\bar{k})^2} = Br\# \quad \frac{\bar{k}^2}{(\bar{k} - 1/\bar{k})^2}$$

where Br is the Brinkman number, one can proceed to recast equation 4.

$$\frac{1}{\S} \frac{d}{d\S} \left(\S \frac{d\theta}{d\S}\right) = -4N \frac{1}{\S^4} \tag{5}$$

The solution of this dimensionless expression is given in equation 6. Two sets of boundary conditions may be

$$\theta = \frac{-N}{\S^2} + C_1 \ln \S + C_2 \tag{6}$$

stipulated. Case I is for an adiabatic inner wall and isothermal outer wall. Case II represents two isothermal walls.

Case I $\qquad \theta = 0 \quad \text{at} \quad \S = 1$

$$\frac{1}{R} \frac{d\theta}{d\S} = 0 \quad \text{at} \quad \S = \bar{k}$$

Case II $\theta = 0$ at $\S = 1$

$\theta = 0$ at $\S = \bar{k}$

The solutions for both cases are given in equations 7 and 8.

$$\text{Case I} \quad \theta = N - \frac{N}{\S^2} - \frac{2N}{\bar{k}^2} \ln \S \tag{7}$$

$$\text{Case II} \quad \theta = \frac{-N}{\S^2} + \left(\frac{N}{\bar{k}^2} - N\right) \frac{\ln \S}{\ln \bar{k}} + N \tag{8}$$

A computer program was written to solve each case for each polymer at three different crystallization temperatures and fifty radial positions across the gap. Figures 8 and 9 show the isothermal and adiabatic results for WSR crystallized at 58.8°C.

References

1. J. Gavis and R. L. Laurence, Ind. and Eng. Chem. Fund., 7, 232 (1968).

APPENDIX II

REGRESSION PROCEDURES

To perform a linear least squares regression on the Avrami equation, it must be transformed as shown below.

$$X_c = X_\infty \left(1 - \exp(-kt_1)^n\right) \tag{1}$$

where $t_1 = t - t_o$

$$1 - X_{cr} = 1 - \frac{X_c}{X_\infty} = \exp(-kt_1^n) \tag{2}$$

The exponential term is expanded in a Taylor series to give equation 3.

$$X_{cr} = kt_1^n - \frac{(kt_1^n)^2}{2} + \frac{(kt_1^n)^3}{6} + \cdots \tag{3}$$

If X_{cr} is less than ten percent, neglecting second and higher order terms in the expression produces an error of approximately five percent. The first computer program fits equation 4 by minimizing the sum of squares, S, between observed and calculated data. This technique will

$$\ln X_{cr} = n \ln t_1 + \ln k \tag{4}$$

$$S = \sum_{i=1}^{N} (y_i - w_i)^2 \tag{5}$$

be discussed in greater detail later in this section. A value for the variance of n and ln k are calculated along

with confidence limits for each parameter[1]. The confidence limits are significant only for experiments with a large number of data points.

The second computer program follows the same method as the first, but each data point is weighted by a factor of $1/\ln(X_{cr,i})$. The results of this technique differ slightly from the non-weighted analysis. The values of n and ln k, on the average, changed by one and five percent respectively, while the variances remained essentially the same. The fit in the weighted analysis was better in the region of higher crystallinity. The error introduced in the approximation (equation 4) increases with increasing X_{cr} so the non-weighted analysis was generally preferred.

The third computer program employs a non-linear analysis detailed by Kittrell[2] and Duffy[3]. For a linear least squares problem, the sum of squares between the predicted and observed values of the dependent variable are minimized with respect to each parameter. In matrix notation one can define the regression parameter matrix {K} for p parameters and N data points as shown where

$$\{K\} = (\{X\}'\{X\})^{-1} \{X\}' \{Y\} \qquad (6)$$

{X} is a N x p matrix of the independent variables and {Y} is a N x 1 vector of the dependent variables. For a non-linear expression, the p simultaneous equations resulting

from the partial differentiation with respect to each parameter are not easily solved. Two methods have generally been used to approach a solution.

The first method uses the first two terms of the functional equation expanded about a set of parameter values in a Taylor series.

$$w_i = f(x_i;\{K\})\Big|_{\{K\}=\{K\}^\circ} + \sum_{u=1}^{p} \frac{\partial f(x_i;\{K\})}{\partial K_u}\Bigg|_{\{K\}=\{K^\circ\}} (K_u - K_u^\circ) \tag{7}$$

This can be linearized by defining

$$z_i = w_i - f(x_i;\{K\}) + e_i \tag{8}$$

where e_i is the experimental error. Then

$$z_i = \sum_{u=1}^{p} f'_{u,i} b_u - e_i \tag{9}$$

where,

$$b_u = K_u - K_u^\circ \tag{10}$$

and

$$f'_{u,i} = \left.\frac{\partial f(x_i;\{K\})}{\partial K_u}\right| \qquad \{K\} = \{K^\circ\} \tag{11}$$

Given initial estimates of all parameters $\{K^\circ\}$, one can use the form of equation 6 to solve for the correction vector $\{b\}$. Values obtained for $\{b\}$ are used in equation 10 to

$$\{b\} = (\{X\}'\{X\})^{-1}\{X\}'\{Z\} \tag{12}$$

determine new parameter estimates. This process is repeated until $\{b\}$ reaches a given tolerance. Convergence is obtained rapidly by this method if initial estimates are good.

A second approach may be applied to the problem if one considers equation 5 as a surface in space. The technique of steepest descent[4] can then be applied to determine the lowest point in the surface (minimum value of S). This is done by numerically evaluating the gradient of sum of squares with respect to each of the parameters. A jump is then made in the direction of maximum gradient proportional to the length of the gradient vector and a new sum of squares is calculated. If the new sum is less than the previous value, the process is repeated with the parameters at that point as the new reference values. If a greater sum is found, the distance travelled is halved and the sum

is recalculated. This process is continued until the difference in calculated sum of squares is within some acceptable tolerance. Convergence with this technique occurs for poor initial estimates but is very slow near the best fit values.

Kittrell has explained a compromise technique given in equation 13.

$$\{b\} = (\{X\}'\{X\} + \lambda\{X\})^{-1} \{X\}'\{Z\} \qquad (13)$$

The parameter λ determines the importance of parameter estimates. The method is begun using large values of λ resulting in the solution by the steepest descent method. As each successive parameter estimate improves, λ is decreased until the solution approaches that given in equation 12.

The initial estimates used in the non-linear regression are those determined as best fit parameters in the linear analysis. Convergence with these estimates occurs after a small number of iterations and changes in the parameters are generally less than five percent. Parameter estimates differing by as much as 50 percent from the best fit estimates were found to converge to the same values.

References

1. O. L. Davies and P. L. Goldsmith, Statistical Methods in Research and Production, 4th edition, Hafner Publishing Co., New York, 1972.

2. J. R. Kittrell, Advances in Chem. Eng., Volume 8, Academic Press, New York, 1970.

3. R. Duffy, Masters Thesis, University of Massachusetts, 1972.

4. G. E. P. Box and H. C. Wilson, Biometrika, 46, 77 (1959).